

Supplementary Material: High dose inactivated influenza vaccine inconsistently improves heterologous antibody responses in an elderly human cohort

Table of contents

Reproducibility instructions	3
Additional background references	5
Expanded Methods	6
Causal model for confounding	6
Analysis of confounders on treatment choice	8
Model formula and explanation	11
Model likelihood and priors	12
Model fitting	16
cACE calculation	17
Effect size transformation from cACE calculation	17
Supplementary results	19
Historical and vaccine strain information	19
Descriptive analysis	25
Birth year and age summary statistics	25
Cohort demographics and assays by year	25
Pre and post-vaccination titer figures	28
Fold change figures	42
Outcome summaries	55
Model diagnostics	61
Trace rank plots	62
Prior and posterior density comparison	65

Homologous model results	69
Model results for other outcomes	69
Post-vaccination titer	70
Seroprotection	75
Seroconversion	80
Session information	85
References	86

Reproducibility instructions

In order to reproduce our results, you should first download the archived repo from Zenodo (here: <https://doi.org/10.5281/zenodo.12666976>) or clone the Git repository (hosted on GitHub here: <https://github.com/ahgroup/Billings-2024-HD-Heterologous>). (You can also download the repository as a zipped folder from the GitHub page). If you use different software or package versions than what we used, or run the results in a different order, you may get errors or inconsistent results.

We ran the analysis on a Windows 10 Enterprise 64-bit (build 19045) machine with 64 GB RAM and a 36-core processor. Any statements we make about the execution time of code will vary across machines, especially if the hardware is different from these specs.

Before you can reproduce our results you will need to install the following software requirements.

- R version 4.4.1, available from <https://cran.r-project.org/>.
- RTools 4.4, also available from CRAN.
- The RStudio IDE, available from <https://posit.co/download/rstudio-desktop/>. We used version 2023.12.1+402 Ocean Storm (desktop).
- Quarto version 1.5.24, available from <https://quarto.org/>.
- Version 1.0.7 of the `renv` package for R, available from <https://cran.r-project.org/web/packages/renv/index.html>.

With the software installed, follow these instructions to reproduce our results.

1. Open the `SD-HD-flu-vaccine.Rproj` file in RStudio.
2. Once `renv` initializes, run the command `renv::restore()` in the Console in order to begin installing the required packages. If you have issues at this stage, you can also run `renv::deactivate()` and install the packages manually. However, if you do not use `renv` or use different package versions than we did, the following instructions might not work for you.
3. (This step is optional. If you do not want to re-run the Bayesian models, you can ignore this step.) If you want to re-run the Bayesian models, you need to install `cmdstan` at this step. You should have the `cmdstanr` package installed if you successfully followed the `renv` instructions, and you can follow the `cmdstanr` quick start guide at <https://mc-stan.org/cmdstanr/articles/cmdstanr.html> to install `cmdstan`. Start at the section titled “Installing CmdStan”. Installing `cmdstan` can be difficult, so make sure to carefully read the instructions. If you have issues with the `cmdstan` path or installation, you may need to open a new R GUI or RStudio window as an administrator (on Windows), install version v1.0.8 of `cmdstanr` manually, and re-run the installation and path setting steps. If you still have issues, the Stan discourse forum (<https://discourse.mc-stan.org/>) is often an excellent place to ask for help.

4. Now you should be able to run our code files. All of the code files are located in the `code` directory. The code files are designed to run in the following order, although multiple steps can potentially be skipped since we provide our results along with the code.
 - `02-Data-Summary.R`: the input files for this code are provided and it does not take a long time to run. This file recreates many of our summary tables.
 - `03-Model-Fitting.R`: this code specifies the `brms` models, and runs the HMC sampling scheme for our bayesian regression models. **This code takes a very long time to execute.** You do not need to run this code to reproduce our model results, as we have provided the model fit files along with the code.
 - `04-Posterior-Summaries.R`: this code computes the (c)ACE estimates from the fitted models. You should be able to run this code without running script 03. **Running this code took about an hour for us**, but will provide time estimates after the first set of cACEs is calculated. Running this code will reconstruct the model fit files.
 - `05-Model-Results.R`: processes the (c)ACE estimates into figures for the manuscript. The `all-cates-combined.Rds` input file is produced by script 04 and is provided with our code.. You can produce all of our figures with the cleaned data and this file of estimates.
 - `06-Supplementary-Analyses.R`: contains additional calculations for the Supplementary Material. You can run the first part of the script, including the DAG and tables, with only the cleaned data, which is provided. You should (at minimum) run script 04 before this code to ensure the model fit files are reconstructed.
 - The `common-functions` directory contains various helper functions and declarations and running the code on its own is not very interesting, although it is possible as long as all of the packages are installed correctly.
5. If you have run all of the code files, you can reproduce an unformatted version of the manuscript and supplement by rendering the files `products/manuscript/manuscript.qmd` and `products/manuscript/supplement.qmd`. When you open these files in RStudio with Quarto installed, you will see a “Render” button in the GUI that will execute the appropriate Quarto commands for you.

Note that the script `01-Data-Processing.R` contains our code for obtaining the finalized data set released in the Supplement: you will not be able to run this file. Se do not provide the input file, `clean-data.Rds` due to data sensitivity concerns. Instead we have provided the output files in the `data/processed` folder along with the code.

Again, we note that our Bayesian models are computationally intensive, especially compared to similar frequentist models. The model fits in script 03 took several days to run on our relatively good computer, but will take a long time even on cutting-edge machines. We recommend only re-running the model fitting process for readers who wish to validate our results.

Additional background references

We also consulted additional references on the immunogenicity benefits [1–12] and clinical benefits [8,13–19] of Fluzone HD vaccine relative to SD, which are included here due to the reference limit in the main text. Some studies which included younger adults did not find a difference between the HD and SD vaccine [20].

Notably, in the main text we do not discuss comparisons with vaccines other than the split-inactivated SD vaccine, but the HD vaccine also appears to perform similarly to other enhanced vaccines like those with adjuvants [12,21,22]. Unfortunately we do not have access to data from study groups that received other enhanced vaccine candidates, but comparing the effects of, among others, adjuvanted and high-dose vaccines on the heterologous antibody response could reveal intriguing differences in the underlying immunology of the different formulations.

Expanded Methods

Causal model for confounding

Since we used observational data rather than clinical trial data to estimate the effect of vaccine dose on immunological responses, we needed to adopt a causal model to control for confounding. A confounder is any other factor which can affect both the treatment an individual receives (i.e., which dose they got) and the outcome. We represented our causal assumptions using a directed acyclic graph (DAG), shown in Figure 1.

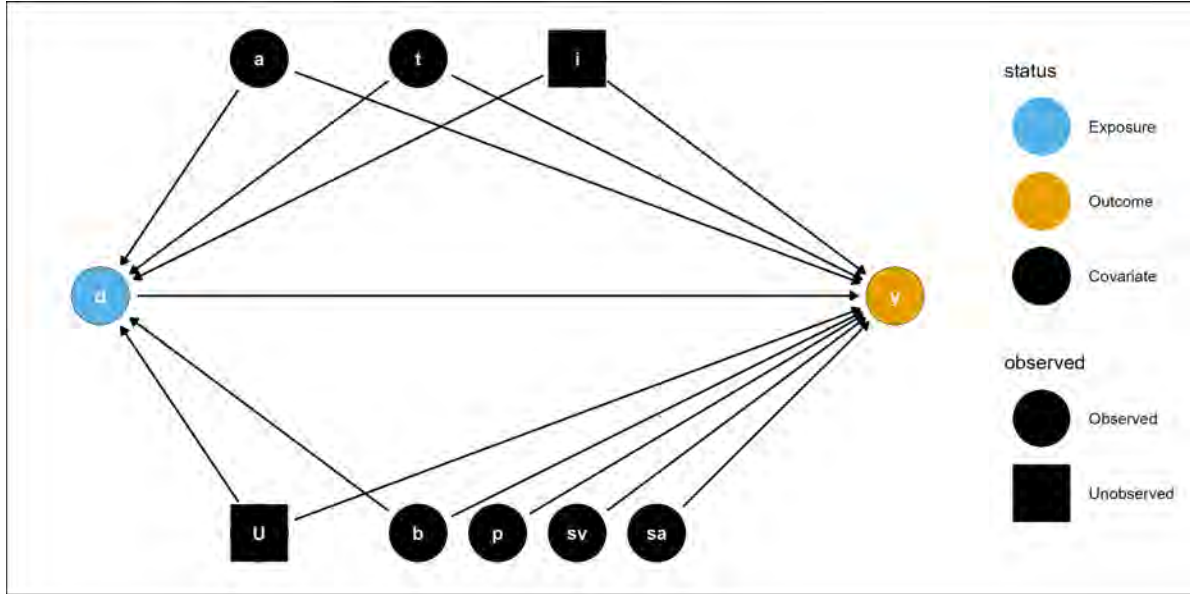


Figure 1: The DAG we adopted as our causal model. Nodes indicated variables and arrows follow the direction of causality, i.e., an arrow from X to Y indicates that X is a cause of Y .

In order to show the DAG nicely, the variable names are abbreviated by single letters. The letters in Figure 1 correspond to the following variables in our data (Table 1).

The observed confounders we included in our model were age, calendar time, and birth year. Age could potentially be a confounder since elderly individuals are more encouraged to get the high dose vaccine, and older individuals tend to have attenuated immune responses [23]. Birth year was included as a confounder for the same reason – older individuals could be more likely to receive HD vaccines, and the cohort effect of birth year imprinting affects vaccine response independently of age [24–27]. Finally, we included the season as the calendar year to account for differences in vaccines between seasons. Some vaccine formulations are more immunogenic than others, which varies by season. Additionally, we included this as a confounder because the production and administration rate of HD vaccines could change by season, although we

have no data with which to test this hypothesis. However, including controlling for a variable which is not actually a confounder does not include bias in the model results (unless collider bias is induced, which we do not believe is the case here as there are no relevant variables that have both season and dose or season and vaccine response as common causes. Any such variables are temporally separated from the treatment and response.)

Table 1: Variable abbreviations used in the DAG.

Abbreviation	Variable
d	Vaccine dose
y	Immunological outcome
a	Age
t	Season
i	Other individual effects
U	Other unobserved confounders
b	Birth year
p	Pre-vaccination titer
sv	Strain included in vaccine
sa	Strain used for assay

We represent unobserved confounding in our DAG as the variable U . There are likely many confounders, like individual variables driving vaccine choice, which we cannot account for because they were not collected as part of the study we used. We attempted to control for unobserved confounding as best as possible by using a random effects model structure which can absorb part of the effect of unobserved confounders by modeling between-individual variability (which we represent as i in the DAG). Not all unobserved confounding effects can be absorbed by individual random effects, but some, such as for demographic characteristics like sex and race, potentially can be.

Even though not all of the variables shown are confounders (p , sv , and sa are only causes of the outcome in our DAG), we include sv and sa so we can obtain stratum-specific effects for those variables. Controlling for p does not open any backdoor paths (under our assumed causal model), so since p is a cause of the outcome we can include p in the model to potentially improve the efficiency of our estimates.

Analysis of confounders on treatment choice

In the study our data were collected in, participants over age 65 were offered the choice between SD and HD vaccine, so the treatment (vaccine dose) was not assigned randomly as it would be in a clinical trial. There are many factors that could affect which treatment group an individual was likely to choose, including prior knowledge about the HD vaccine, batch effects in receiving shipments of HD vaccines at the clinical study site, demographic characteristics, risk-taking behavior, prior adverse events from vaccination, and others. While we cannot assess many of these characteristics, we did assess the demographic characteristics that were available to us to inform our selection of confounders in the model.

Table 2 shows the results of our analysis. We used Bayesian logistic regression to calculate the odds ratio for receiving the HD vaccine (relative to receiving the SD vaccine). Each model used the dose as the outcome (with HD coded as an event, that is, SD was coded as 0 and HD was coded as 1) and we included a single categorical predictor in each model. The ORs are calculated by exponentiating the mean beta coefficient from 2000 post-warmup Hamiltonian Monte Carlo samples, implemented using the `brms` package. We used the same priors and setup as our main logistic regression model, which are explained in detail in the model fitting section. The credible interval shown is the highest density continuous interval over the post-warmup samples.

Our results (Table 2) show that several demographic and study-specific variables affected the odds of receiving an HD vaccine. More HD vaccines were available at the UGA study site than the PA and FL study sites, and in general HD vaccine uptake increased as the study continued, although the effect was not strong (the credible interval was wide and had a large amount of posterior density on either side of 1). Patients who were assigned female at birth (AFAB) and assigned male at birth (AMAB) had nearly equal odds of receiving HD vaccines, as did White patients and patients of color. Finally, older patients were somewhat more likely to receive HD vaccination, although estimating the OR was unstable for the oldest groups since there were very few patients over age 80. Since our study was conducted over a small temporal scale, the results for birth year are very similar to the results for age at enrollment. These odds ratios matched our causal hypotheses about age, birth year, study site, and calendar time (represented by influenza season) and help justify our inclusion of these terms in the model as confounders. Since sex assigned at birth and race/ethnicity did not appear to be associated with which dose was received, we elected not to include these variables in the model.

Table 2: Odds ratio for receiving HD vaccine. I.e., each OR is the odds of receiving the HD vaccine in the relevant group compared to the reference group for each variable. Each model was a univariable (simple) logistic regression model where the dose was the outcome (a patient who received SD was coded as 0 and a patient who received HD was coded as 1) and one single categorical covariate was included in the model. OR was calculated by exponentiating the relevant slope coefficient from the logistic regression model, and thus an OR higher than one indicates a group with higher odds of receiving the HD vaccine than the reference group for a given variable. A dash indicates the reference group for a given variable, which means an OR could not be calculated.

Variable	OR ¹²
Study	
UGA	—
PA	0.64 (0.44 to 0.94)
FL	0.16 (0.10 to 0.25)
Season	
2013 - 2014	—
2014 - 2015	1.88 (0.88 to 3.80)
2015 - 2016	3.71 (1.90 to 7.77)
2016 - 2017	5.84 (2.88 to 12.2)
2017 - 2018	1.85 (0.72 to 4.32)
2018 - 2019	1.82 (0.61 to 5.97)
2019 - 2020	8.48 (4.00 to 18.7)
2020 - 2021	29.6 (11.2 to 80.5)
2021 - 2022	34.1 (12.2 to 97.4)
Sex assigned at birth	
Female	—
Male	0.94 (0.68 to 1.32)
Age at enrollment	
65 - 70	—
71 - 75	1.15 (0.77 to 1.70)

Variable	OR ¹²
76 - 80	1.56 (0.88 to 2.87)
81 - 85	0.57 (0.14 to 1.99)
Birth year	
1930 - 1935	—
1936 - 1940	1.99 (0.77 to 5.64)
1941 - 1945	2.22 (0.80 to 5.80)
1946 - 1950	2.30 (0.92 to 5.90)
1951 - 1955	3.24 (1.23 to 8.56)
1956 - 1960	7.29 (0.54 to 116)
Race/Ethnicity	
White or Caucasian	—
Black or African American	0.87 (0.55 to 1.39)
Other	0.97 (0.42 to 2.07)

¹OR = Odds Ratio

²CI = Confidence Interval

Model formula and explanation

The full mathematical equations for our model are shown in the next section. Here, we briefly explain the model we used and the implementation in **brms**.

The model formula for our hierarchical models was chosen based on *a priori* covariate information from our causal model, along with constraints induced by the estimability of random effects. We elected not to include interaction terms or any other nuisance covariates due to the complexity of the model. Notably, our model is unlikely to converge under frequentist maximum likelihood estimation, such as by the **nlme** R package, or other similar methods. The random effects in the model are overdetermined, which leads to near-zero (boundary) estimates of random effect covariance terms, which prevents the maximum likelihood model from reaching convergence. However, having random effects which are all similar does not prevent the NUTS algorithm implemented by Stan/**brms** from exploring the implied posterior distribution.

We specified our models in **brms** using the following model formula:

```
outcome ~ dose +
  s(birth_year_c, k = 5) + s(age_c, k = 5) +
  s(log_pretiter, k = 5) + s(year_c, k = 5, by = study) +
  (1 | id) + (1 | study) +
  (1 + dose | strain_type) + (1 + dose | strain_type:strain_name) +
  (1 + dose | vaccine_name) + (1 + dose | vaccine_name:strain_type).
```

The **brms** model syntax is explained more fully in the **brms** documentation, but we will briefly explain the model formula. The `outcome ~` specification declares that `outcome` is the outcome variable in the model, and everything after the `~` will be an independent variable. The term `dose` specifies a fixed effect of the variable `dose`, which by default will use indicator encoding (as will all qualitative variables). The model also includes a global intercept term by default.

All of the terms which look like `s(variable_name, k = 5)` specify smoothing splines. The smoothing spline basis matrix is constructed by the **mgcv** package before being passed to the Stan code generated by **brms**, and so the smoothing splines are parametrized in the same way as for frequentist models. We used penalized thin-plate bases with $k = 5$ basis functions – since some of our predictor variables are integer-valued, choosing a low value of k provides reasonable flexibility for modeling nonlinear relationships while preventing the spline from being overdetermined. Finally, the specification `by = study` in the smoothing term for the variable `year_c` fits separate smoothing splines over the variable `year_c` for each stratum defined by the `study` variable. Since the three different studies did not all align temporally, we allowed the effect to be

Finally, all the terms in parenthesis with vertical bars (`|`) indicate random or varying effect terms. A `(1 | g)` term indicates a varying intercept for each unique level of the variable `g`,

while a $(1 + v | g)$ indicates a random effect of the variable v , which is allowed to differ for each unique level of the group variable g . Our model includes random intercepts for individuals (`id`) and the three different studies represented in our data (`study`), which allows all individuals and each of the studies to have different baseline effects on the model outcome. When the varying intercept and slope are specified together, they are assumed to be correlated, and the covariance matrix for the random effects is estimated.

We also include random intercepts for each `strain_type`, which refers to the influenza strain used to conduct an HAI assay: for our model, this is either H1N1 or H3N2. Furthermore, the specification $(1 + \text{dose} | \text{strain_type}) + (1 + \text{dose} | \text{strain_type}:\text{strain_name})$ adds random effects (on both the baseline and the effect of dose) for `strain_type`, and for `strain_name` *nested within* the `strain_type`. In our dataset, `strain_name` refers to the specific strain that was used to conduct an HAI assay. In other words, the random effects for all H1N1 strains are allowed to share information, and the random effects for all H3N2 strains are allowed to share information, but information cannot be borrowed across the strain types. The similar terms for `vaccine_name` and `strain_type` imply the same effects, but varying by the strain that was used in the vaccine formulation an individual received, rather than the strain used for the HAI assay.

In short, our model controls for correlated measurements between individuals, for correlated responses to the same strains, and for strains of the same subtype to be more similar to each other than to the opposing subtype. The effect of dose is allowed to vary across all of these subgroups, with the same patterns of correlation.

The model is complicated, and not all combinations of random effects are observed in our data (in fact, they cannot be due to the update schedule of the influenza vaccine). That means our random effects are neither completely nested nor completely crossed, but we allow random effects to be correlated with each other where appropriate.

Finally, the variable names specified with `_c` as a suffix have been centered to improve numerical estimation of the model. We performed all data transformation steps like log transformations and centering prior to passing any data to `brms` or `Stan`.

Model likelihood and priors

For the post-vaccination titer and titer increase outcomes, we used a Gaussian (Normal distribution) likelihood function for the model. Letting the outcome be y , we assumed that

$$\begin{aligned} y[i] &\sim \text{Normal}(\mu[i], \sigma^2) \\ \sigma &\sim t^+(3, 0, 3) \\ i &= 1, \dots, N \end{aligned}$$

where σ is the residual variance, and $\mu[i]$ is described by the **brms** equation above, which builds a model for the conditional mean of $y[i]$ given the predictor data. Here, N is the number of data points passed to the model and the index variable i indexes the current data record.

The model for the mean and the priors we used for the Gaussian outcomes are shown below.

$$\begin{aligned}
\mu[i] &= \alpha + \beta \cdot \text{HD}[i] + f[1](\text{birth_year_c}[i]) + f[2](\text{age_c}[i]) + \\
&\quad f[3](\log \text{pre_titer}[i]) + f[4, \text{study}[i]](\text{year_c}[i]) + \\
&\quad u[1, \text{id}[i]] + u[2, \text{study}[i]] + \\
&\quad b[1, 0, \text{strain_type}[i]] + b[1, 1, \text{strain_type}[i]] \cdot \text{HD}[i] + \\
&\quad b[2, 0, \text{strain_type}[i]] \cdot \text{strain_name}[i] + \\
&\quad b[2, 1, \text{strain_type}[i]] \cdot \text{strain_name}[i] \cdot \text{HD}[i] + \\
&\quad b[3, 0, \text{vaccine_name}[i]] + b[3, 1, \text{vaccine_name}[i]] \cdot \text{HD}[i] + \\
&\quad b[4, 0, \text{strain_type}[i]] \cdot \text{vaccine_name}[i] + \\
&\quad b[4, 1, \text{strain_type}[i]] \cdot \text{vaccine_name}[i] \cdot \text{HD}[i] \\
f[j](\cdot) &= \sum_{k=1}^5 \gamma[j, k] \cdot \phi[j, k](\cdot); \quad j = 1, 2, 3 \\
f[4, \text{study}[i]](\text{year_c}[i]) &= \sum_{k=1}^5 \eta[k, \text{study}[i]] \cdot \phi[4, k](\text{year_c}[i]) \\
\alpha &\sim \mathcal{N}(0, 5) \\
\beta &\sim \mathcal{N}(0, 5) \\
\gamma[j, k] &\sim \mathcal{N}(0, \tau[j]) \quad j = 1, 2, 3; \quad k = 1, \dots, 5 \\
\tau[s] &\sim t^+(3, 0, 3) \\
\eta[k, \text{study}[i]] &\sim \mathcal{N}(0, \zeta[\text{study}[i]]) \quad k = 1, \dots, 5 \\
\zeta[\cdot] &\sim t^+(3, 0, 3) \\
u[r, \cdot] &\sim \mathcal{N}(0, \omega[r]) \quad r = 1, 2 \\
\omega[r] &\sim t^+(3, 0, 1) \\
\begin{pmatrix} b[q, 0, \cdot] \\ b[q, 1, \cdot] \end{pmatrix} &\sim \text{MVN}\left(\mathbf{0}, (\text{diag}(\psi[q])L[q])(\text{diag}(\psi[q])L[q])^T\right) \quad q = 1, \dots, 4 \\
\psi[q] &\sim t^+(3, 0, 1) \\
L[q] &\sim \text{LKJ}(2)
\end{aligned}$$

Note that instead of using subscript notation in our model, because of the large number of nested subscripts and the use of index-variable coding, we elected to use brackets to show indexing. For example, the notation $L[q]$ in our model is identical to the common notation L_q , but for index variables such as in the equation for $\mu[i]$, the bracket notation avoids small text which is often difficult to read. Additionally, we use the centered dot symbol (\cdot) to indicate when there are many valid arguments that would all have the exact same right hand side (RHS)

in a formula. For example, $\zeta(\cdot)$ indicates that all subscripts for ζ follow the same independent distributions, and writing out another index variable would only serve to make the formula more confusing.

In our model, the $\phi(\cdot)$ functions represent basis functions for thin plate splines. Internally, `brms` uses `mgcv` to create the spline basis design matrix, which uses a low-rank (in our case, rank $k = 5$) approximation of the eigenvalue matrix to create the thin plate spline, which allows for similar performance to the full-rank eigendecomposition while substantially saving computational time by elementing dimensions with small eigenvalues which contribute little to the fitting process. Since our data values are integer-valued (year, birth year, pretiter, and age are all integer values), the maximum k rank we can choose is equal to the number of unique values recorded in each variable, but we chose $k = 5$ in order to preserve the first five components after eigendecomposition because this balances performance with loss of data [28–33].

The distributions we refer to are: $\mathcal{N}(\cdot, \cdot)$ for the Normal distribution, parametrized in terms of the mean and variance; $t^+(\nu, \cdot, \cdot)$ for the location-scale **half** Student’s t distribution with ν degrees of freedom, which can take on only positive values; $MVN(\cdot, \cdot)$ for the multivariate normal distribution parametrized in terms of a mean vector and a covariance matrix; and $LKJ(\cdot)$ for the Lewandowski-Kurowicka-Joe distribution for Cholesky factors [34].

To specify the covariance structures for our correlated varying effects, we used the Cholesky factor parametrization, which is more numerically stable and computationally efficient than other methods like individually parametrizing each term of the covariance matrix or specifying an inverse-Wishart prior [35,36]. We represent the covariance matrix, say Σ , using a Cholesky factor and scale parameter as follows:

$$\begin{aligned}\Sigma &= \text{diag}(\sigma)\Omega_{\Sigma}\text{diag}(\sigma) \\ &= \text{diag}(\sigma)(LL^T)\text{diag}(\sigma) \\ &= (\text{diag}(\sigma)L)(\text{diag}(\sigma)L)^T.\end{aligned}$$

Here, L is the Cholesky factor of Ω . We can then specify a strictly positive prior on σ , the scale parameter, and an LKJ prior on L . Specify, we use an **LKJ**(2) prior. An **LKJ**(1) indicates that all correlations are equally likely, while parameter values less than one indicate that strong correlations are more likely while parameter values greater than one indicate that strong correlations are less likely. Therefore, using a parameter value of 2 presumes slightly weaker correlations *a priori*, but large and weak correlations can still be learned from the data.

For the seroconversion and seroprotection outcomes, we used a Bernoulli likelihood with a logit link function. That is, we assumed that

$$\begin{aligned}y_i &\sim \text{Bernoulli}(p_i), \\ p_i &= \text{logit}^{-1}(\mu_i),\end{aligned}$$

where μ_i is again described by the right-hand side of the **brms** formula.

While the structure of the model for the mean is the same for the logistic regression models, we have to reduce the width of the priors because our outcome is fitted on the logit scale for the binary outcomes. Using these relatively narrow priors actually gives a more uniform prior distribution of effects, because of the nonlinear transformation of the linear predictor, which severely deflates low values and severely inflates high values. There is no residual variance to estimate in the binary outcome models.

The mean structure and priors used for the logistic regression models are as follows.

$$\begin{aligned}
\mu[i] &= \alpha + \beta \cdot \text{HD}[i] + f[1](\text{birth_year_c}[i]) + f[2](\text{age_c}[i]) + \\
&\quad f[3](\text{log pre_titer}[i]) + f[4, \text{study}[i]](\text{year_c}[i]) + \\
&\quad u[1, \text{id}[i]] + u[2, \text{study}[i]] + \\
&\quad b[1, 0, \text{strain_type}[i]] + b[1, 1, \text{strain_type}[i]] \cdot \text{HD}[i] + \\
&\quad b[2, 0, \text{strain_type}[i] \cdot \text{strain_name}[i]] + \\
&\quad b[2, 1, \text{strain_type}[i] \cdot \text{strain_name}[i]] \cdot \text{HD}[i] + \\
&\quad b[3, 0, \text{vaccine_name}[i]] + b[3, 1, \text{vaccine_name}[i]] \cdot \text{HD}[i] + \\
&\quad b[4, 0, \text{strain_type}[i] \cdot \text{vaccine_name}[i]] + \\
&\quad b[4, 1, \text{strain_type}[i] \cdot \text{vaccine_name}[i]] \cdot \text{HD}[i] \\
f[j](\cdot) &= \sum_{k=1}^5 \gamma[j, k] \cdot \phi[j, k](\cdot); \quad j = 1, 2, 3 \\
f[4, \text{study}[i]](\text{year_c}[i]) &= \sum_{k=1}^5 \eta[k, \text{study}[i]] \cdot \phi[4, k](\text{year_c}[i]) \\
\alpha &\sim \mathcal{N}(0, 1) \\
\beta &\sim \mathcal{N}(0, 1) \\
\gamma[j, k] &\sim \mathcal{N}(0, \tau[j]) \quad j = 1, 2, 3; \quad k = 1, \dots, 5 \\
\tau[s] &\sim t^+(3, 0, 1) \\
\eta[k, \text{study}[i]] &\sim \mathcal{N}(0, \zeta[\text{study}[i]]) \quad k = 1, \dots, 5 \\
\zeta[\cdot] &\sim t^+(3, 0, 1) \\
u[r, \cdot] &\sim \mathcal{N}(0, \omega[r]) \quad r = 1, 2 \\
\omega[r] &\sim t^+(3, 0, 1) \\
\begin{pmatrix} b[q, 0, \cdot] \\ b[q, 1, \cdot] \end{pmatrix} &\sim \text{MVN}\left(\mathbf{0}, (\text{diag}(\psi[q])L[q])(\text{diag}(\psi[q])L[q])^T\right) \quad q = 1, \dots, 4 \\
\psi[q] &\sim t^+(3, 0, 1) \\
L[q] &\sim \text{LKJ}(2)
\end{aligned}$$

The details on notation and priors are the same as for the Gaussian model. The only changes are for the outcome distribution, the lack of a residual unexplained variance parameter to

estimate, and the narrower variances specified for the prior distributions.

We chose our priors with three major criteria in mind. 1. The priors should reflect true constraints on parameters, but should not impose arbitrary constraints. So variance parameters should have strictly positive priors, correlations should be bounded between -1 and 1, etc. The parameter space of each prior is unbounded other than actual, scientific limitations of parameters. 1. The priors should be skeptical and regularizing. The priors for all of our effects have a mode of zero – we have effectively presupposed that there are no true effects, and any effects need to be learned from the data. This is similar to the idea of falsification in a frequentist framework – we need the data to convince us that an effect is present, rather than presupposing an effect and working to find it. 1. The priors should allow for large effects if the data support large effects.

Due to our third point, for variance parameters, we have chosen half Student’s t priors. These are a compromise between half-Gaussian (or half-Normal) priors, which have most of their mass in the bulk of the distribution, and normal tails, and the Cauchy distribution, which has fat tails and more easily allows for large effects. The Cauchy distribution is poorly behaved and hard to sample from because of its pathological properties (e.g. it has no mean and infinite variance, which certainly does not reflect our prior beliefs about observable effects). The degrees of freedom parameter for the Student’s t prior controls how “Cauchy-like” the distribution is, i.e., how fat the tails are. A half- t distribution with $\nu = 3$ degrees of freedom (the value we have chosen for all of our priors) provides the fattest tails that are easy to sample from without pathological problems, therefore allowing all of our parameters to become large if the data support large parameters. This principle also reflects why we chose an LKJ(2) prior for correlation matrices, as explained previously.

Model fitting

We implemented our models in `brms` [37,38], an R package which interfaces with the `cmdstanr` R package [39] and the `cmdstan` interface to the Stan probabilistic programming language [35]. Stan is a programming language designed to efficiently implement Hamiltonian Monte Carlo (HMC) for sampling from the posterior distribution of a Bayesian model [40]. HMC is a modern method which improves upon several limitations of other MCMC methods (such as random walk Metropolis-Hastings or Gibbs sampling) for models with continuous parameters.

We sampled all of our models across 16 chains (in parallel), with 500 warmup iterations and 1250 sampling iterations per chain, for a total of 20000 post-warmup samples per model. We increased the adaptive delta to 0.99 (which controls the ratio of accepted Metropolis proposals; increasing this parameter helps to prevent divergent transitions). We also seed the seed for each HMC run, but otherwise we used the default `cmdstan` control parameters.

cACE calculation

Our primary measure of effect size after fitting the model was the (C)ACE, or (Conditional) Average Causal Effect. The cACE represents the difference in model predictions for the two counterfactual potential outcomes. Let y_i be the observed outcome for individual i , and let t_i be the treatment for individual i (where $t_i \in \{\text{SD}, \text{HD}\}$). Using our fitted model, we can predict two counterfactual potential outcomes for individual i , which we call $\hat{y}_i(\text{HD})$, the predicted outcome if an individual had received the HD vaccine, and $\hat{y}_i(\text{SD})$, the predicted outcome if an individual had received the SD vaccine. Even though only one of these potential outcomes corresponds to the actual observed data, we can make predictions for both using the model. The individual causal effect (ICE) for individual i is defined as

$$\tau_i = \hat{y}_i(\text{HD}) - \hat{y}_i(\text{SD}).$$

We can then summarize the posterior distribution of τ_i measurements to estimate the average causal effect (ACE). If the ACE is positive, then our model predicts that the HD vaccine elicits a stronger immune response on average in our study sample.

While the most common way to calculate the ACE is by taking the sample mean and associated 95% confidence interval over all of the calculated ICEs, in a Bayesian framework, we have k samples (in our specific case, 20000) from the posterior distribution of the ICE for each individual. We can pool these samples either all together to obtain the posterior distribution of the overall ACE for our sample, or we can pool samples together within strata to obtain estimates for various cACEs, where “conditional” refers to an observation being in a specific stratum (for example, all assays conducted on samples given by donors who had received a vaccine containing CA/09-like virus particles).

Specifically, we summarized all (c)ACEs in our study using the mean point estimate from the relevant posterior samples, along with the 95% highest density continuous interval (HDCI). We estimated the mean and HDCI using the `ggdist` R package [41,42], which (at the time of writing) calculates the HDCI using a CDF-bounded density estimator with a Gaussian kernel using the reflection method [43,44]. The density estimate is trimmed to the bounds of the data, the bandwidth is estimated using the Sheather-Jones Direct Plug-In method [45], and we evaluated the density estimator at 4096 grid points.

Effect size transformation from cACE calculation

The cACE (as described in a previous section) is calculated by taking a difference of predicted model outcomes. Since the model predictions are in units of log titer measurements (regardless of whether the outcome is post-vaccination titer or titer increase), the cACE is expressed in log titer units. In order to better communicate the effect size, we transformed the cACE. As before, let $\hat{y}_i(\text{SD})$ be the predicted treatment effect for individual i if that individual had

received an SD vaccine, and let $\hat{y}_i(\text{HD})$ be the predicted treatment effect for individual i if that individual had received an HD vaccine. The estimated ICE is

$$\hat{\tau}_i = \hat{y}_i(\text{HD}) - \hat{y}_i(\text{SD}),$$

which represents the estimated benefit that individual i would receive from the HD vaccine. Our model generates a posterior distribution of the estimated ICE for each individual

The (c)ACE over the study sample is estimated as

$$\widehat{ACE}_i = E(\hat{\tau}_i) = E(\hat{y}_i(\text{HD}) - \hat{y}_i(\text{SD})),$$

and we compute this by pooling together the posterior distributions of the ICEs and summarizing them. However, each ICE is in log2-titer units, and so the ACE is also in log2-titer units. To facilitate interpretation, we can exponentiate (a monotone strictly increasing transformation) the estimated ACE to obtain an estimate in more interpretable titer units.

The transformed ACE, which we (arbitrarily) denote as $\hat{\varphi}_i$ is then

$$\hat{\varphi}_i = 2^{\tau_i} = 2^{E(\hat{y}_i(\text{HD}) - \hat{y}_i(\text{SD}))},$$

and is in HAI titer units. This number represents the average treatment effect as a ratio of fold changes, for the results presented in the main text. It can be interpreted analogously for the other three outcomes we used as sensitivity analyses in a later section of this Supplement.

Supplementary results

Historical and vaccine strain information

Throughout our manuscript and supplement, we used the abbreviated names of each strain throughout the paper in order to simplify tables and graphics. The complete strain names along with the abbreviated names are shown for H1N1 strains in Table 3 and for H3N2 strains in Table 4.

Table 3: Abbreviated strain names used in figures and tables, along with complete strain names. This table shows all H1N1 strains in our study.

Strain name	Short name
A/H1N1/South Carolina/1/1918	SC/18
A/H1N1/Puerto Rico/8/1934	PR/34
A/H1N1/Weiss/43	Wei/43
A/H1N1/Fort Monmouth/1/1947	FM/47
A/H1N1/Denver/1957	Den/57
A/H1N1/New Jersey/8/1976	NJ/76
A/H1N1/Ussr/90/1977	USSR/77
A/H1N1/Brazil/11/1978	Bra/78
A/H1N1/California/10/1978	CA/78
A/H1N1/Chile/1/1983	Chi/83
A/H1N1/Singapore/6/1986	Sing/86
A/H1N1/Texas/36/1991	TX/91
A/H1N1/Beijing/262/1995	Bei/95
A/H1N1/New Caledonia/20/1999	NC/99
A/H1N1/Solomon Islands/3/2006	SI/06
A/H1N1/Brisbane/59/2007	Bris/07
A/H1N1/California/07/2009	CA/09
A/H1N1/Michigan 45/2015	MI/15
A/H1N1/Brisbane/02/2018	Bris/18

Strain name	Short name
A/H1N1/Guangdong-Maonan/SWL1536/201	GD/19
A/H1N1/Victoria/2570/2019	Vic/19

Table 4: Abbreviated strain names used in figures and tables, along with complete strain names. This table shows all H3N2 strains in our study.

Strain name	Short name
A/H3N2/Hong Kong/8/1968	HK/68
A/H3N2/Port Chalmers/1/1973	PC/73
A/H3N2/Texas/1/1977	TX/77
A/H3N2/Mississippi/1/1985	MI/85
A/H3N2/Sichuan/2/1987	Sich/87
A/H3N2/Shangdong/9/1993	Shan/93
A/H3N2/Nanchang/933/1995	Nan/95
A/H3N2/Sydney/5/1997	Syd/97
A/H3N2/Panama/2007/1999	Pan/99
A/H3N2/Fujian/411/2002	Fuj/02
A/H3N2/New York/55/2004	NY/04
A/H3N2/Brisbane/10/2007	Br/07
A/H3N2/Wisconsin/67/2005	WI/05
A/H3N2/Uruguay/716/2007	Uru/07
A/H3N2/Perth/16/2009	Per/09
A/H3N2/Victoria/361/2011	Vic/11
A/H3N2/Texas/50/2012	TX/12
A/H3N2/Switzerland/9715293/2013	Switz/13
A/H3N2/Hong Kong/4801/2014	HK/14
A/H3N2/Singapore/inflimh-16-0019/2016	Sing/16
A/H3N2/Kansas/14/2017	KS/17

Strain name	Short name
A/H3N2/Hong Kong/2671/2019	HK/19
A/H3N2/South Australia/34/2019	SA/19
A/H3N2/Tasmania/503/2020	Tas/20
A/H3N2/Darwin/9/2021	Dar/21

The strains included in influenza vaccines are reviewed annually based on estimates of the ability of a lab strain to elicit an immune response and antigenic similarity to strains which are predicted to circulate. If major changes in circulating strains are expected, the vaccine composition is updated to hopefully induce better immunity to the expected strains. The vaccine composition for each year is shown in Table 5.

Table 5: Composition of the Fluzone vaccine during each influenza season. The strains used were matched to ACIP/CDC recommendations, and were the same for both the SD and HD vaccine formulations.

season	H1N1	H3N2
2013 - 2014	CA/09	TX/12
2014 - 2015	CA/09	TX/12
2015 - 2016	CA/09	Switz/13
2016 - 2017	CA/09	HK/14
2017 - 2018	MI/15	HK/14
2018 - 2019	MI/15	Sing/16
2019 - 2020	Bris/18	KS/17
2020 - 2021	GD/19	HK/19
2021 - 2022	Vic/19	Tas/20

The panel of historical assays used in each year is shown in Table 6 for the H1N1 subtype strains, and in Table 7 for the H3N2 subtype strains. **Note that the strains for the historical panel are chosen by our clinical research collaborators. We did not control which strains were used in each year of the study, and we used all strains available to us for analysis without omitting any. For the historical panels, strains were chosen to represent a broad spectrum of historical clades, along with representing all contemporary lineages used for vaccine development. For example, H1N1 strains cover the 1918-like clade, the 1976 Fort Dix-like strain, the pre-2009**

lineage, and the 2009 pandemic-like viruses. H3N2 strains were chosen roughly as new clades emerged through time.

Additionally, the influenza viruses used for HAI assays were propagated in eggs, and may have egg-derived mutations. Some H3N2 strains perform poorly [46,47] in HAI essays due to these mutations, but we used all of the heterologous assay available.

Table 6: Number of assays performed using each component of the historical panel for a given season. Over the different seasons, strains were added and removed from the historical panel, indicated by the zeros in the table. The H1N1 strains are shown in this table.

Strain	13/14	14/15	15/16	16/17	17/18	18/19	19/20	20/21	21/22	Total
SC/18	42	92	98	111	38	0	0	0	0	381
PR/34	42	0	0	0	0	0	0	0	0	42
Wei/43	42	92	98	111	38	0	0	0	0	381
FM/47	42	92	98	111	38	0	0	0	0	381
Den/57	42	92	98	111	38	0	0	0	0	381
NJ/76	42	92	98	111	38	0	0	0	0	381
USSR/77	42	92	98	111	38	0	0	0	0	381
Bra/78	42	0	0	111	38	0	0	0	0	191
Chi/83	42	92	98	111	38	19	90	0	0	490
Sing/86	56	92	98	111	38	19	0	0	0	414
TX/91	56	92	98	111	38	19	0	0	0	414
Bei/95	56	92	98	111	38	19	0	0	0	414
NC/99	55	92	98	111	38	19	0	0	0	413
SI/06	56	92	98	111	38	19	0	0	0	414
Bris/07	56	92	98	111	38	19	90	0	0	504
CA/09	56	92	98	111	38	19	90	83	81	668
CA/78	0	92	98	0	0	0	0	0	0	190
MI/15	0	0	0	111	38	19	90	83	0	341
Bris/18	0	0	0	0	0	0	90	83	81	254
GD/19	0	0	0	0	0	0	90	83	81	254

Strain	13/14	14/15	15/16	16/17	17/18	18/19	19/20	20/21	21/22	Total
Vic/19	0	0	0	0	0	0	0	0	81	81

Table 7: Number of assays performed using each component of the historical panel for a given season. The H3N2 strains are shown in this table.

Strain	13/14	14/15	15/16	16/17	17/18	18/19	19/20	20/21	21/22	Total
HK/68	56	92	98	111	38	0	0	0	0	395
PC/73	56	92	98	111	38	0	0	0	0	395
TX/77	56	92	98	111	38	0	0	0	0	395
MI/85	56	92	97	111	38	0	0	0	0	394
Sich/87	42	92	97	111	38	0	0	0	0	380
Shan/93	42	92	98	111	38	0	0	0	0	381
Nan/95	42	92	98	111	38	0	0	0	0	381
Syd/97	56	92	98	111	38	0	0	0	0	395
Pan/99	56	92	98	111	38	19	90	0	0	504
Fuj/02	42	92	98	0	0	0	0	0	0	232
NY/04	56	92	98	111	38	19	0	0	0	414
Br/07	42	0	0	0	0	0	0	0	0	42
WI/05	56	92	98	111	38	19	0	0	0	414
Per/09	56	92	98	111	38	19	0	0	0	414
Vic/11	56	92	98	111	38	19	0	0	0	414
TX/12	56	92	98	111	38	19	90	0	0	504
Switz/13	36	91	98	111	38	19	90	0	0	483
Uru/07	0	92	98	111	38	19	0	0	0	358
HK/14	0	91	98	111	38	19	90	83	81	611
Sing/16	0	0	0	0	38	19	90	83	81	311
KS/17	0	0	0	0	0	0	90	83	81	254
HK/19	0	0	0	0	0	0	90	83	81	254

Strain	13/14	14/15	15/16	16/17	17/18	18/19	19/20	20/21	21/22	Total
SA/19	0	0	0	0	0	0	90	0	81	171
Tas/20	0	0	0	0	0	0	0	0	81	81
Dar/21	0	0	0	0	0	0	0	0	81	81

Descriptive analysis

First, we conducted a descriptive analysis of the outcomes, stratified by vaccine dose. In order to determine how different the effect of dose was across the different vaccines and assay strains, we further conducted stratified analyses.

Birth year and age summary statistics

Table 8 shows the number of unique individuals who were recruited at each study site, along with summaries of their age at first enrollment in the study and birth year. The ages at enrollment and birth years were very similar across the three study sites.

Table 8: Number of unique individuals who were recruited at each study site, along with summaries of the age at first enrollment and birth year of participants at each study site and overall.

Characteristic	FL, N = 52	PA, N = 83	UGA, N = 119	Overall, N = 254
Age at first enrollment, Median (Range)	68 (65 - 80)	68 (65 - 82)	68 (65 - 85)	68 (65 - 85)
Birth year, Median (Range)	1946 (1933 - 1951)	1945 (1932 - 1951)	1950 (1934 - 1956)	1948 (1932 - 1956)

Cohort demographics and assays by year

The study was collected at two different sites (PA and FL) from 2013/14 through 2016/17, but moved to the UGA site in January 2017. The demographic information stratified by study site is shown in Table 9. The FL study site gave fewer HD vaccinations, but there were no noticeable differences in the age or birth cohort of individuals from the three study sites.

Table 9: Demographics of the study sample stratified by the three study sites. The only season when all three study sites recruited individuals was 2016/17.

Characteristic	FL, N = 123	PA, N = 219	UGA, N = 326	Overall, N = 668
Season, n (%)				
2013 - 2014	20 (16)	36 (16)	0 (0)	56 (8)
2014 - 2015	35 (28)	57 (26)	0 (0)	92 (14)
2015 - 2016	35 (28)	63 (29)	0 (0)	98 (15)
2016 - 2017	33 (27)	63 (29)	15 (5)	111 (17)
2017 - 2018	0 (0)	0 (0)	38 (12)	38 (6)
2018 - 2019	0 (0)	0 (0)	19 (6)	19 (3)
2019 - 2020	0 (0)	0 (0)	90 (28)	90 (13)
2020 - 2021	0 (0)	0 (0)	83 (25)	83 (12)
2021 - 2022	0 (0)	0 (0)	81 (25)	81 (12)
Dose, n (%)				
SD	82 (67)	73 (33)	79 (24)	234 (35)
HD	41 (33)	146 (67)	247 (76)	434 (65)

In addition, several individuals returned to the study site in multiple years. Table 10 shows the number of recurring individuals at each study site, with how many times a participant returned to the study. The PA and FL study sites ran for four years (2013/14 influenza season through 2016/17 influenza season) while the UGA study site had six years of data we could use for our secondary analysis (2016/17 influenza season through 2021/22 influenza season) and is ongoing.

Since individuals were not required to choose the same vaccine (SD or HD) they received at their previous visit, some individuals received different doses at subsequent visits, which is accounted for in our statistical analyses. From Table 10, we can see that the majority of individuals did not switch vaccine doses at subsequent visits, and out of all of the times an individual switched vaccine doses, almost all of them were switching from HD to SD vaccines. While a history of adverse events or side effects could account for switching from HD to SD vaccines, the likely explanation is the availability of HD vaccination at the study site.

While we do not have access to detailed shipping and receiving logs along with individual dates of vaccination to confirm this, the study site ordered fewer HD vaccines than SD vaccines and it is likely that some individuals who would have preferred an HD vaccine received an SD

vaccine since no HD vaccines were available. Most individuals are likely to prefer receiving an SD vaccine while at the study site rather than returning to receive an HD vaccine at a later date. To our knowledge, there are no studies, either empirical or computational, showing whether receiving an SD vaccination instead of HD vaccination is preferable (in terms of intraseason waning immunity and overall protection from influenza disease) to waiting to receive an HD vaccine.

Table 10: Summary statistics of how many individuals participated in the study in multiple years at each study site. Individuals were not required to choose the same vaccine (SD or HD) at subsequent visits, so we also show summary statistics for the number of times individuals switched which vaccine they received at subsequent visits.

Characteristic	UGA, N = 119	FL, N = 52	PA, N = 83	Overall, N = 254
Number of total visits by same individual, n (%)				
1	27 (23)	19 (37)	16 (19)	62 (24)
2	23 (19)	7 (13)	20 (24)	50 (20)
3	46 (39)	14 (27)	25 (30)	85 (33)
4	8 (6.7)	12 (23)	22 (27)	42 (17)
5	7 (5.9)	0 (0)	0 (0)	7 (2.8)
6	8 (6.7)	0 (0)	0 (0)	8 (3.1)
Number of SD vaccinations for same individual, n (%)				
0	74 (62)	1 (1.9)	36 (43)	111 (44)
1	27 (23)	32 (62)	27 (33)	86 (34)
2	9 (7.6)	12 (23)	15 (18)	36 (14)
3	5 (4.2)	2 (3.8)	4 (4.8)	11 (4.3)
4	2 (1.7)	5 (9.6)	1 (1.2)	8 (3.1)
5	1 (0.8)	0 (0)	0 (0)	1 (0.4)
6	1 (0.8)	0 (0)	0 (0)	1 (0.4)
Number of HD vaccinations for same individual, n (%)				
0	19 (16)	30 (58)	11 (13)	60 (24)
1	24 (20)	3 (5.8)	33 (40)	60 (24)
2	23 (19)	19 (37)	13 (16)	55 (22)

Characteristic	UGA, N = 119	FL, N = 52	PA, N = 83	Overall, N = 254
3	42 (35)	0 (0)	17 (20)	59 (23)
4	4 (3.4)	0 (0)	9 (11)	13 (5.1)
5	7 (5.9)	0 (0)	0 (0)	7 (2.8)
Number of times an individual switched from HD to SD, n (%)				
0	93 (78)	31 (60)	49 (59)	173 (68)
1	25 (21)	21 (40)	34 (41)	80 (31)
2	1 (0.8)	0 (0)	0 (0)	1 (0.4)
Number of times an individual switched from SD to HD, n (%)				
0	116 (97)	52 (100)	79 (95)	247 (97)
1	3 (2.5)	0 (0)	4 (4.8)	7 (2.8)

Pre and post-vaccination titer figures

In order to better conceptualize the data we use for our models, we have included plots of the pre and post-vaccination titers. Due to technical limitations with how LaTeX processes the layout for large images, the raw data for each vaccine strain is included in a separate figure.

In each of the following figures, every person-year of data is represented as a line segment and a pair of points, one for the recorded pre-vaccination titer and one for the recorded post-vaccination titer. The line is a visual aid to help gauge the relative titer increase for that person-year, and to more easily understand for which strains the relevant vaccine candidate induced an immunogenic response at the cohort level. Each subplot in each figure corresponds to one assay strain, showing all person-years of data where the noted vaccine was administered and a response was measured to the noted assay strain.

The following figure numbers correspond to the listed vaccine strains. Please reference Table 3 and Table 4 for the complete strain names.

- Figure 2: Ca/09 (H1N1) vaccine strain;
- Figure 3: MI/15 (H1N1) vaccine strain;
- Figure 4: Bris/18 (H1N1) vaccine strain;
- Figure 5: GD/19 (H1N1) vaccine strain;
- Figure 6: Vic/19 (H1N1) vaccine strain;
- Figure 7: TX/12 (H3N2) vaccine strain;

- Figure 8: Switz/13 (H3N2) vaccine strain;
- Figure 9: HK/14 (H3N2) vaccine strain;
- Figure 10: Sing/16 (H3N2) vaccine strain;
- Figure 11: KS/17 (H3N2) vaccine strain;
- Figure 12: HK/19 (H3N2) vaccine strain; and
- Figure 13: Tas/20 (H3N2) vaccine strain.

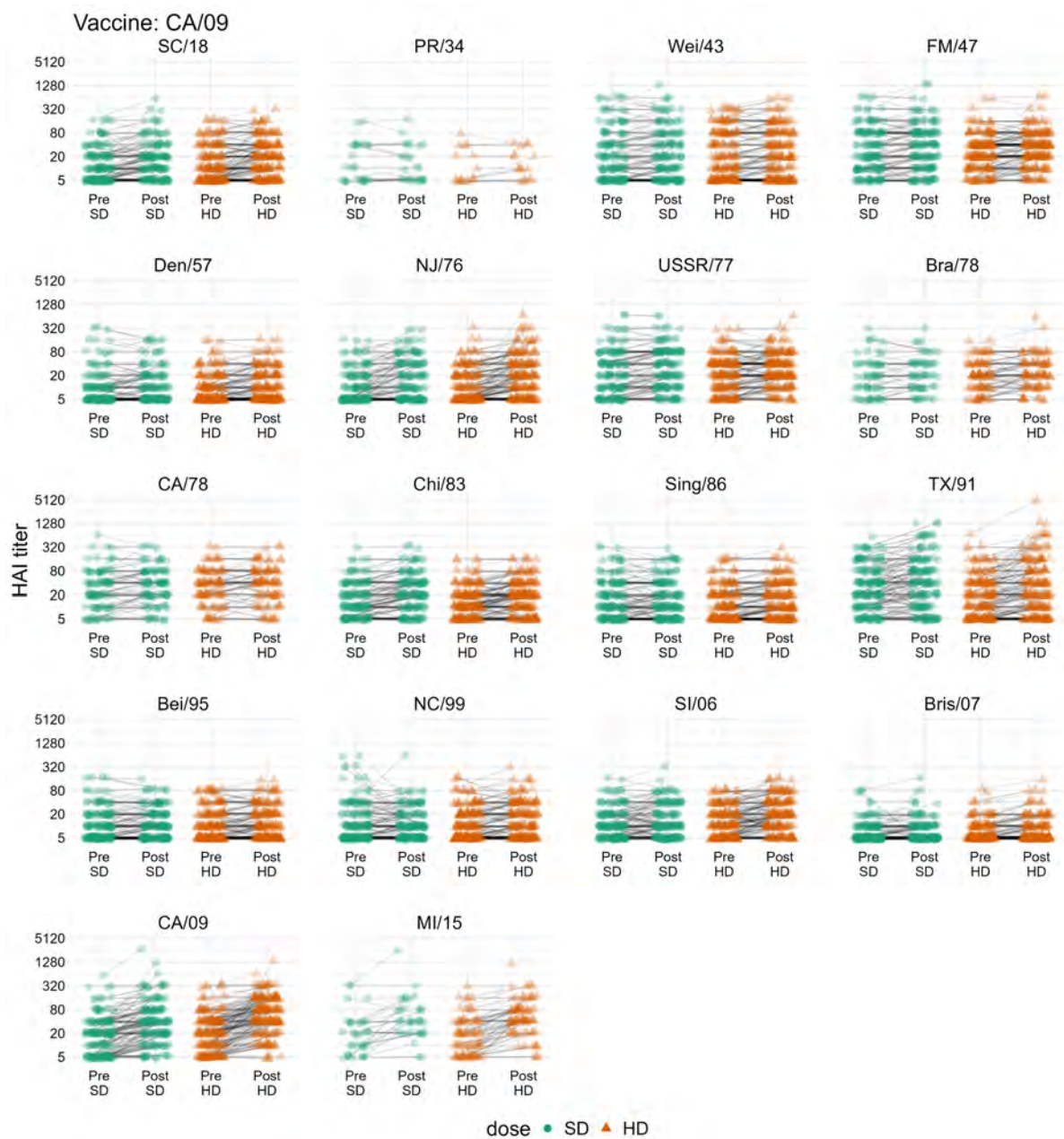


Figure 2: Pre and post vaccination titers for all person-years where a participant was administered a vaccine containing CA/09-like split inactivated virus. Each panel shows a historical strain which was used for HAI assays, and all H1N1 subtype historical strains that were used for running assays against CA/09 vaccinated individual samples are shown.



Figure 3: Pre and post vaccination titers for all person-years where a participant was administered a vaccine containing MI/15-like split inactivated virus. Each panel shows a historical strain which was used for HAI assays, and all H1N1 subtype historical strains that were used for running assays against MI/15 vaccinated individual samples are shown.

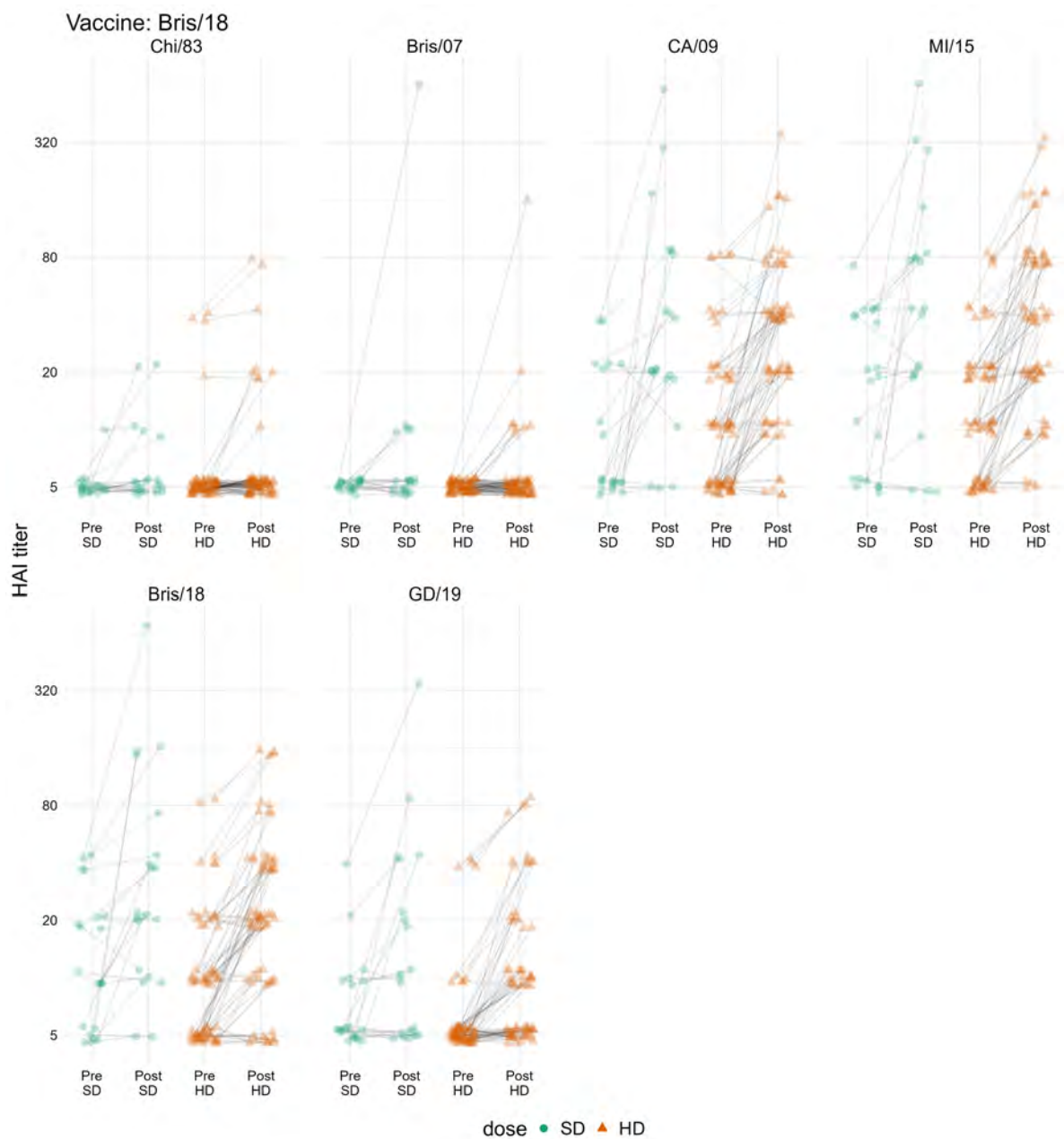


Figure 4: Pre and post vaccination titers for all person-years where a participant was administered a vaccine containing Bris/18-like split inactivated virus. Each panel shows a historical strain which was used for HAI assays, and all H1N1 subtype historical strains that were used for running assays against Bris/18 vaccinated individual samples are shown.

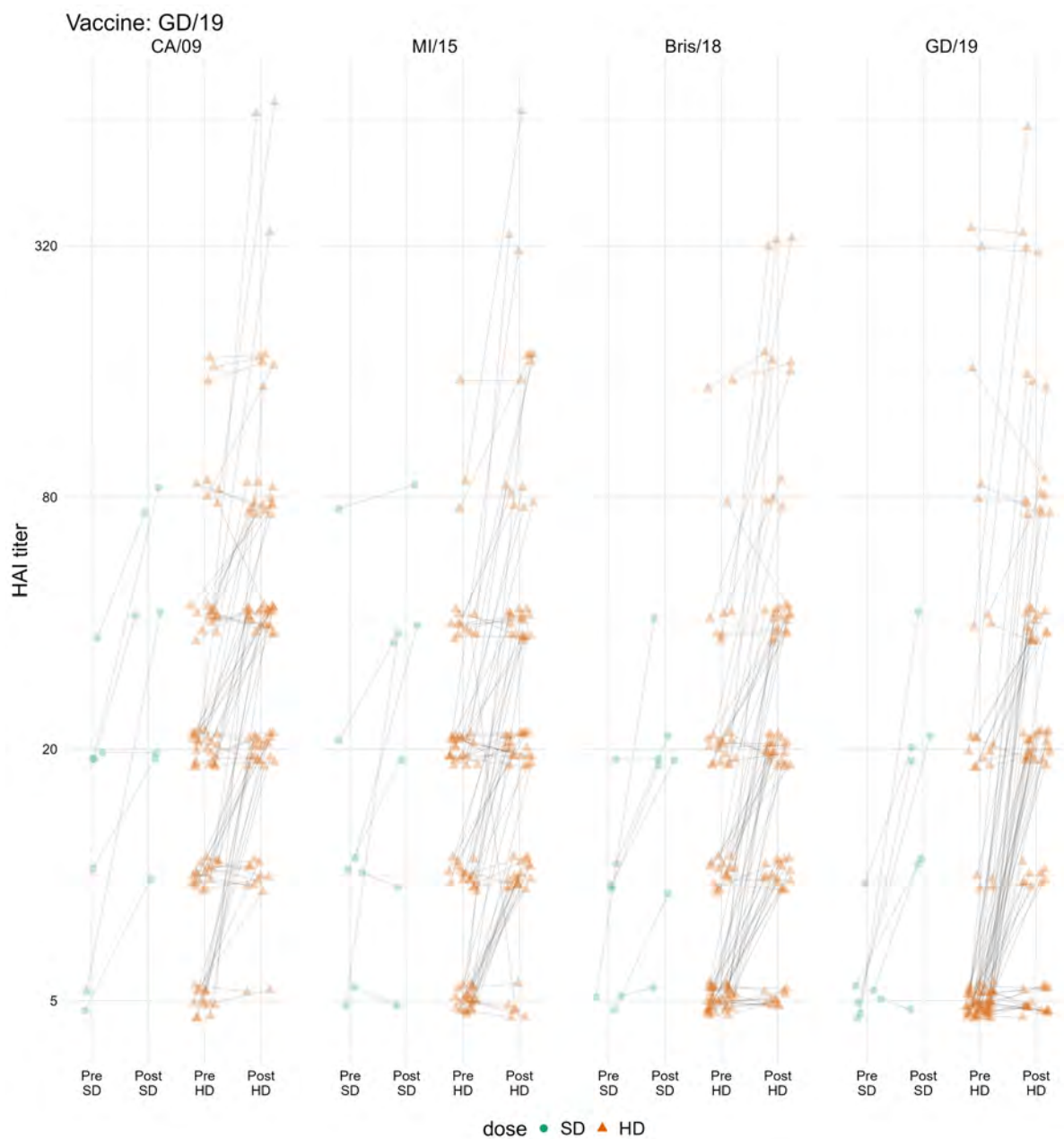


Figure 5: Pre and post vaccination titers for all person-years where a participant was administered a vaccine containing GD/19-like split inactivated virus. Each panel shows a historical strain which was used for HAI assays, and all H1N1 subtype historical strains that were used for running assays against GD/19 vaccinated individual samples are shown.

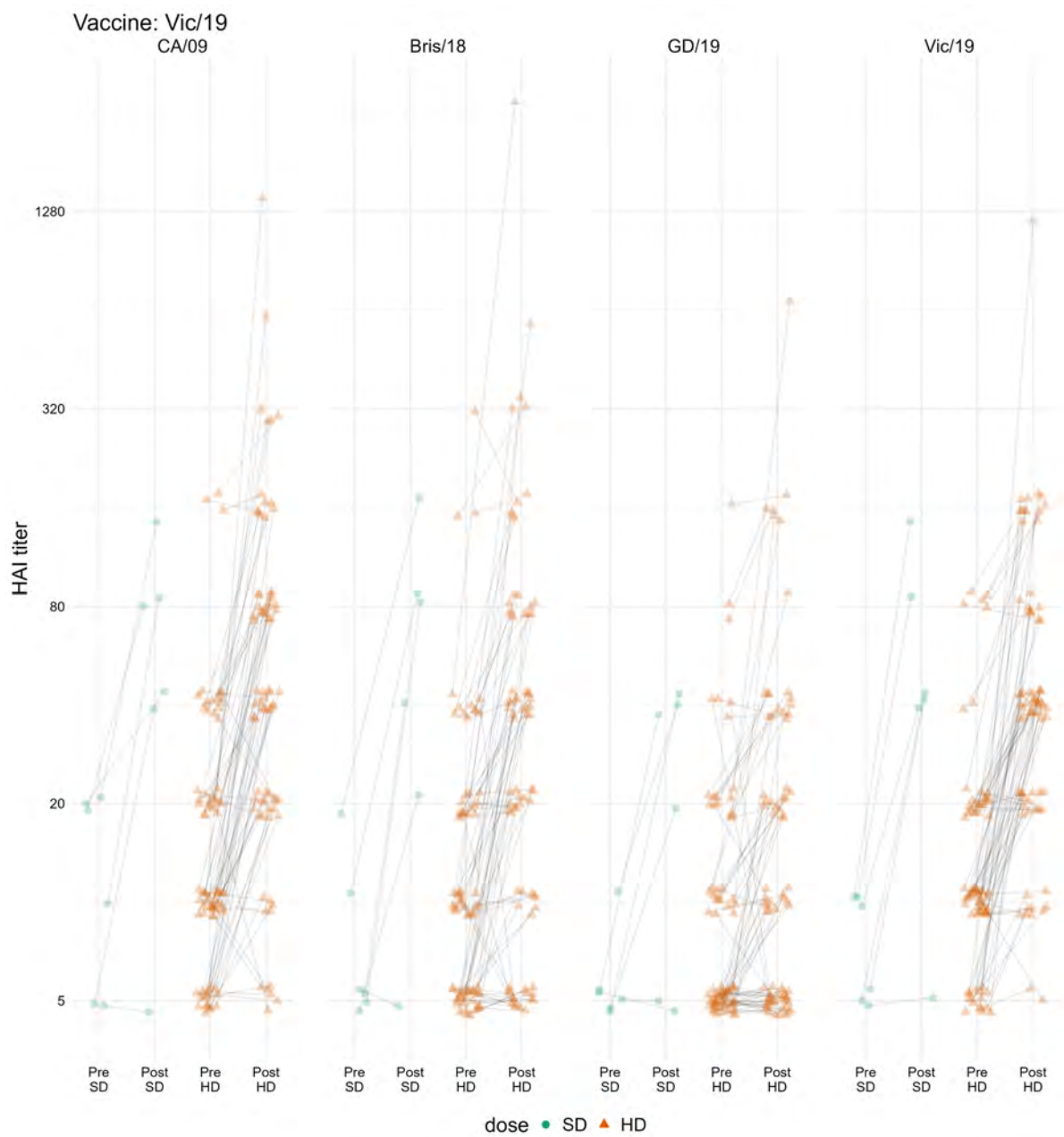


Figure 6: Pre and post vaccination titers for all person-years where a participant was administered a vaccine containing Vic/19-like split inactivated virus. Each panel shows a historical strain which was used for HAI assays, and all H1N1 subtype historical strains that were used for running assays against Vic/19 vaccinated individual samples are shown.



Figure 7: Pre and post vaccination titers for all person-years where a participant was administered a vaccine containing Tx/12-like split inactivated virus. Each panel shows a historical strain which was used for HAI assays, and all H3N2 subtype historical strains that were used for running assays against TX/12 vaccinated individual samples are shown.



Figure 8: Pre and post vaccination titers for all person-years where a participant was administered a vaccine containing Switz/13-like split inactivated virus. Each panel shows a historical strain which was used for HAI assays, and all H3N2 subtype historical strains that were used for running assays against Switz/13 vaccinated individual samples are shown.



Figure 9: Pre and post vaccination titers for all person-years where a participant was administered a vaccine containing HK/14-like split inactivated virus. Each panel shows a historical strain which was used for HAI assays, and all H3N2 subtype historical strains that were used for running assays against HK/14 vaccinated individual samples are shown.

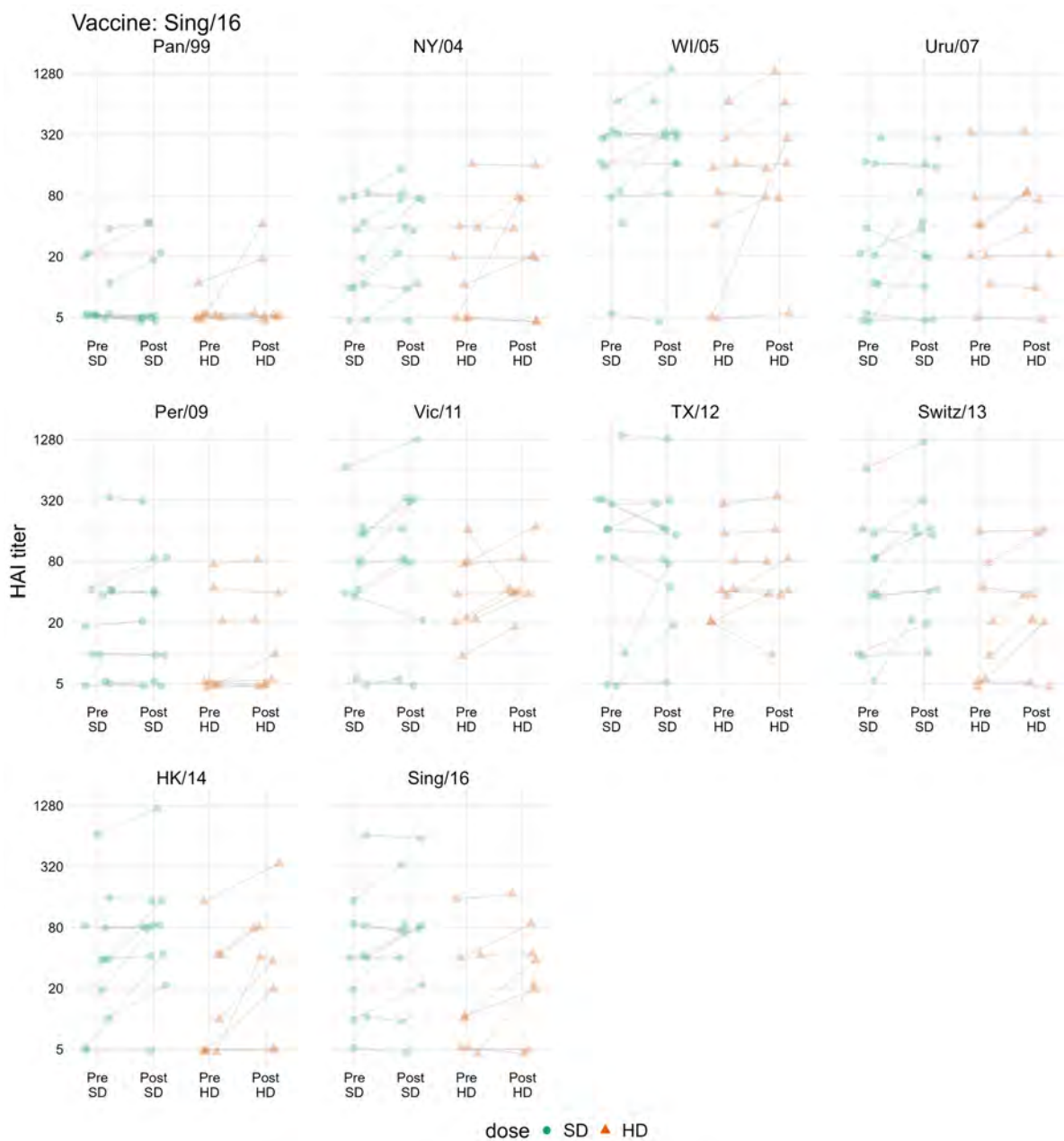


Figure 10: Pre and post vaccination titers for all person-years where a participant was administered a vaccine containing Sing/16-like split inactivated virus. Each panel shows a historical strain which was used for HAI assays, and all H3N2 subtype historical strains that were used for running assays against Sing/16 vaccinated individual samples are shown.

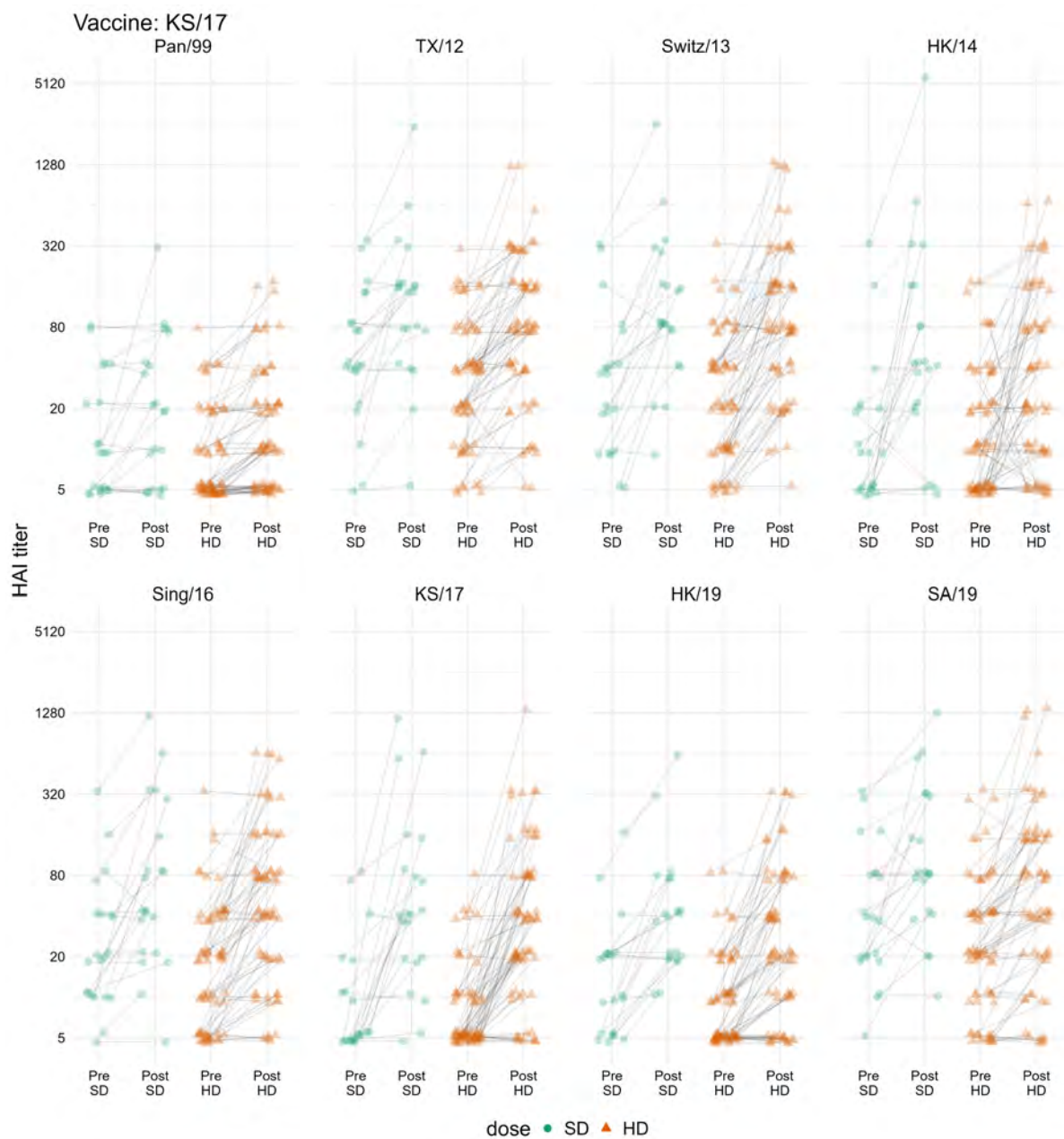


Figure 11: Pre and post vaccination titers for all person-years where a participant was administered a vaccine containing KS/17-like split inactivated virus. Each panel shows a historical strain which was used for HAI assays, and all H3N2 subtype historical strains that were used for running assays against KS/17 vaccinated individual samples are shown.

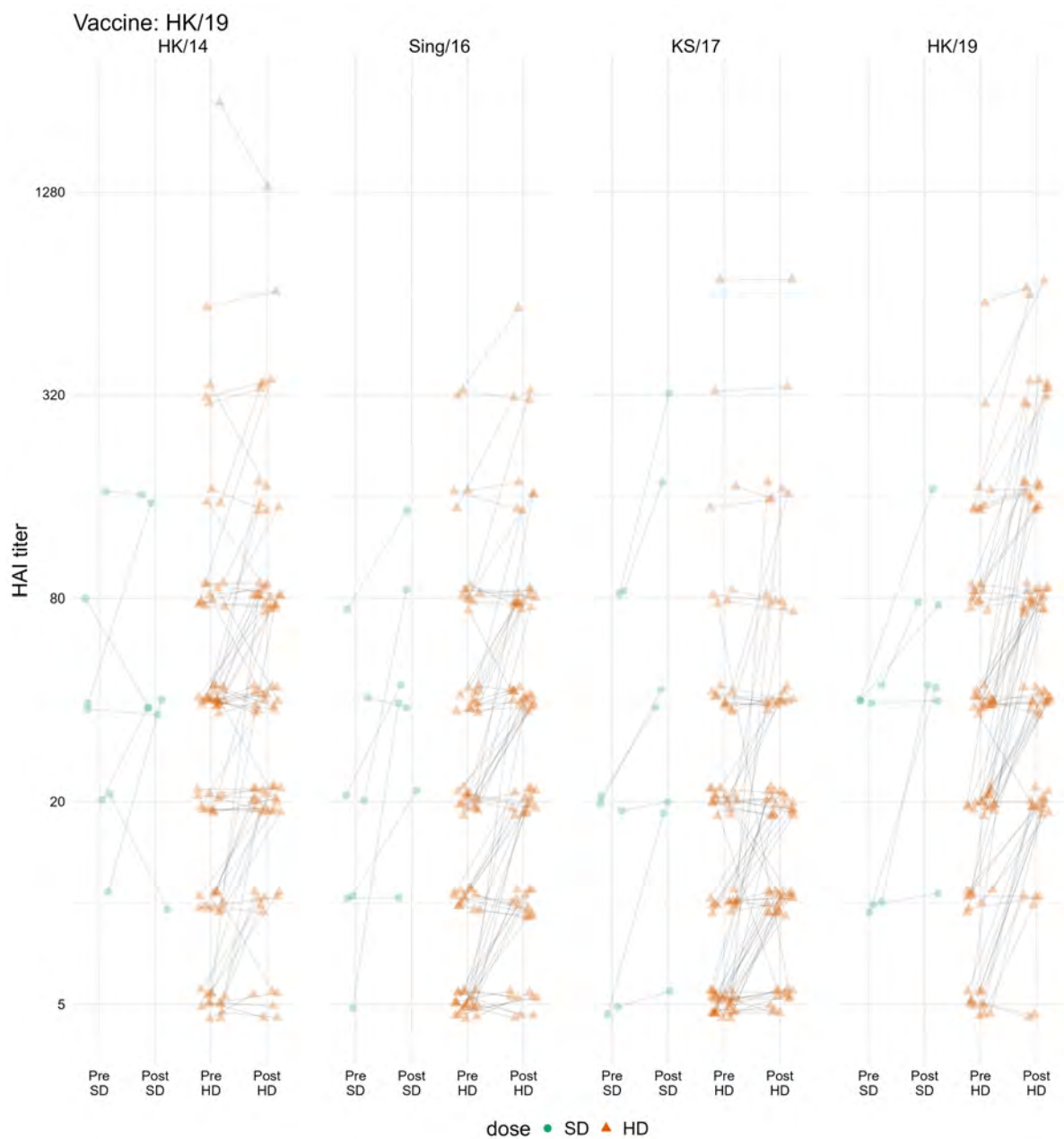


Figure 12: Pre and post vaccination titers for all person-years where a participant was administered a vaccine containing HK/19-like split inactivated virus. Each panel shows a historical strain which was used for HAI assays, and all H3N2 subtype historical strains that were used for running assays against KH/19 vaccinated individual samples are shown.

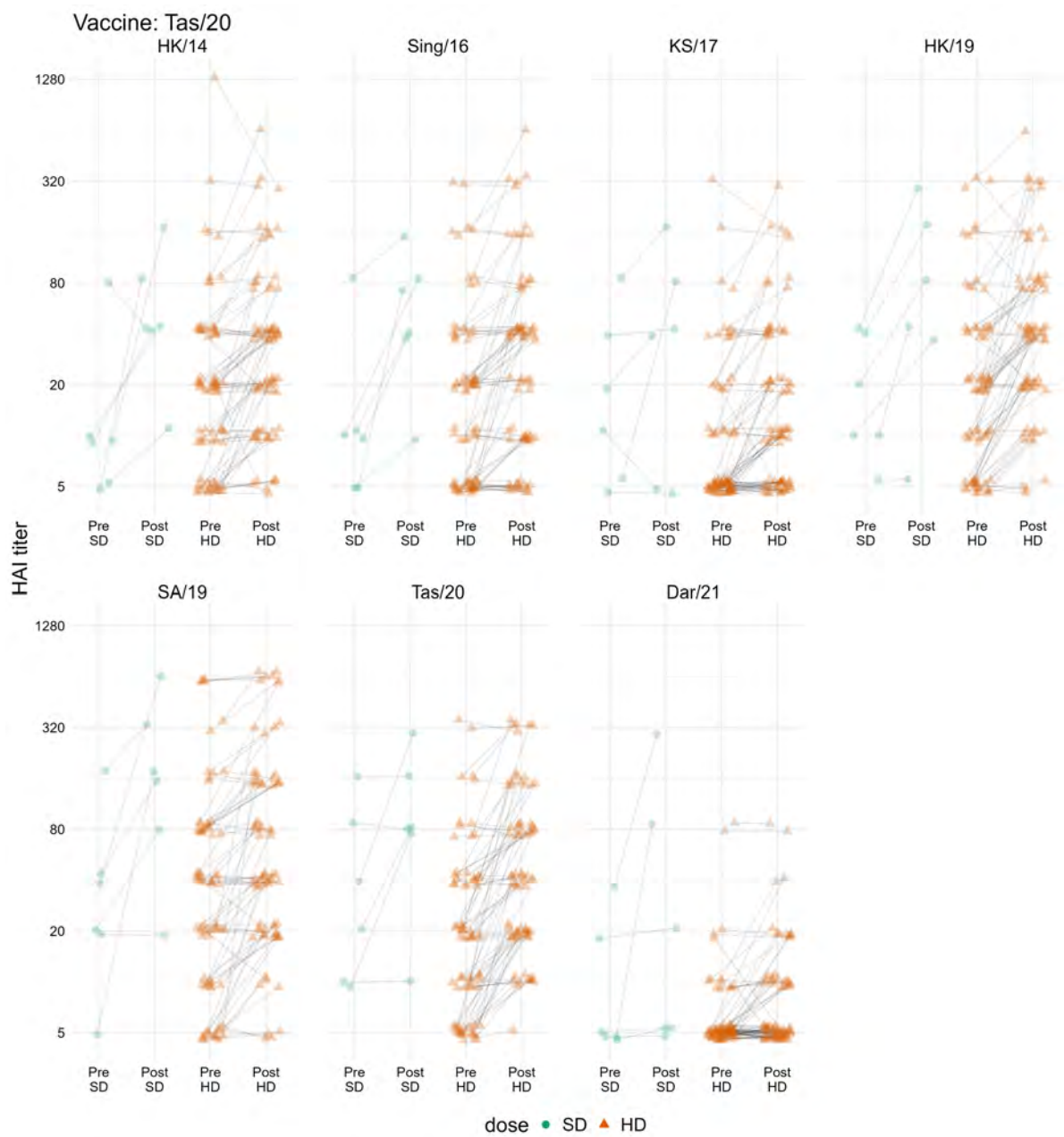


Figure 13: Pre and post vaccination titers for all person-years where a participant was administered a vaccine containing Tas/20-like split inactivated virus. Each panel shows a historical strain which was used for HAI assays, and all H3N2 subtype historical strains that were used for running assays against Tas/20 vaccinated individual samples are shown.

Fold change figures

In addition to the previous figures, we also show the distribution of fold changes to each assay strain that were induced by each vaccine component.

Similar to the previous section, in each of the following figures, every person-year of data is represented as one point, representing the fold change (i.e., post-vaccination titer divided by pre-vaccination titer) for that person in a particular season.

The following figure numbers correspond to the listed vaccine strains. Please reference Table 3 and Table 4 for the complete strain names.

- Figure 14: Ca/09 (H1N1) vaccine strain;
- Figure 15: MI/15 (H1N1) vaccine strain;
- Figure 16: Bris/18 (H1N1) vaccine strain;
- Figure 17: GD/19 (H1N1) vaccine strain;
- Figure 18: Vic/19 (H1N1) vaccine strain;
- Figure 19: TX/12 (H3N2) vaccine strain;
- Figure 20: Switz/13 (H3N2) vaccine strain;
- Figure 21: HK/14 (H3N2) vaccine strain;
- Figure 22: Sing/16 (H3N2) vaccine strain;
- Figure 23: KS/17 (H3N2) vaccine strain;
- Figure 24: HK/19 (H3N2) vaccine strain; and
- Figure 25: Tas/20 (H3N2) vaccine strain.

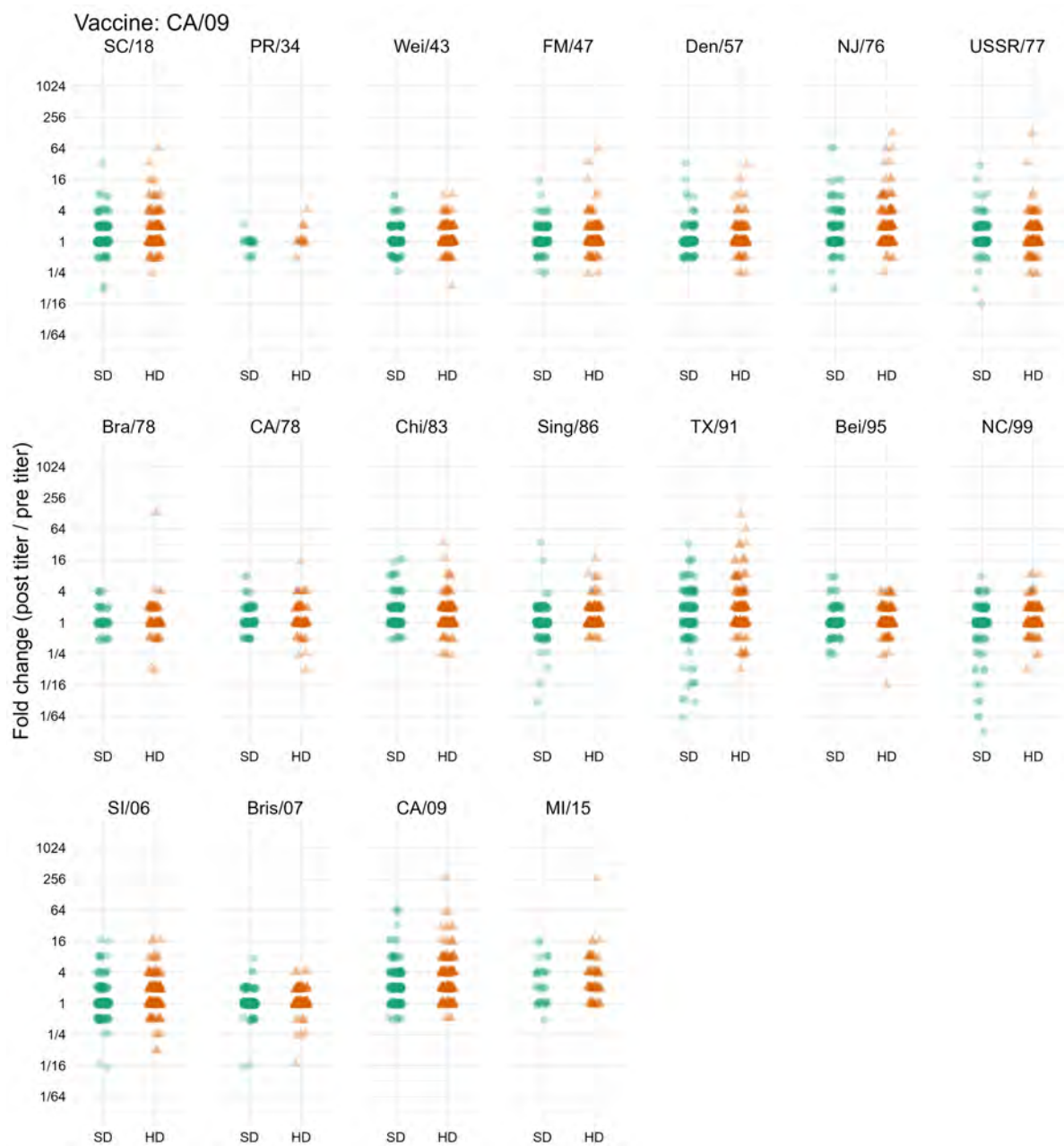


Figure 14: Fold-change (post-vaccination titer / pre-vaccination titer) for all person-years where a participant was administered a vaccine containing CA/09-like split inactivated virus. Each panel shows a historical strain which was used for HAI assays, and all H1N1 subtype historical strains that were used for running assays against CA/09 vaccinated individual samples are shown.

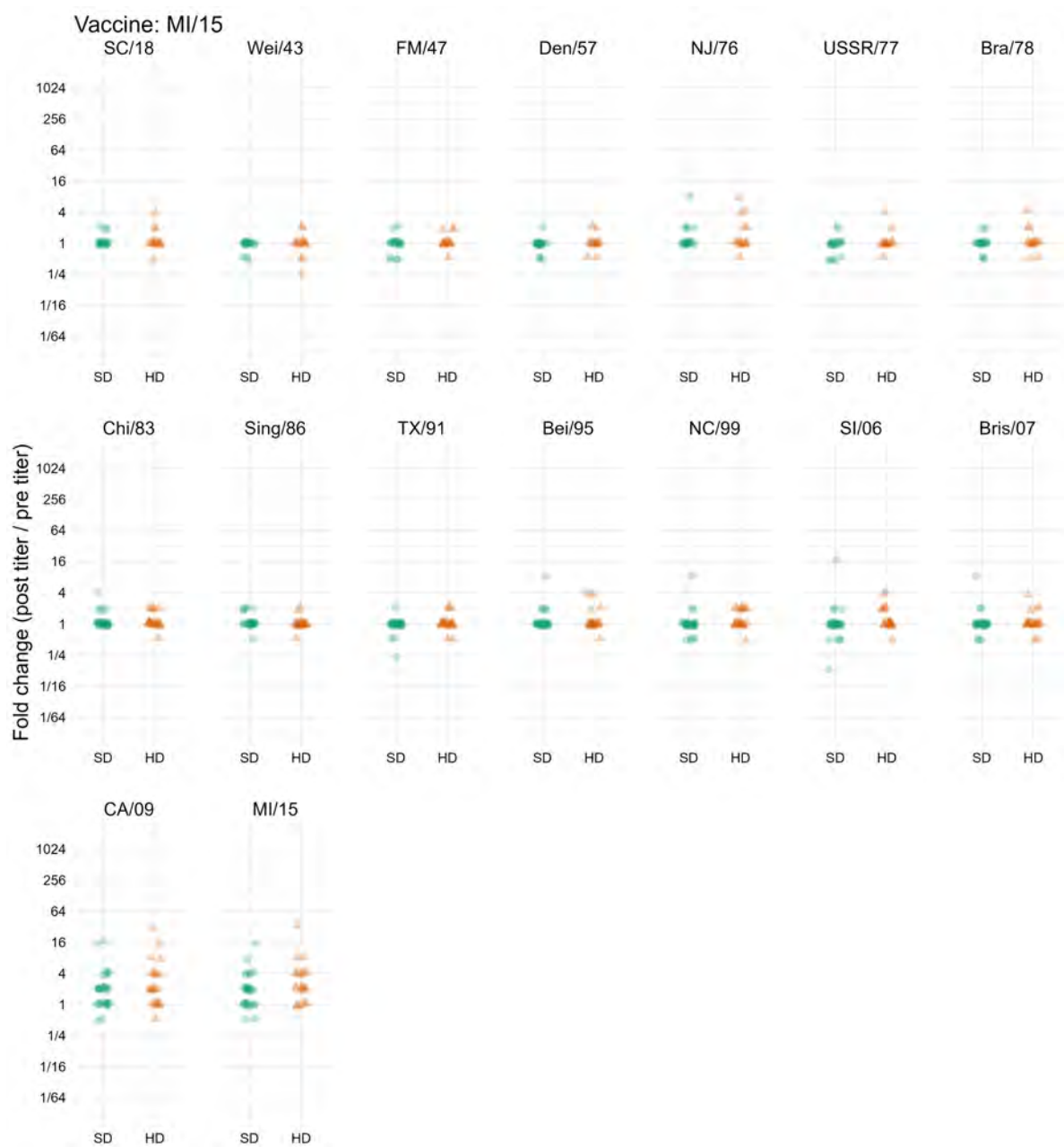


Figure 15: Fold-change (post-vaccination titer / pre-vaccination titer) for all person-years where a participant was administered a vaccine containing MI/15-like split inactivated virus. Each panel shows a historical strain which was used for HAI assays, and all H1N1 subtype historical strains that were used for running assays against MI/15 vaccinated individual samples are shown.

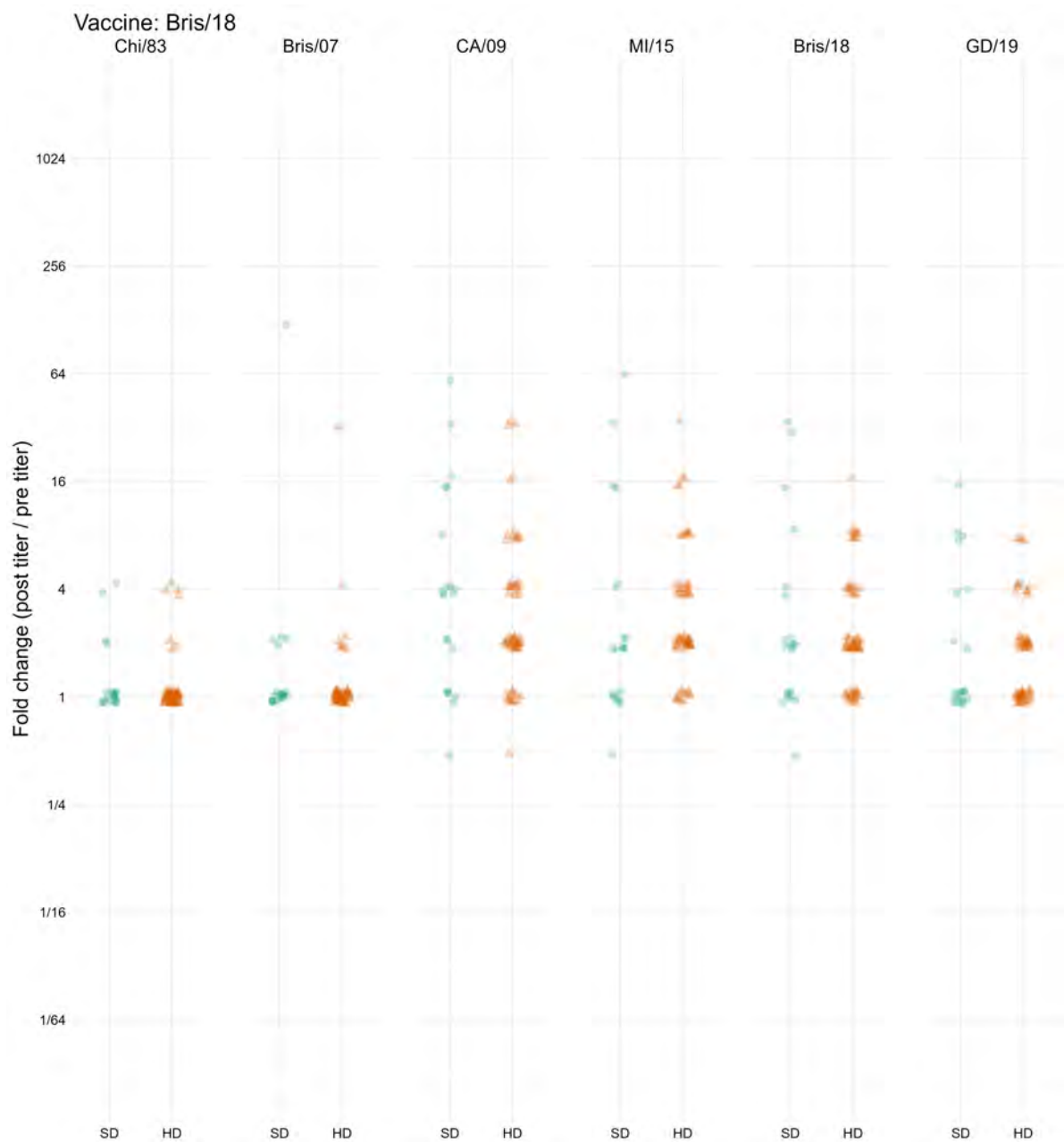


Figure 16: Fold-change (post-vaccination titer / pre-vaccination titer) for all person-years where a participant was administered a vaccine containing Bris/18-like split inactivated virus. Each panel shows a historical strain which was used for HAI assays, and all H1N1 subtype historical strains that were used for running assays against Bris/18 vaccinated individual samples are shown.

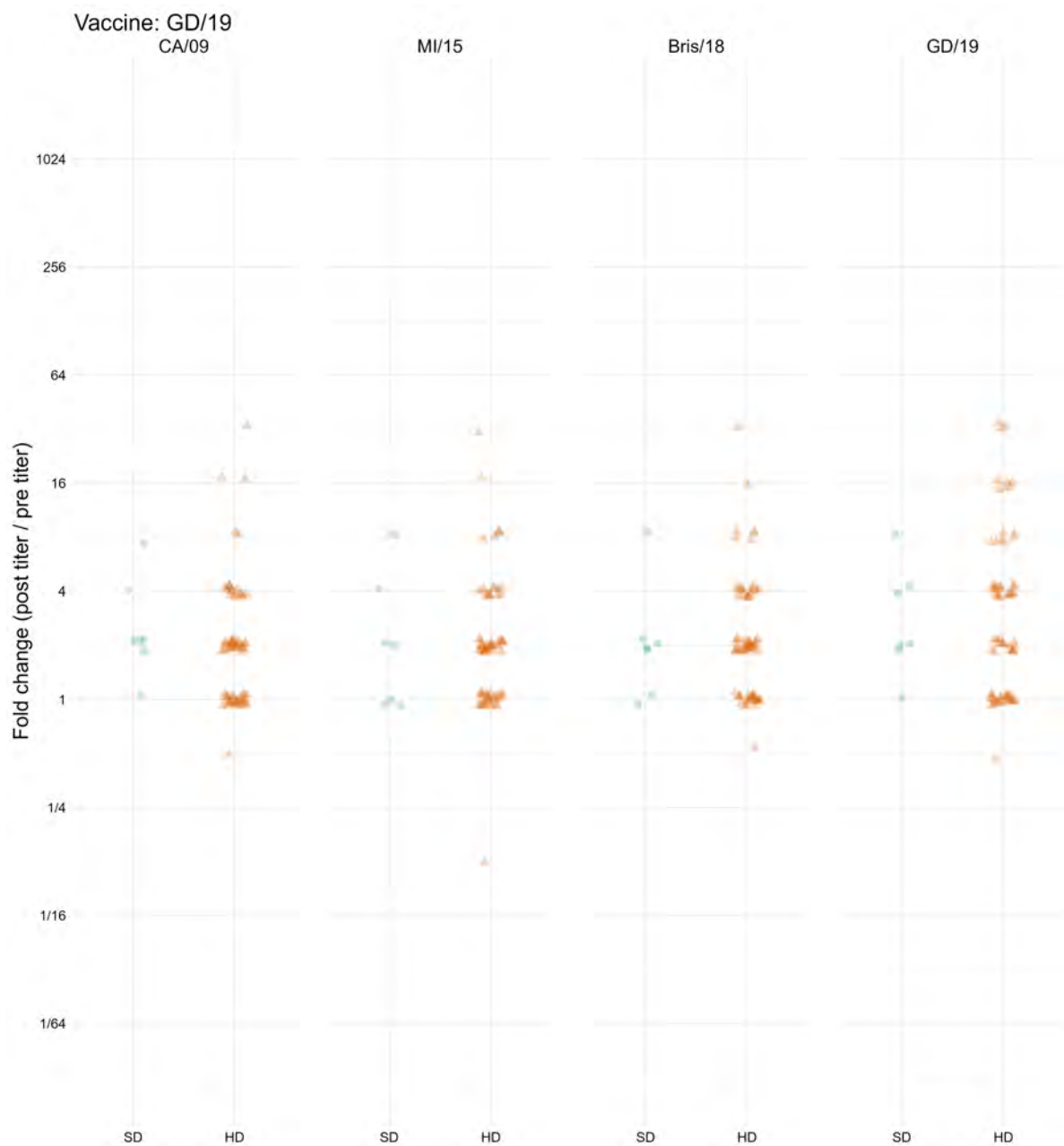


Figure 17: Fold-change (post-vaccination titer / pre-vaccination titer) for all person-years where a participant was administered a vaccine containing GD/19-like split inactivated virus. Each panel shows a historical strain which was used for HAI assays, and all H1N1 subtype historical strains that were used for running assays against GD/19 vaccinated individual samples are shown.

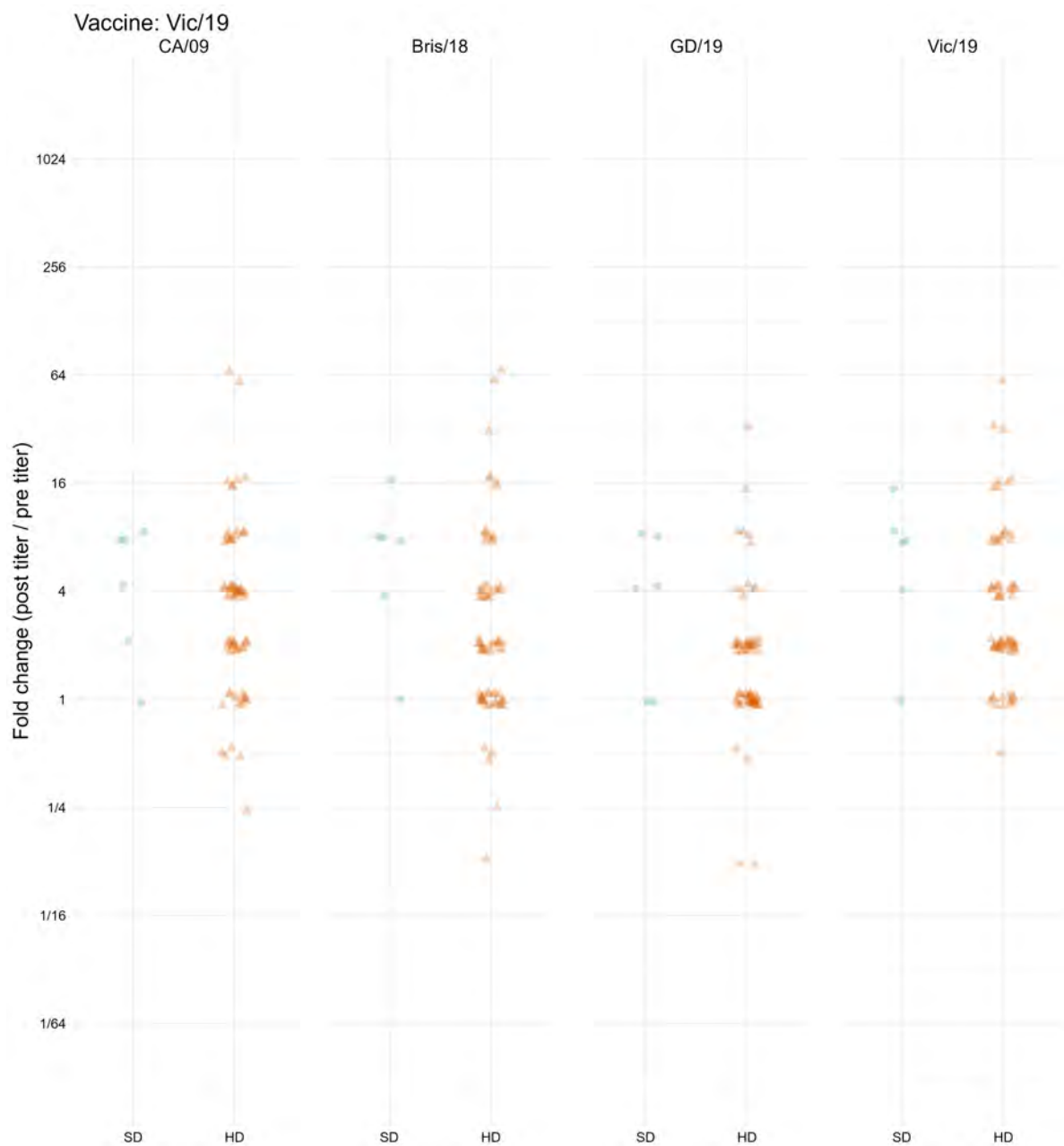


Figure 18: Fold-change (post-vaccination titer / pre-vaccination titer) for all person-years where a participant was administered a vaccine containing Vic/19-like split inactivated virus. Each panel shows a historical strain which was used for HAI assays, and all H1N1 subtype historical strains that were used for running assays against Vic/19 vaccinated individual samples are shown.

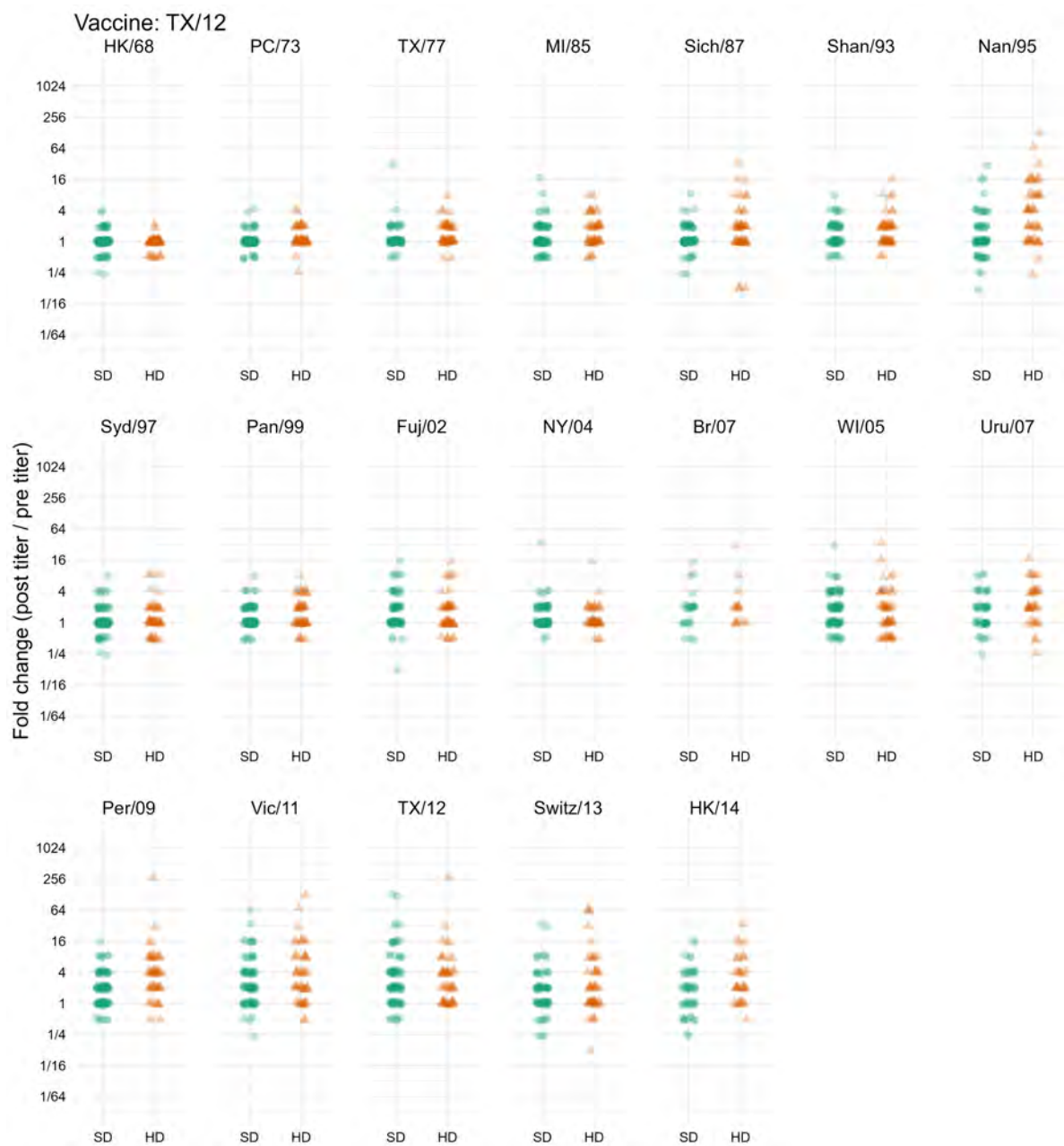


Figure 19: Fold-change (post-vaccination titer / pre-vaccination titer) for all person-years where a participant was administered a vaccine containing Tx/12-like split inactivated virus. Each panel shows a historical strain which was used for HAI assays, and all H3N2 subtype historical strains that were used for running assays against TX/12 vaccinated individual samples are shown.

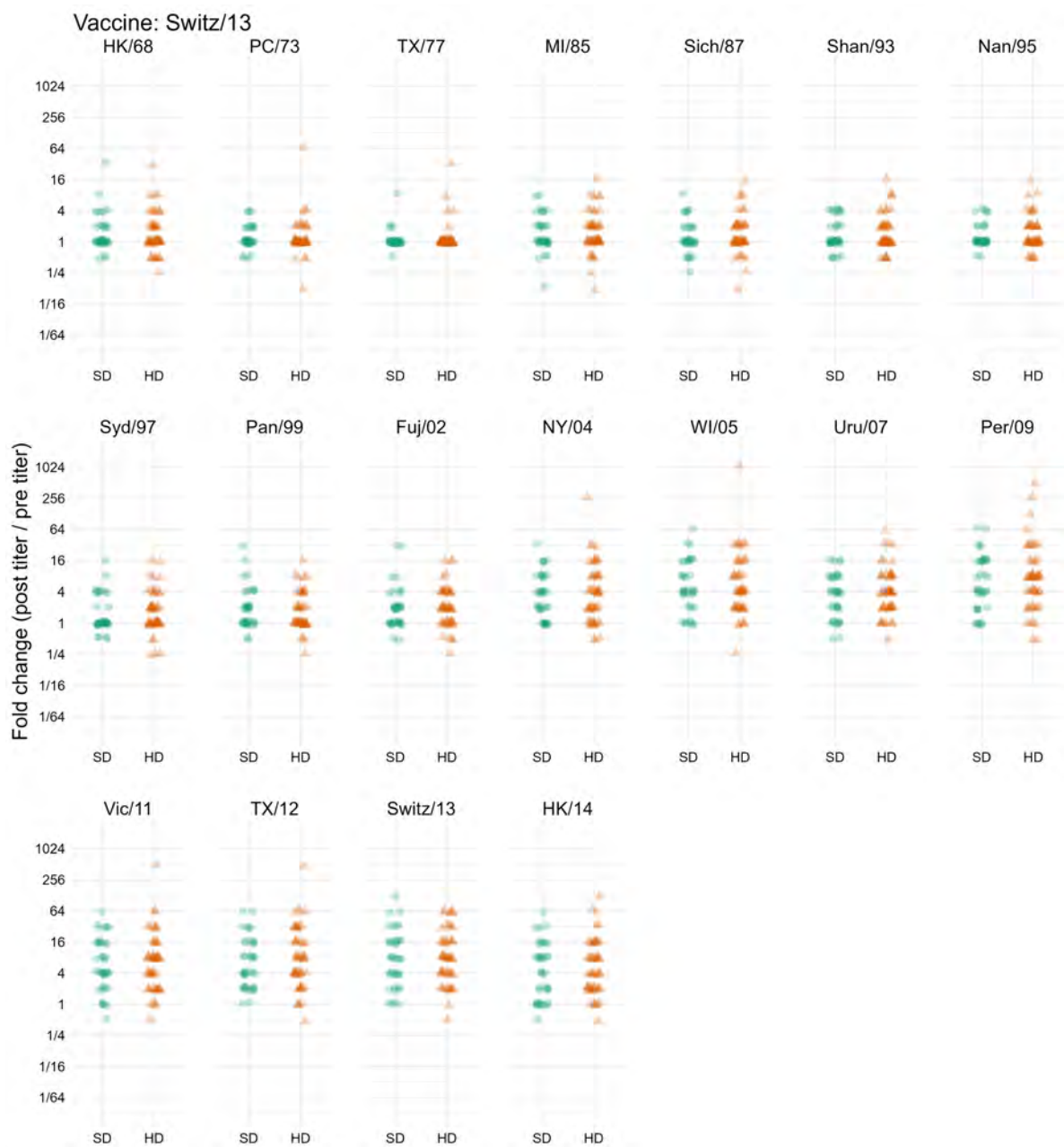


Figure 20: Fold-change (post-vaccination titer / pre-vaccination titer) for all person-years where a participant was administered a vaccine containing Switz/13-like split inactivated virus. Each panel shows a historical strain which was used for HAI assays, and all H3N2 subtype historical strains that were used for running assays against Switz/13 vaccinated individual samples are shown.

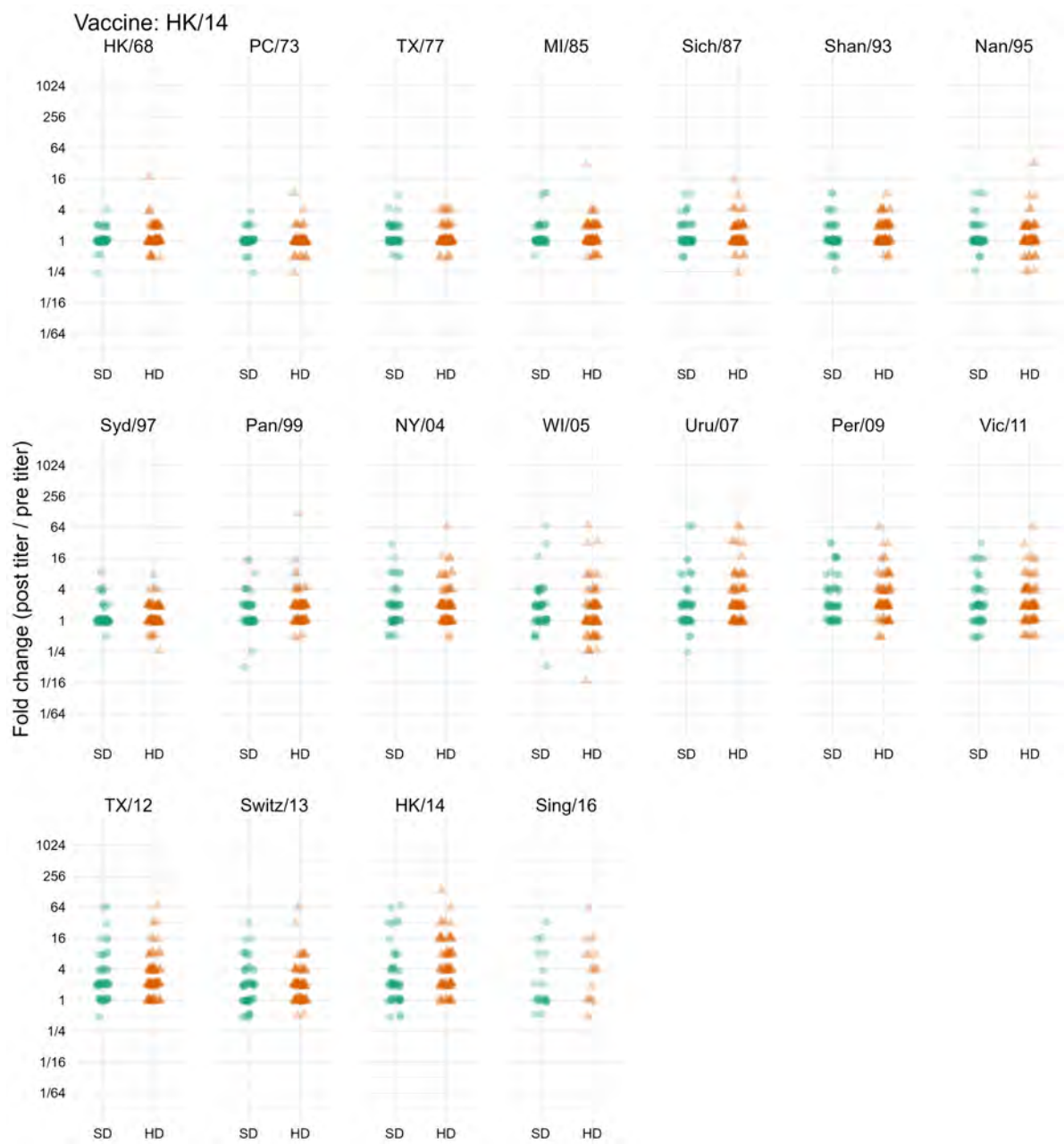


Figure 21: Fold-change (post-vaccination titer / pre-vaccination titer) for all person-years where a participant was administered a vaccine containing HK/14-like split inactivated virus. Each panel shows a historical strain which was used for HAI assays, and all H3N2 subtype historical strains that were used for running assays against HK/14 vaccinated individual samples are shown.

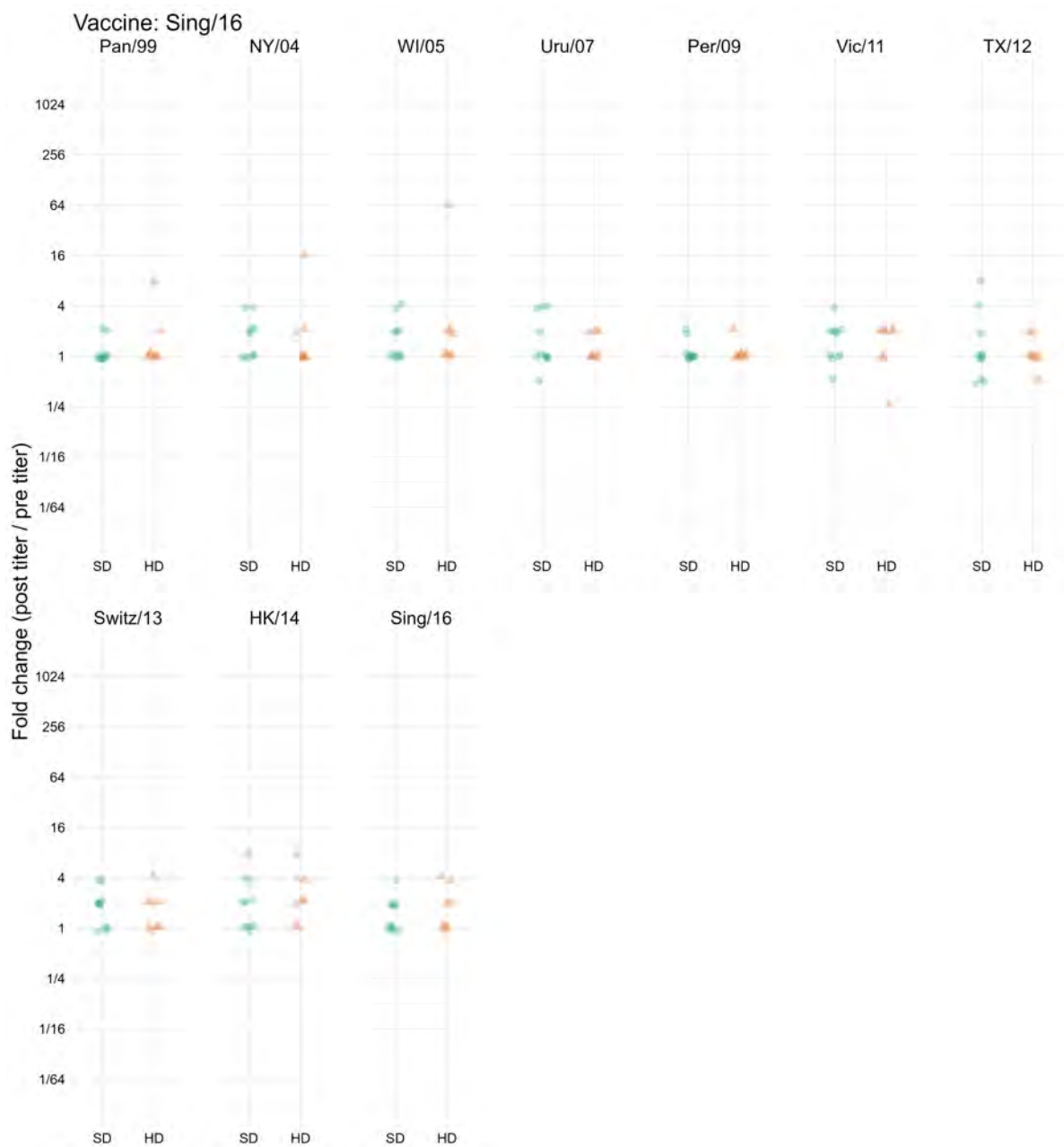


Figure 22: Fold-change (post-vaccination titer / pre-vaccination titer) for all person-years where a participant was administered a vaccine containing Sing/16-like split inactivated virus. Each panel shows a historical strain which was used for HAI assays, and all H3N2 subtype historical strains that were used for running assays against Sing/16 vaccinated individual samples are shown.

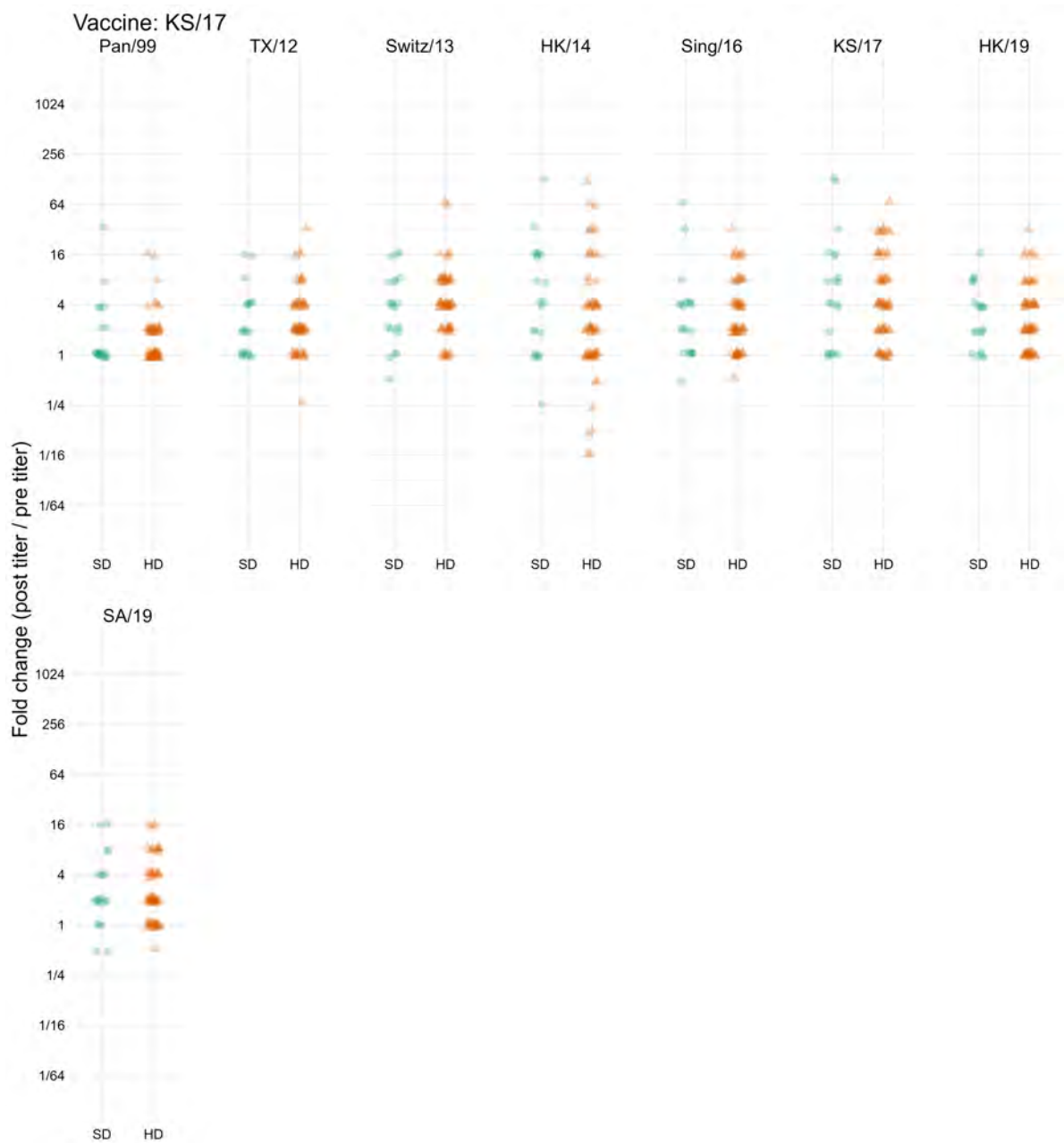


Figure 23: Fold-change (post-vaccination titer / pre-vaccination titer) for all person-years where a participant was administered a vaccine containing KS/17-like split inactivated virus. Each panel shows a historical strain which was used for HAI assays, and all H3N2 subtype historical strains that were used for running assays against KS/17 vaccinated individual samples are shown.

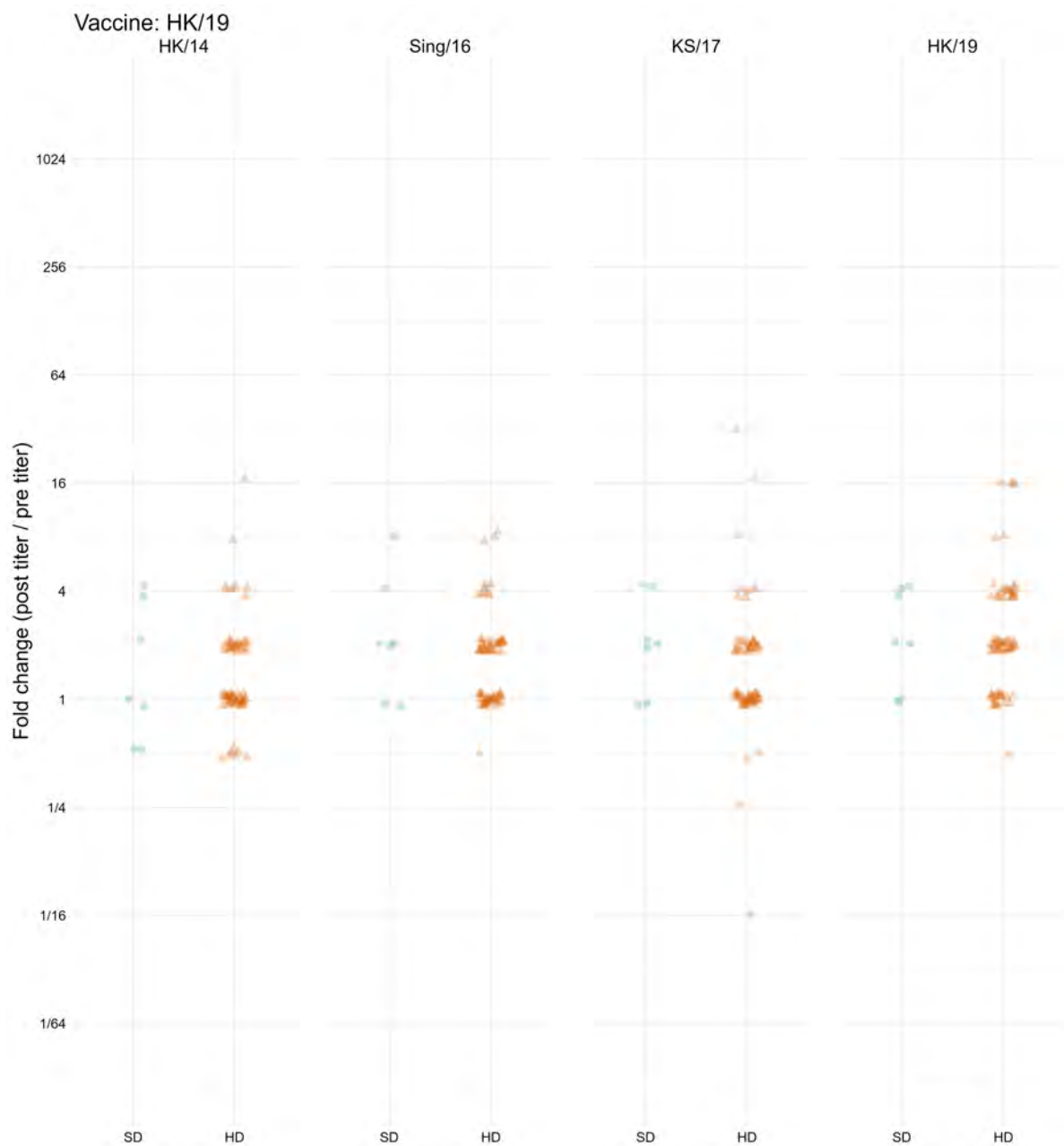


Figure 24: Fold-change (post-vaccination titer / pre-vaccination titer) for all person-years where a participant was administered a vaccine containing HK/19-like split inactivated virus. Each panel shows a historical strain which was used for HAI assays, and all H3N2 subtype historical strains that were used for running assays against KH/19 vaccinated individual samples are shown.

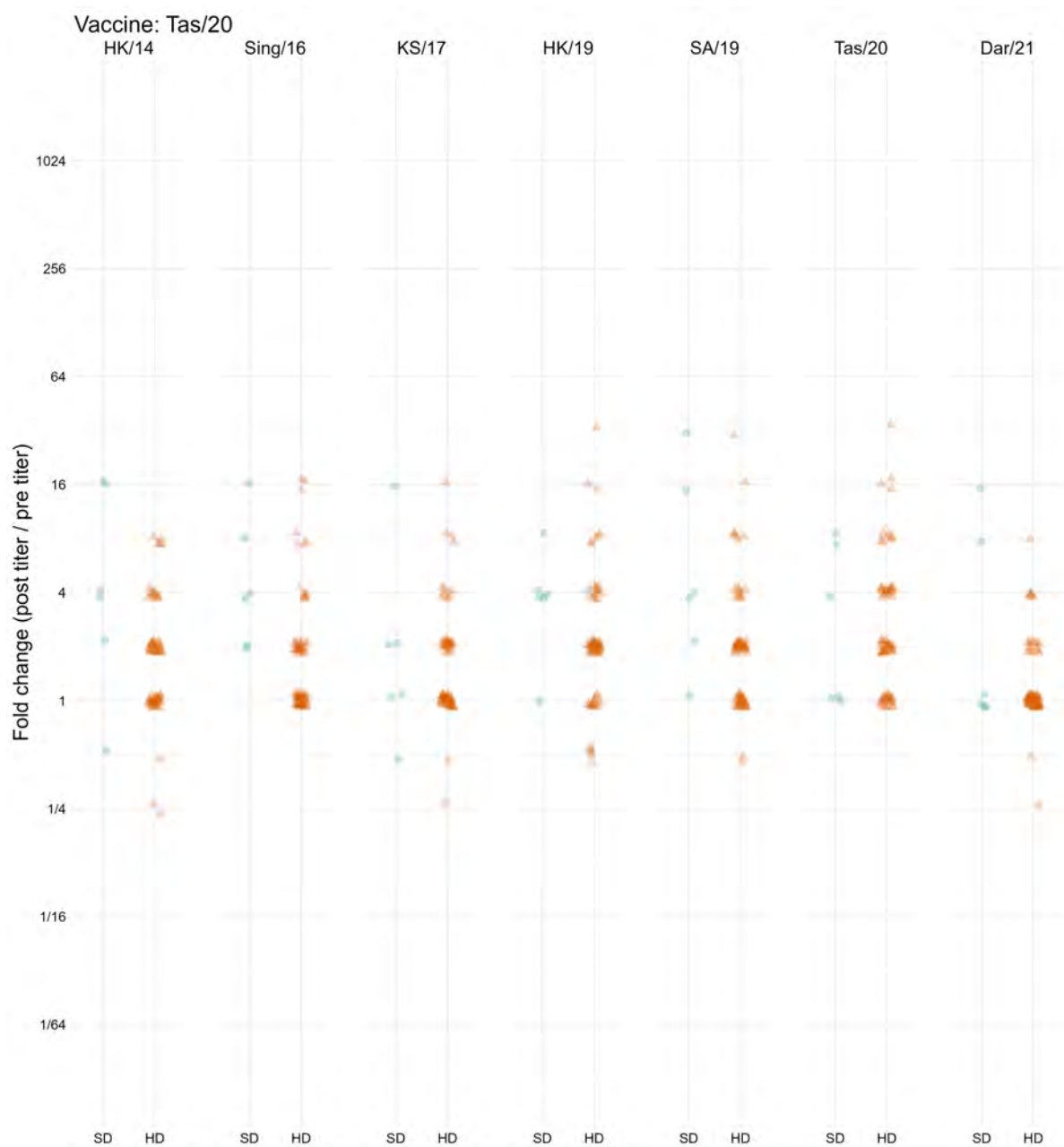


Figure 25: Fold-change (post-vaccination titer / pre-vaccination titer) for all person-years where a participant was administered a vaccine containing Tas/20-like split inactivated virus. Each panel shows a historical strain which was used for HAI assays, and all H3N2 subtype historical strains that were used for running assays against Tas/20 vaccinated individual samples are shown.

Outcome summaries

For each outcome (and additionally the pre-vaccination titer), we computed crude summary statistics for the SD and HD groups in order to obtain a measure of the crude effect size. For the pre-vaccination titer, post-vaccination titer, and fold change, we computed the geometric mean and geometric SD, while for the seroprotection and serconversion, we computed the number and percentage of individuals for which each event occurred. We also computed standardized mean differences (SMDs) to compare the groups using the method of Yang and Dalton [48] via the R package `smd` [49].

We did not further stratify by each assay strain during the crude analysis, because the low sample size and number of comparisons would greatly inflate the amount of noise in the analysis, and understanding the stratified results would be very difficult. Notably, SMDs can be roughly interpreted by the guidelines shown in Table 11, although these should not be strictly or decisively used to make decisions based on the qualitative guidelines alone [50,51].

Table 11: Suggested qualitative interpretations of the Cohen’s d effect sizes represented by our SMD calculations. Note that these are only rough guidelines.

Cohen’s d	Interpretation
0.01	Very small
0.20	Small
0.50	Medium
0.80	Large
1.20	Very large
2.0	Huge

Pre-vaccination titer

Table 12 shows the crude analysis of the pre-vaccination titer. In contrast to the results shown in the main paper, the overall effect and subtype overall effects are all near zero. For some vaccine strains, the titer was clearly higher for the HD group, potentially due to the effect of receiving HD vaccines in multiple years. We using a flexible smoothing spline to control for the effect of pre-vaccination titer in our main model to reduce confounding by pre-vaccination titer in our main results.

Table 12: Crude analysis of the pre-vaccination titer, stratified by dose.

Subtype	Vaccine strain	n ¹		Pre-vaccination titer ²		SMD ³
		SD	HD	SD	HD	
Overall	Overall	6,668	9,360	16.27 (±3.31)	16.29 (±3.21)	0.00 (-0.03, 0.03)
H1N1	Overall	3,082	4,288	13.40 (±3.04)	12.94 (±2.78)	-0.03 (-0.08, 0.01)
	CA/09	2,453	2,942	14.53 (±3.17)	13.96 (±2.88)	-0.04 (-0.09, 0.02)
	MI/15	451	328	10.46 (±2.43)	15.07 (±2.84)	0.38 (0.23, 0.52)
	Bris/18	126	414	8.16 (±2.14)	7.66 (±2.06)	-0.08 (-0.28, 0.11)
	GD/19	28	304	9.28 (±2.09)	12.03 (±2.57)	0.31 (-0.08, 0.70)
	Vic/19	24	300	7.49 (±1.71)	11.57 (±2.34)	0.61 (0.20, 1.03)
H3N2	Overall	3,586	5,072	19.22 (±3.46)	19.79 (±3.46)	0.02 (-0.02, 0.07)
	TX/12	1,544	972	19.42 (±3.43)	22.34 (±3.56)	0.11 (0.03, 0.19)
	Switz/13	720	1,042	15.90 (±3.11)	17.04 (±3.22)	0.06 (-0.04, 0.15)
	HK/14	974	1,597	20.16 (±3.62)	24.06 (±3.66)	0.14 (0.06, 0.22)
	Sing/16	110	80	36.39 (±4.62)	21.07 (±3.93)	-0.38 (-0.67, -0.09)
	KS/17	168	552	19.92 (±3.39)	14.80 (±2.94)	-0.26 (-0.43, -0.09)
	HK/19	28	304	23.20 (±2.54)	21.46 (±3.34)	-0.07 (-0.46, 0.31)
	Tas/20	42	525	15.87 (±2.88)	15.08 (±3.27)	-0.05 (-0.36, 0.27)

¹Total number of HAI assays across all assay strains and seasons.

²Pre-vaccination HAI titer. Geometric mean (± geometric standard deviation).

³Standardized mean difference (HD - SD); SMD (95% CI).

Post-vaccination titer

Table 13 shows the crude dose-stratified analysis of the post-vaccination titer outcome. We saw a weakly positive effect of the HD vaccine overall, which matched what we saw in our primary adjusted analysis. Notably, some strains showed a negative effect of the HD vaccine, which tended to correspond with the strains where the HD group had higher pre-vaccination titers (Table 12) in the crude analysis.

Table 13: Crude analysis of the post-vaccination titer, stratified by dose.

Subtype	Vaccine strain	n ¹		Post-vaccination titer ²		SMD ³
		SD	HD	SD	HD	
Overall	Overall	6,668	9,360	24.68 (±4.10)	28.99 (±4.01)	0.12 (0.08, 0.15)
H1N1	Overall	3,082	4,288	17.29 (±3.35)	20.09 (±3.24)	0.13 (0.08, 0.17)
	CA/09	2,453	2,942	18.44 (±3.40)	19.92 (±3.22)	0.06 (0.01, 0.12)
	MI/15	451	328	11.68 (±2.74)	19.01 (±3.19)	0.45 (0.30, 0.59)
	Bris/18	126	414	16.86 (±3.82)	14.07 (±3.01)	-0.15 (-0.35, 0.05)
	GD/19	28	304	21.02 (±2.22)	26.29 (±2.96)	0.24 (-0.15, 0.62)
	Vic/19	24	300	33.64 (±3.13)	28.95 (±3.49)	-0.13 (-0.54, 0.29)
H3N2	Overall	3,586	5,072	33.52 (±4.47)	39.53 (±4.39)	0.11 (0.07, 0.15)
	TX/12	1,544	972	28.48 (±3.96)	40.86 (±4.00)	0.26 (0.18, 0.34)
	Switz/13	720	1,042	39.09 (±5.33)	45.21 (±5.54)	0.09 (-0.01, 0.18)
	HK/14	974	1,597	32.43 (±4.55)	41.23 (±4.41)	0.16 (0.08, 0.24)
	Sing/16	110	80	52.78 (±4.80)	31.93 (±4.01)	-0.34 (-0.63, -0.05)
	KS/17	168	552	60.43 (±4.21)	40.81 (±4.09)	-0.28 (-0.45, -0.10)
	HK/19	28	304	44.16 (±2.70)	35.37 (±3.37)	-0.20 (-0.59, 0.19)
	Tas/20	42	525	50.40 (±3.82)	26.71 (±3.61)	-0.49 (-0.80, -0.17)

¹Total number of HAI assays across all assay strains and seasons.

²Post-vaccination HAI titer. Geometric mean (± geometric standard deviation).

³Standardized mean difference (HD - SD); SMD (95% CI).

Fold change

The crude analysis of the fold change (Table 14) was similar to our main adjusted analysis. The only qualitatively different result was the significant overall SMD, and the significant SMDs for all H1N1 and all H3N2 strains, indicating a small positive effect of the HD vaccine. These results are consistent with our main adjusted analysis.

Table 14: Crude analysis of the fold change, stratified by dose.

Subtype	Vaccine strain	n ¹		Fold change ²		SMD ³
		SD	HD	SD	HD	
Overall	Overall	6,668	9,360	1.52 (±2.42)	1.78 (±2.51)	0.18 (0.15, 0.21)
H1N1	Overall	3,082	4,288	1.29 (±2.19)	1.55 (±2.24)	0.23 (0.19, 0.28)
	CA/09	2,453	2,942	1.27 (±2.19)	1.43 (±2.15)	0.15 (0.10, 0.21)
	MI/15	451	328	1.12 (±1.68)	1.26 (±1.83)	0.22 (0.07, 0.36)
	Bris/18	126	414	2.07 (±3.05)	1.84 (±2.15)	-0.12 (-0.32, 0.08)
	GD/19	28	304	2.26 (±1.98)	2.19 (±2.33)	-0.05 (-0.43, 0.34)
	Vic/19	24	300	4.49 (±2.48)	2.50 (±2.84)	-0.60 (-1.02, -0.19)
H3N2	Overall	3,586	5,072	1.74 (±2.56)	2.00 (±2.69)	0.14 (0.10, 0.18)
	TX/12	1,544	972	1.47 (±2.19)	1.83 (±2.62)	0.25 (0.17, 0.33)
	Switz/13	720	1,042	2.46 (±3.12)	2.65 (±3.44)	0.06 (-0.03, 0.16)
	HK/14	974	1,597	1.61 (±2.40)	1.71 (±2.36)	0.07 (-0.01, 0.15)
	Sing/16	110	80	1.45 (±1.79)	1.52 (±2.11)	0.07 (-0.22, 0.35)
	KS/17	168	552	3.03 (±3.19)	2.76 (±2.83)	-0.09 (-0.26, 0.09)
	HK/19	28	304	1.90 (±2.02)	1.65 (±2.04)	-0.21 (-0.59, 0.18)
	Tas/20	42	525	3.17 (±2.97)	1.77 (±2.11)	-0.63 (-0.95, -0.31)

¹Total number of HAI assays across all assay strains and seasons.

²Fold change (post-vaccination titer divided by pre-vaccination titer. Geometric mean (± geometric standard deviation)).

³Standardized mean difference (HD - SD); SMD (95% CI).

Seroprotection

Table 15 shows the crude analysis for the seroprotection outcome. The results were consistent with our main analysis, as well as the crude analyses of the other outcomes.

Table 15: Crude analysis of the seroprotection rate, stratified by dose.

Subtype	Vaccine strain	n ¹		Seroprotection ²		SMD ³
		SD	HD	SD	HD	
Overall	Overall	6,668	9,360	2822 (42%)	4533 (48%)	0.12 (0.09, 0.15)
H1N1	Overall	3,082	4,288	998 (32%)	1638 (38%)	0.12 (0.08, 0.17)
	CA/09	2,453	2,942	847 (35%)	1116 (38%)	0.07 (0.02, 0.12)
	MI/15	451	328	88 (20%)	117 (36%)	0.37 (0.22, 0.51)
	Bris/18	126	414	36 (29%)	117 (28%)	-0.01 (-0.21, 0.19)
	GD/19	28	304	10 (36%)	133 (44%)	0.16 (-0.22, 0.55)
	Vic/19	24	300	17 (71%)	155 (52%)	-0.40 (-0.82, 0.02)
H3N2	Overall	3,586	5,072	1824 (51%)	2895 (57%)	0.12 (0.08, 0.17)
	TX/12	1,544	972	733 (47%)	599 (62%)	0.29 (0.21, 0.37)
	Switz/13	720	1,042	378 (52%)	616 (59%)	0.13 (0.04, 0.23)
	HK/14	974	1,597	471 (48%)	904 (57%)	0.17 (0.09, 0.25)
	Sing/16	110	80	72 (65%)	46 (57%)	-0.16 (-0.45, 0.12)
	KS/17	168	552	118 (70%)	318 (58%)	-0.27 (-0.44, -0.09)
	HK/19	28	304	21 (75%)	166 (55%)	-0.44 (-0.83, -0.05)
	Tas/20	42	525	31 (74%)	246 (47%)	-0.57 (-0.89, -0.26)

¹Total number of HAI assays across all assay strains and seasons.

²Seroprotection (indicator for post-titer $\geq 1:40$); n (%).

³Standardized mean difference (HD - SD); SMD (95% CI).

Seroconversion

Table 16 shows the crude analysis for the seroconversion outcome. The results were consistent with our main analysis, as well as the crude analyses of the other outcomes. Notably, some of the vaccines have a much lower rate of seroconversion than seroprotection, and the SMDs for seroconversion between the two groups are quite negative, which is affected by both the smaller sample size in those groups as well as the higher pre-vaccination titers in the HD group.

Table 16: Crude analysis of the seroconversion rate, stratified by dose.

Subtype	Vaccine strain	n ¹		Seroconversion ²		SMD ³
		SD	HD	SD	HD	
Overall	Overall	6,668	9,360	981 (15%)	1710 (18%)	0.10 (0.06, 0.13)
H1N1	Overall	3,082	4,288	267 (09%)	535 (12%)	0.12 (0.08, 0.17)
	CA/09	2,453	2,942	203 (08%)	282 (10%)	0.05 (-0.01, 0.10)
	MI/15	451	328	19 (04%)	25 (08%)	0.14 (0.00, 0.29)
	Bris/18	126	414	23 (18%)	65 (16%)	-0.07 (-0.27, 0.13)
	GD/19	28	304	6 (21%)	62 (20%)	-0.03 (-0.41, 0.36)
	Vic/19	24	300	16 (67%)	101 (34%)	-0.70 (-1.12, -0.28)
H3N2	Overall	3,586	5,072	714 (20%)	1175 (23%)	0.08 (0.04, 0.12)
	TX/12	1,544	972	206 (13%)	211 (22%)	0.22 (0.14, 0.30)
	Switz/13	720	1,042	240 (33%)	378 (36%)	0.06 (-0.03, 0.16)
	HK/14	974	1,597	155 (16%)	276 (17%)	0.04 (-0.04, 0.12)
	Sing/16	110	80	13 (12%)	6 (08%)	-0.15 (-0.43, 0.14)
	KS/17	168	552	69 (41%)	191 (35%)	-0.13 (-0.31, 0.04)
	HK/19	28	304	8 (29%)	36 (12%)	-0.43 (-0.81, -0.04)
	Tas/20	42	525	23 (55%)	77 (15%)	-0.93 (-1.25, -0.61)

¹Total number of HAI assays across all assay strains and seasons.

²Seroconversion (indicator for post-titer $\geq 1:40$ only after vaccination); n (%).

³Standardized mean difference (HD - SD); SMD (95% CI).

Model diagnostics

We assessed model convergence and sampling using the \hat{R} statistic and the effective sample size (ESS) of the parameters. Detailed explanations of these metrics can be found in other sources [e.g. 52]. Briefly, \hat{R} assesses the mixing of the chains, and a large value indicates that chains have explored separate regions of the posterior or do not agree about the posterior density. The bulk ESS and tail ESS are two measures of the ESS, which provide information about how many draws of the parameters we would have if all of our draws were completely uncorrelated (typically draws from the posterior are correlated and thus have less information than independent draws)

Since each of the models contains hundreds of parameters, it is not feasible to display every diagnostic statistic in the summary. Table 17 contains an abbreviated summary of the most important diagnostic criteria, which were within acceptable bounds ($\hat{R} \lesssim 1.01$ and both ESS $\gtrsim 1000$ for all parameters). While there were a handful of divergent transitions, they were negligible compared to the total amount of samples.

The main exception is the model for the seroprotection outcome, which had a high number of divergent transitions. While a few divergences are no cause for concern, and the number of post-warmup divergences for this model was around 1%, this may indicate that the seroprotection outcome is more difficult to model than the others. The lower ESS values for this model also support this assertion. Since the seroconversion model sampled normally, we attribute this problem to the data collected rather than the parametrization of the model. Since we encourage the use of the titer increase and post-vaccination titer models instead, rather than the binary outcome models, we did not attempt any reparametrizations or extended sampling of the seroprotection model.

Table 17: Summarized diagnostic criteria for each of the four Bayesian models we fit.

Model	Num. Divergences	min E-BFMI	min ESS (tail)	min ESS (bulk)	max R_{hat}
Post-vaccination titer	2 / 20000	0.615	3682	1982	1.013
Seroconversion	2 / 20000	0.636	5956	2718	1.006
Seroprotection	249 / 20000	0.636	1118	1660	1.012
Titer increase	4 / 20000	0.609	2779	1550	1.013

Our models have many parameters (451 for the Gaussian models and 450 for the logistic models due to the lack of a residual variance), so we cannot show parameter-level diagnostics for all parameters. However, we selected a representative parameter of each major class to include representative diagnostics for each model. The parameters we selected are:

- `b_doseHD`, the population-level slope term for the effect of HD vaccination;
- `bs_sbirth_year_c_1`, the first population-level slope term for the smoothing spline effect of birth year;
- `cor_strain_type__Intercept__doseHD`, the correlation between the varying intercept effect and the varying effect of HD vaccination for the strain type variable;
- `Intercept`, the population-level global intercept parameter;
- `sd_id__Intercept`, the variance parameter for the distribution of intercept effects which vary by subject ID;
- `sd_strain_type__doseHD`, the variance parameter for the distribution of HD slope effects which vary by strain type;
- `sd_strain_type__Intercept`, the variance parameter for the distribution of intercept effects which vary by strain type; and
- `sds_sage_c_1`, the variance parameter for the distribution of slope effects for the smoothing spline parameters for the effect of age.

Note that diagnostic statistics for every parameter can be generated from our provided code, and our code can easily be modified to create diagnostic plots for any other parameters.

Trace rank plots

We show trace rank plots (also called rank histograms) for each of these parameters for the titer increase model in Figure 26, for the post-vaccination titer model in Figure 27, for the seroprotection model in Figure 28, and for the seroconversion model in Figure 29. A rank histogram is created by ranking the relative value of each draw of a parameter across all chains, binning the ranks (we used a bin size of 500), and creating a separate histogram for each chains, which are superimposed in each plot. A parameter with chains that have mixed will show histograms which constantly swap positions [53]. These plots indicate good mixing for each of our models, and there is no indication from these plots that hints at the higher number of divergent transitions for the seroprotection model.

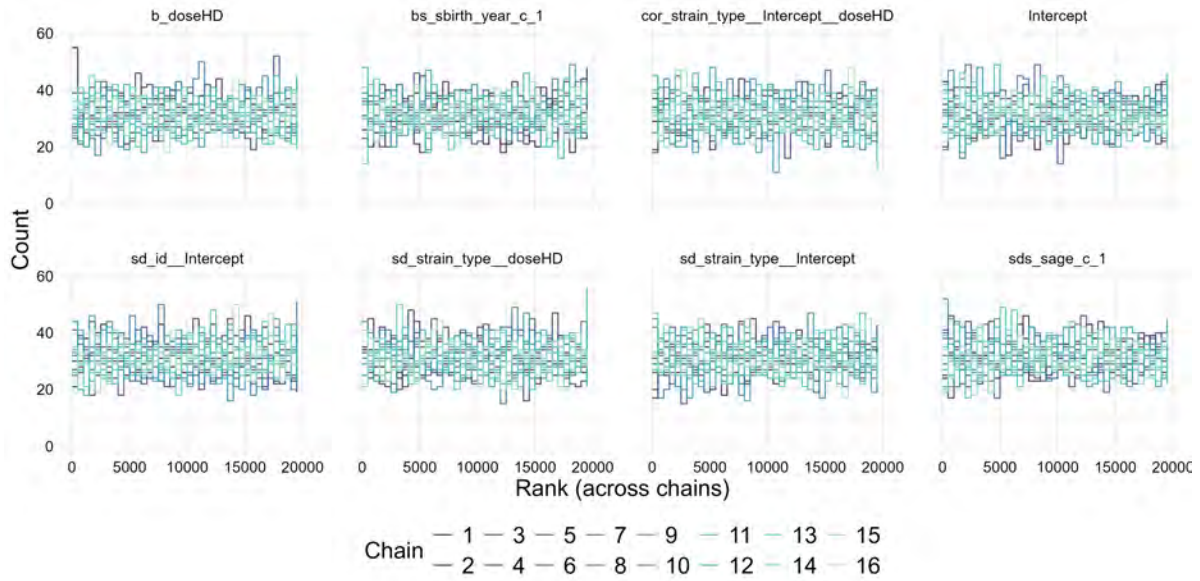


Figure 26: Trace rank plot of the representative parameters from the model with titer increase as the outcome. The histograms oscillate randomly, and constantly swap positions, indicating good chain mixing.

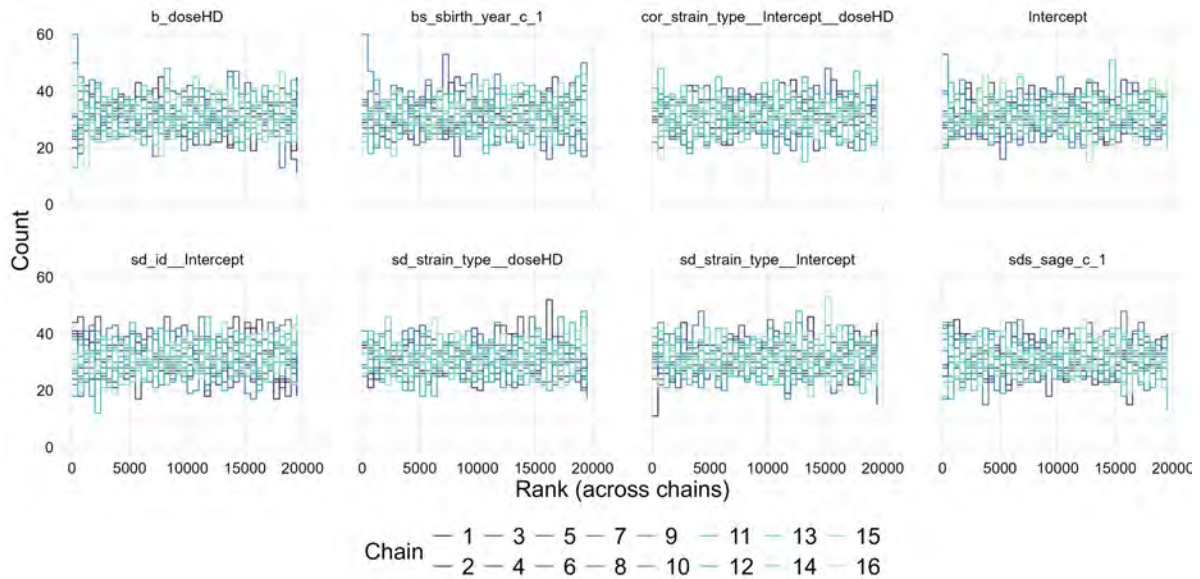


Figure 27: Trace rank plot of the representative parameters from the model with post-vaccination titer as the outcome. The histograms oscillate randomly, and constantly swap positions, indicating good chain mixing.

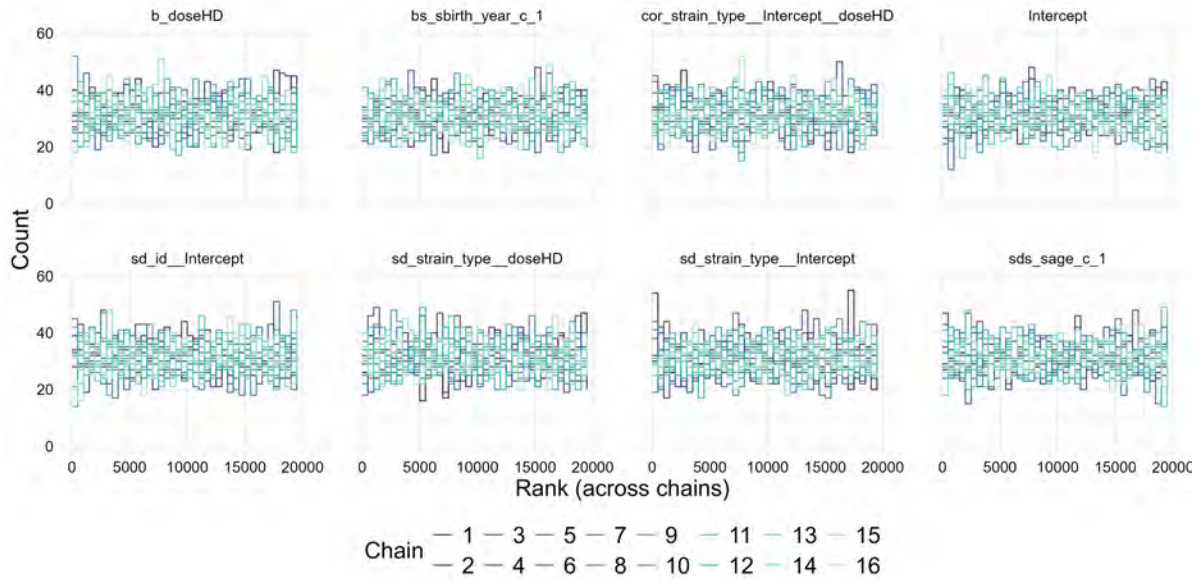


Figure 28: Trace rank plot of the representative parameters from the model with seroprotection as the outcome. The histograms oscillate randomly, and constantly swap positions, indicating good chain mixing.

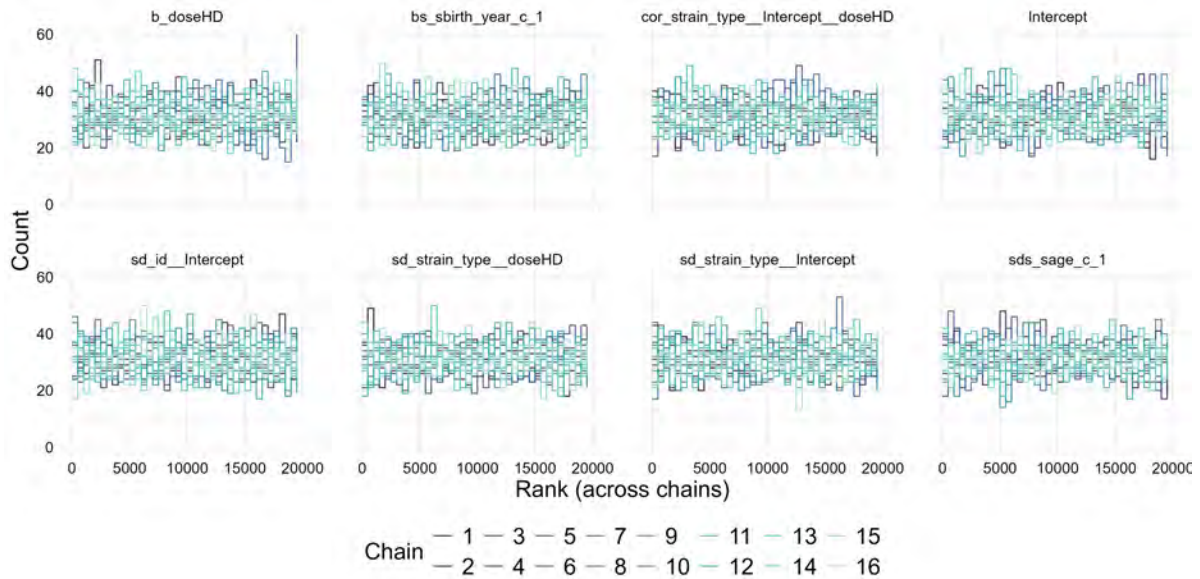


Figure 29: Trace rank plot of the representative parameters from the model with seroconversion as the outcome. The histograms oscillate randomly, and constantly swap positions, indicating good chain mixing.

Prior and posterior density comparison

In order to understand which parameters are affected the most by our priors, we compared the prior and posterior densities visually for the same set of representative parameters. Figure 30 shows the density comparison for the model with titer increase as the outcome, Figure 31 for the model with post-vaccination titer as the outcome, Figure 32 for the model with seroprotection as the outcome, and Figure 33 for the model with seroconversion as the outcome. In order to construct the densities, we sampled from the priors (without updating them with our data) using the same sampling algorithm parameters as we did for the posterior samples – that is, we obtained 20000 prior samples. For both the prior and posterior samples, we computed the gaussian kernel density estimate across all samples for each of the representative parameters, which is the density curve shown in each of the figures.

In Figure 30, we can see that many of the parameters behaved as expected. All of the parameters except for the correlation parameter have clearly moved towards a peak, indicating strong convergence to a value away from the prior distribution. The posterior distribution for the correlation parameter, `cor_strain_type__Intercept__doseHD`, has some differences from the prior but is largely the same. This is not surprising, because these correlation parameters can often be difficult to infer. There is no real alternative prior for the correlation parameters to use as a sensitivity analysis (shrinking the LKJ parameter would bias our model towards more extreme correlations, whereas 2 is a sensible default), and the posterior distribution of the correlation parameter merely indicates uncertainty in the posterior distribution of the correlation, since it is already constrained in the values which it can take. We do not expect changing the correlation parameter to strongly affect the model results.

While some of the variance parameters, represented here by `sd_strain_type__doseHD` and `sd_strain_type__Intercept` stay relatively similar in shape to the priors, they have more pronounced peaks. These terms are often very small (near zero) and would induce boundary convergence errors in a frequentist ML formulation of our model, so it is unsurprising that they stay relatively similar to our priors, which are close to zero, but allow for the parameter to move away from zero if the data allow this – in our case, the data do not appear to support a random effects variance far away from zero. This boundary variance also compounds the difficulties in estimating the random effects correlation parameters.]{color="#FF2400"}

The conclusions from Figure 31 are nearly identical to the conclusions from Figure 30. We expect this, because the models are mathematically very similar.

In contrast to the conclusions from Figure 30 and Figure 31, some of the conclusions in Figure 32 are quite different. In a frequentist context, we would say that this model, with a dichotomous outcome, has much lower statistical power than the models with continuous outcomes. The majority of titers in our sample data were below 40, leading to a lack of events when we analyze seroprotection as a dichotomous outcome, especially for strains which are very antigenically different from the vaccine. We can see that the Intercept and `bs_sbirt_year_c_1`

parameters have moved slightly away from the priors, but not much, indicating that we cannot learn much from the data about these parameters under this model. The random effects variance parameters (with the exception of the variance for the random effect of subject id) are all very close to zero, near the priors, indicating that these parameters are not informative for learning about the seroprotection outcome. Since our priors were chosen as regularizing, skeptical priors (that allow the effects to become large easily if large effects are suggested by the data), the difficulty of predicting our underpowered dichotomous outcome is the cause of posterior densities similar to the prior densities – changing our priors to differently shaped skeptical priors would not make a difference. This analysis is not suggestive of any issues which would cause the higher number of divergent transitions for the seroprotection outcome.

The conclusions for the seroconversion model, shown in Figure 33, are the same as those shown in Figure 32. The seroconversion outcome contains even less events than the seroprotection outcome, leading to an even larger issue with statistical power. Because the logistic regression models have so little power and many parameters did not move away from the skeptical prior distributions, we do not recommend interpreting the binary outcome results directly, which is one reason we focus on the models for titer increase as our main results.

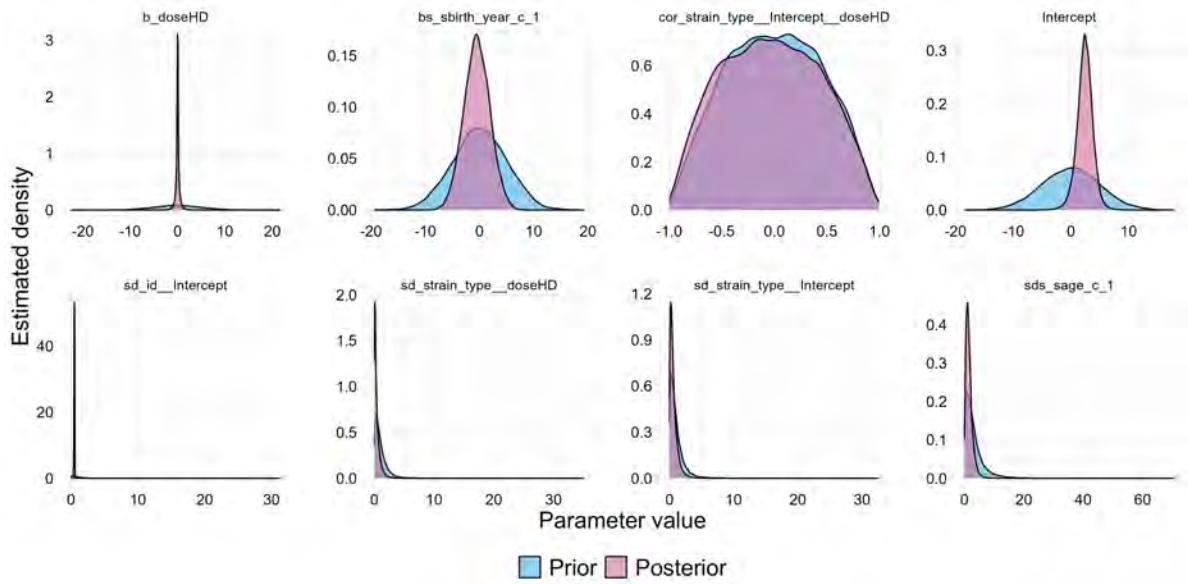


Figure 30: Prior and posterior density plots for each of the representative parameters for the model where titer increase was the outcome.

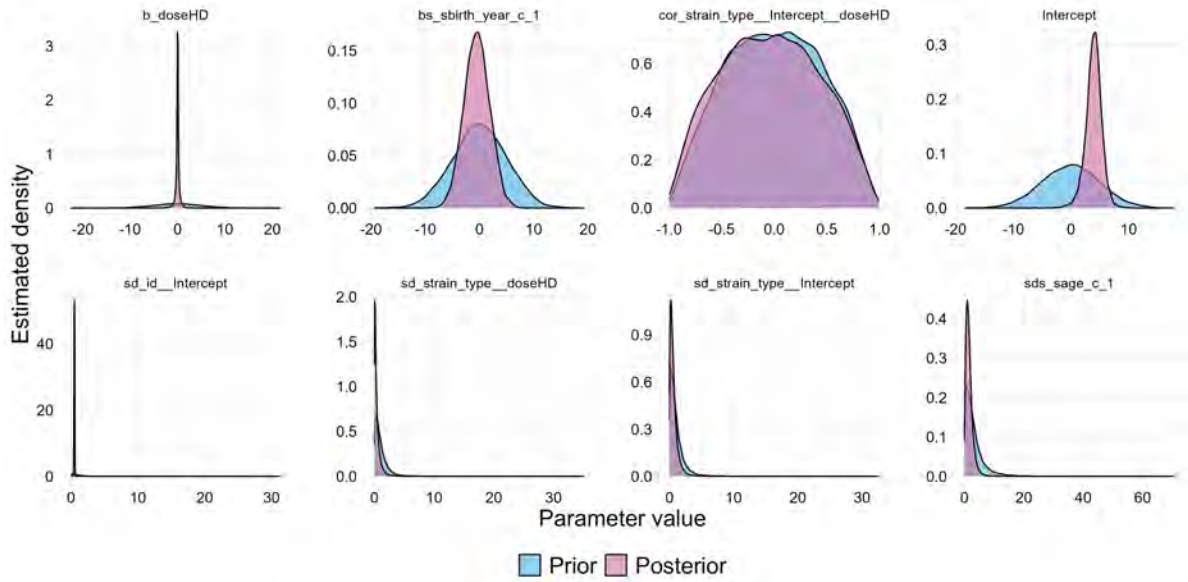


Figure 31: Prior and posterior density plots for each of the representative parameters for the model where post-vaccination titer was the outcome.

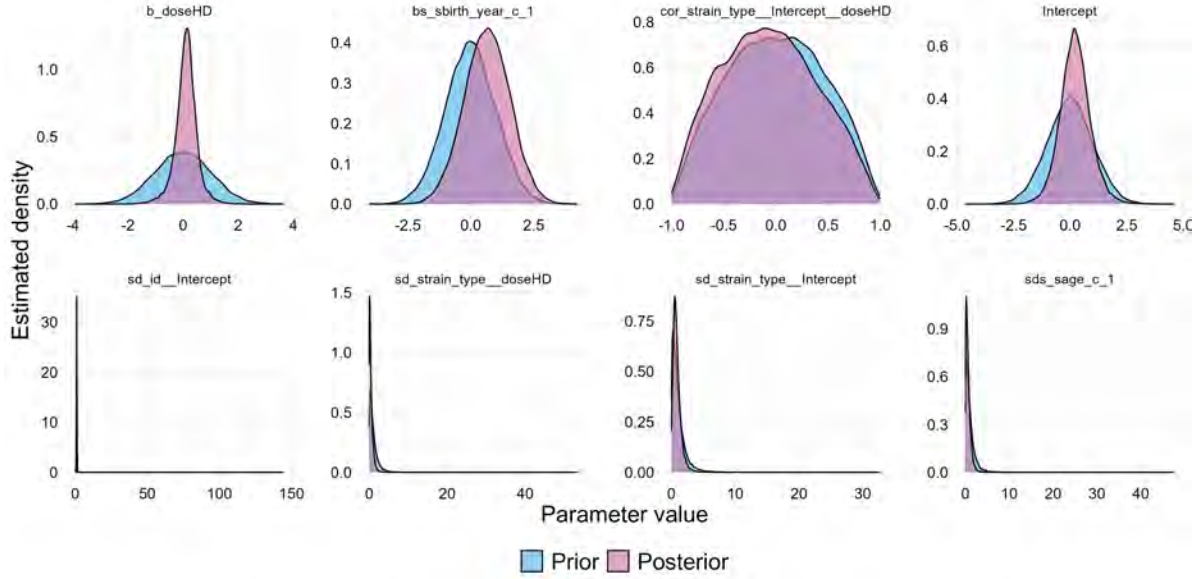


Figure 32: Trace rank plot of the representative parameters from the model with seroprotection as the outcome. The histograms oscillate randomly, and constantly swap positions, indicating good chain mixing.

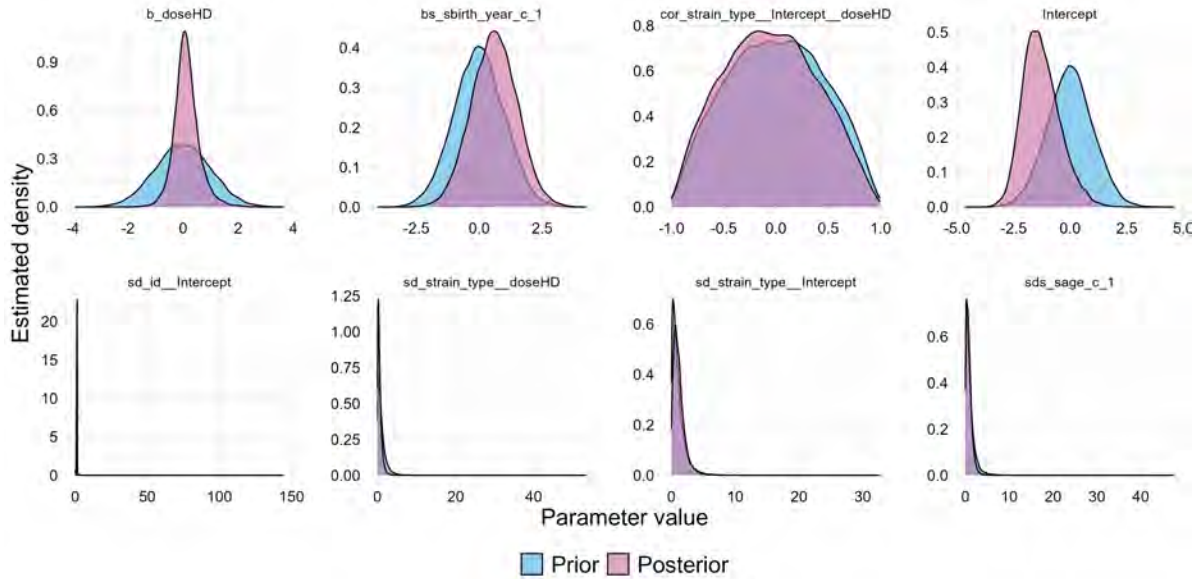


Figure 33: Trace rank plot of the representative parameters from the model with seroconversion as the outcome. The histograms oscillate randomly, and constantly swap positions, indicating good chain mixing.

Homologous model results

In the main text, we briefly mentioned that results which compared only the homologous vaccine response supported a positive effect of the HD vaccine compared to the SD vaccine, as shown in previous literature. Figure 34 shows our results when considering only the homologous response to each vaccine.

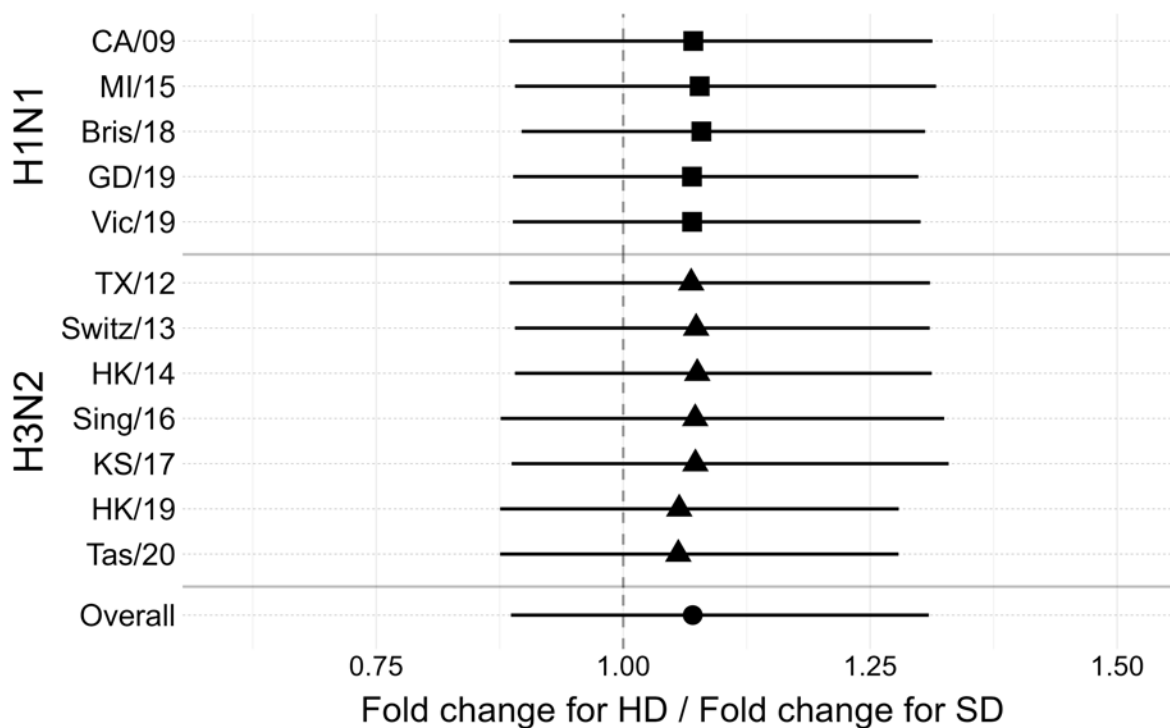


Figure 34: Exponentiated cACE estimates for each vaccine strain and overall. Only homologous responses to each vaccine were considered.

The credible intervals are wide, consistent with our other findings and in general with this type of complex observational data. However, all of the point estimates are positive, which matches previous literature on the effect of the HD vaccine on the homologous response.

Model results for other outcomes

While we think that modeling titer increase most directly answers our research question of interest (namely, whether the HD vaccine induces a stronger heterologous immune response than the SD vaccine), titer increase is not the only outcome with clinical interest. We also fit models with post-vaccination titer, seroprotection, and seroconversion as the outcomes,

detailed in the previous sections on model fitting. Here, we show the three figures from our main results, but using the alternative model outcomes.

Post-vaccination titer

All of the figures in this section show the results for post-vaccination titer as the model outcome. All of our results agreed with the results in the main text and there were no major qualitative differences.

Figure 35 shows the cACEs for each vaccine strain when only the heterologous strains were included.

Figure 36 shows the cACEs for all assay strains.

Figure 37 shows the cACEs for all vaccine strains, pooling assay strains together within each vaccine strain.

Figure 38 shows the cACEs for each season, with the vaccine strain and assay strains for that season all pooled together.

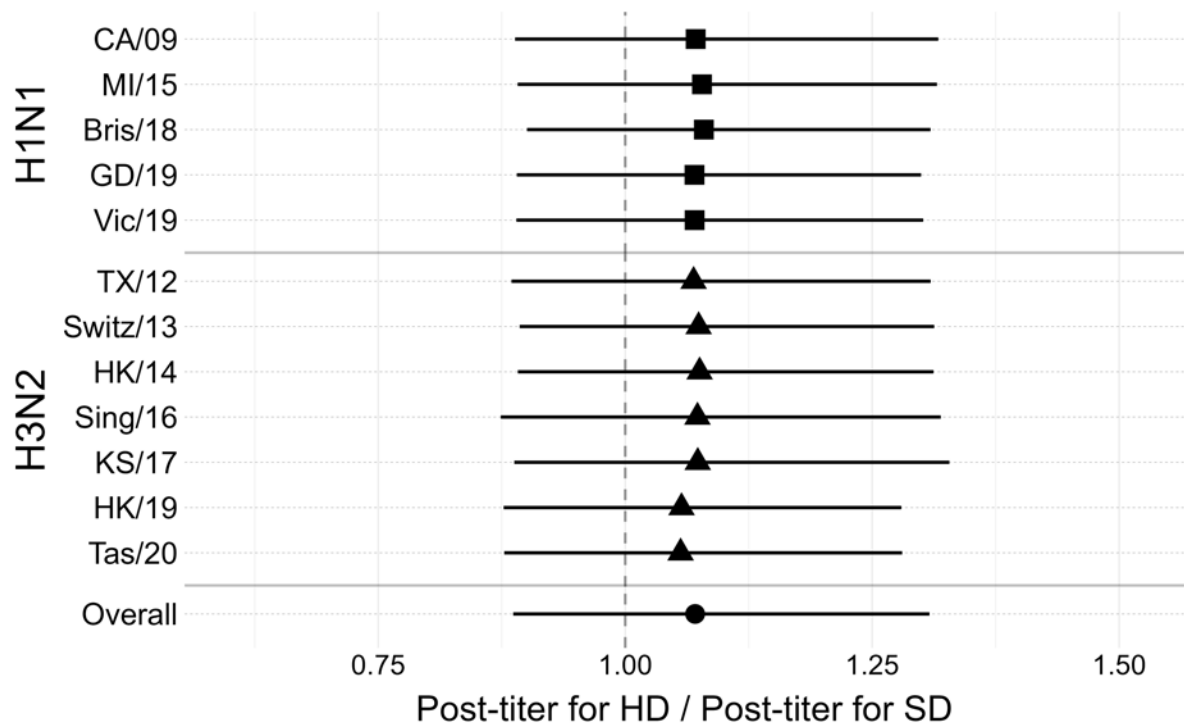


Figure 35: Exponentiated ACE estimates for each vaccine strain and overall. Only homologous responses to each vaccine were considered.

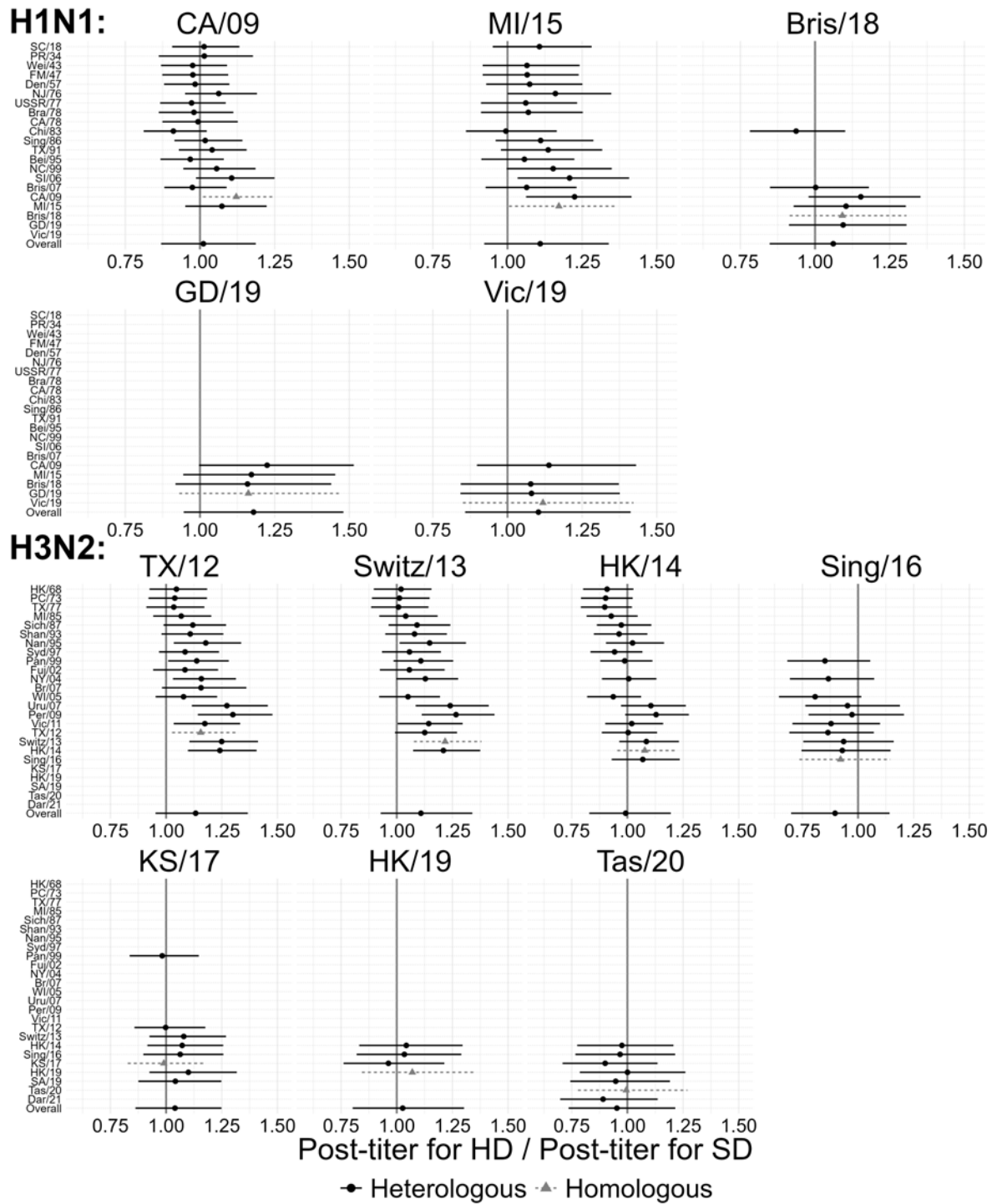


Figure 36: Exponentiated cACE estimates for each assay strain, within vaccine strains

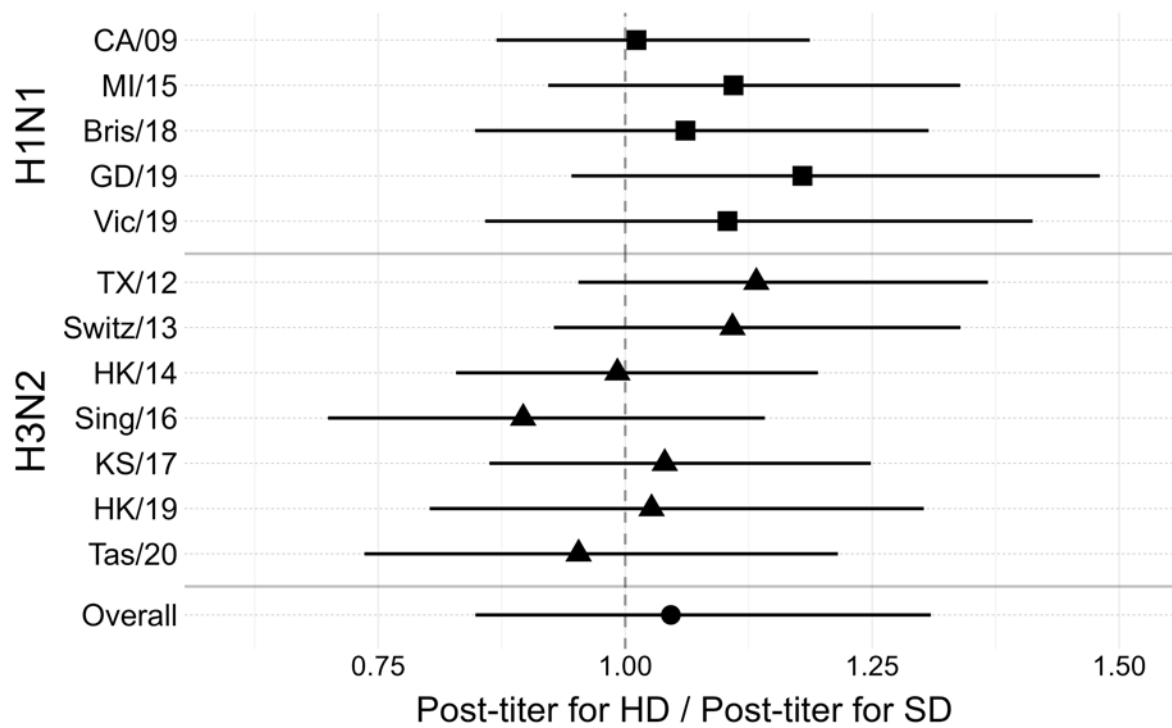


Figure 37: Exponentiated ACE estimates for each vaccine strain and overall.

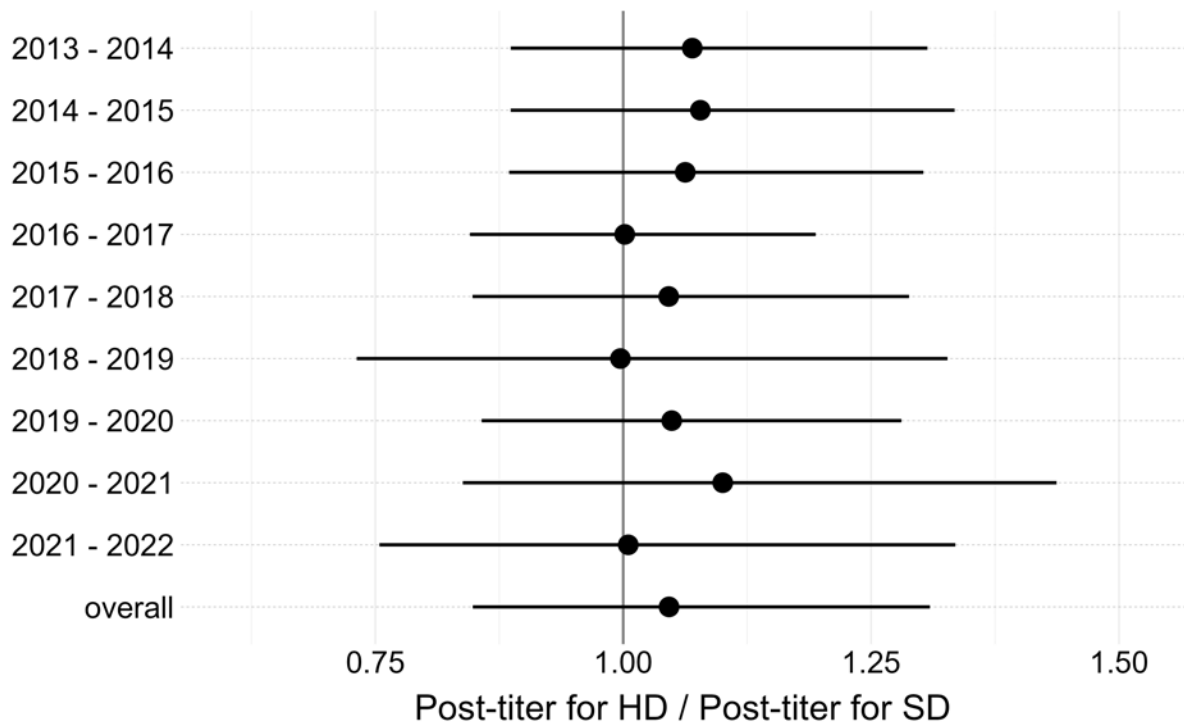


Figure 38: Exponentiated cACE for each season, over all vaccine strains and assay strains.

Seroprotection

All of the figures in this section show the results for seroprotection as the model outcome. All of our results agreed with the results in the main text and there were no major qualitative differences.

Figure 39 shows the cACEs for each vaccine strain when only the heterologous strains were included.

Figure 40 shows the cACEs for all assay strains.

Figure 41 shows the cACEs for all vaccine strains, pooling assay strains together within each vaccine strain.

Figure 42 shows the cACEs for each season, with the vaccine strain and assay strains for that season all pooled together.

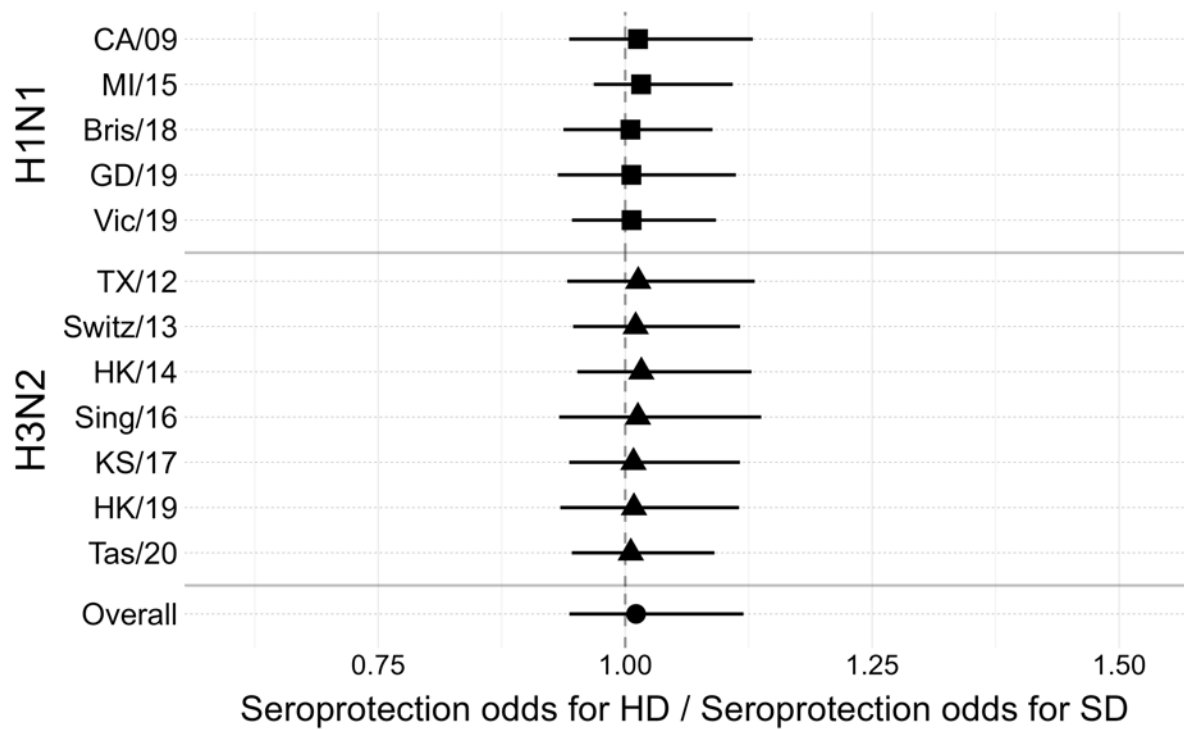


Figure 39: Exponentiated ACE estimates for each vaccine strain and overall. Only homologous responses to each vaccine were considered.

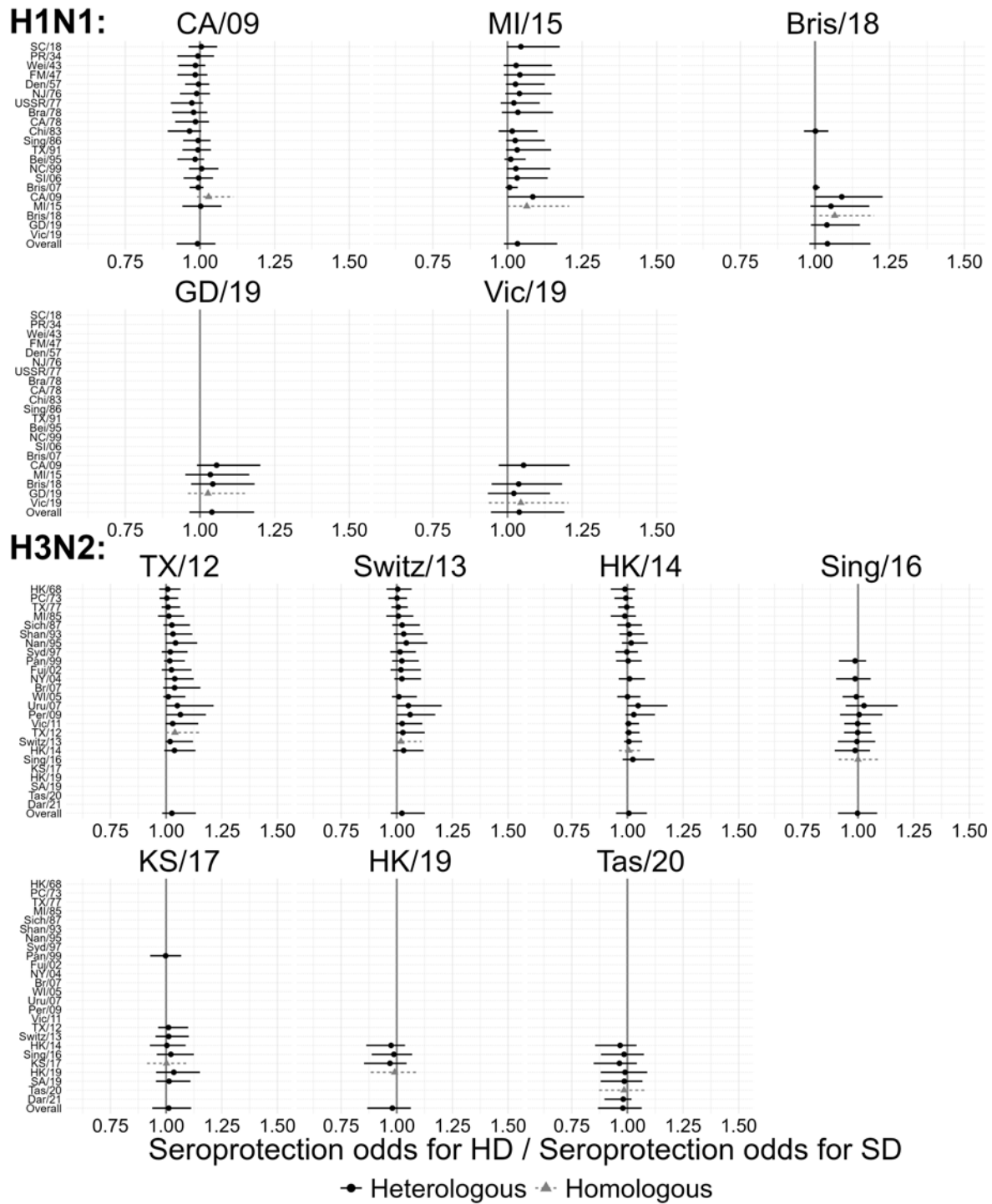


Figure 40: Exponentiated cACE estimates for each assay strain, within vaccine strains

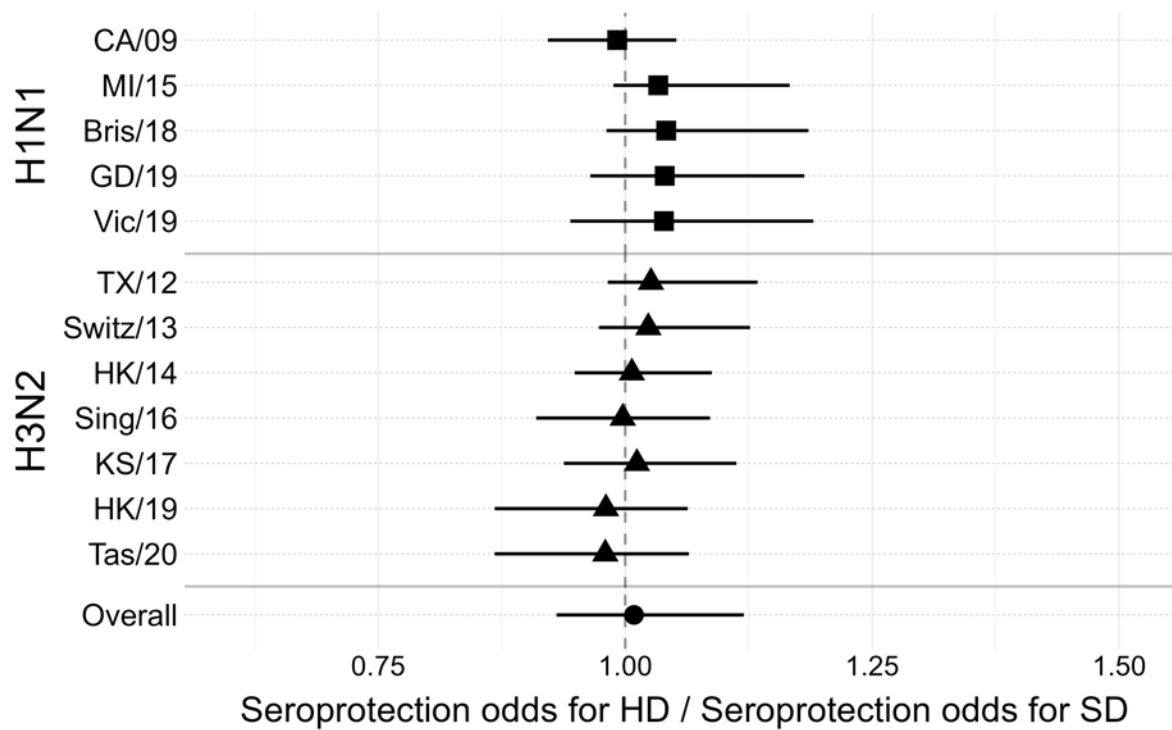


Figure 41: Exponentiated ACE estimates for each vaccine strain and overall.

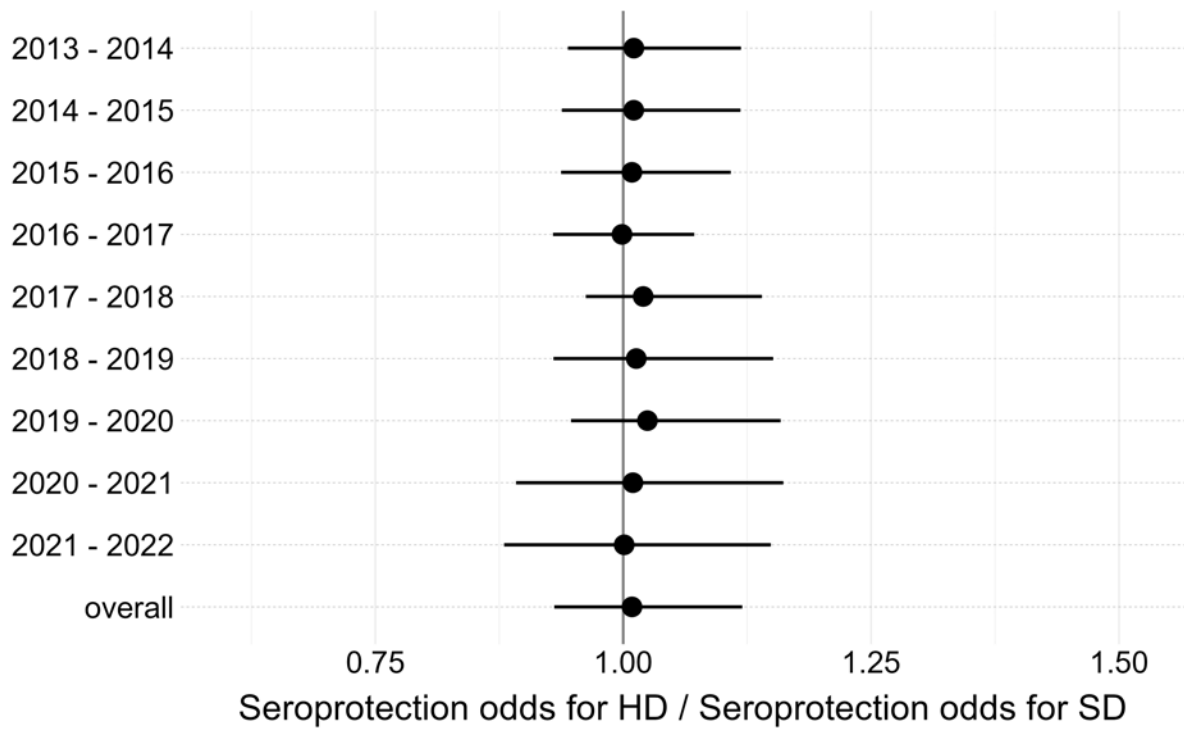


Figure 42: Exponentiated cACE for each season, over all vaccine strains and assay strains.

Seroconversion

All of the figures in this section show the results for seroconversion as the model outcome. All of our results agreed with the results in the main text and there were no major qualitative differences.

Figure 43 shows the cACEs for each vaccine strain when only the heterologous strains were included.

Figure 44 shows the cACEs for all assay strains.

Figure 45 shows the cACEs for all vaccine strains, pooling assay strains together within each vaccine strain.

Figure 46 shows the cACEs for each season, with the vaccine strain and assay strains for that season all pooled together.

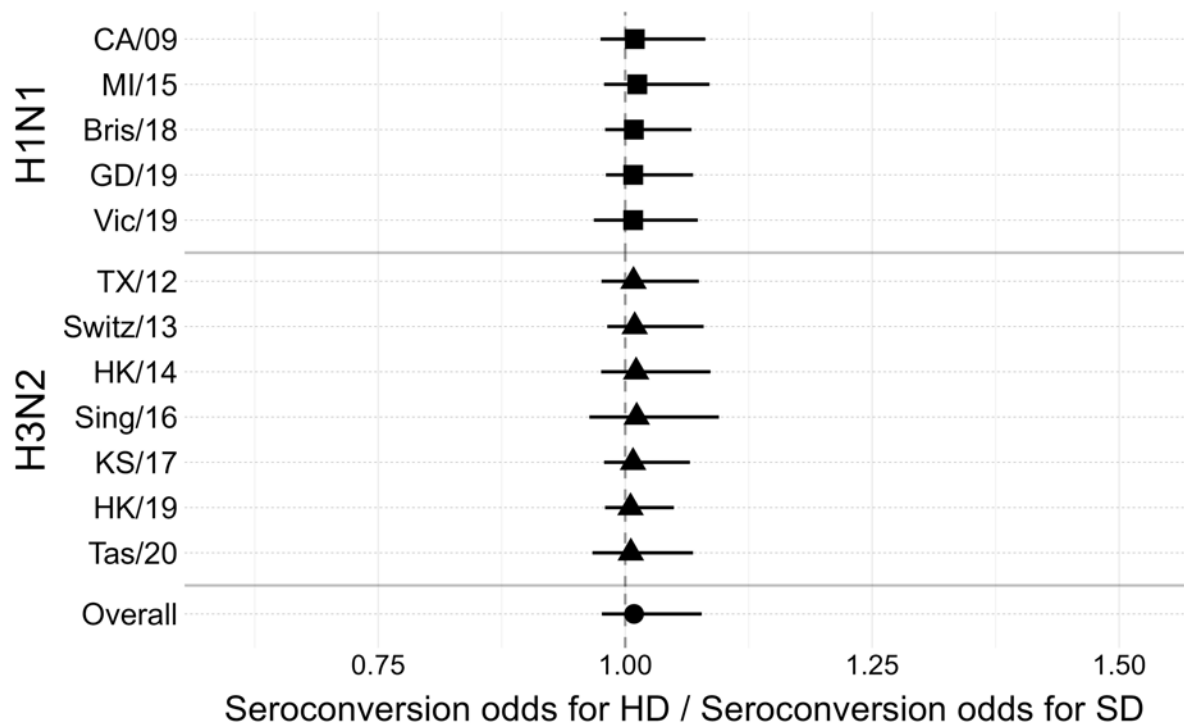


Figure 43: Exponentiated ACE estimates for each vaccine strain and overall. Only homologous responses to each vaccine were considered.

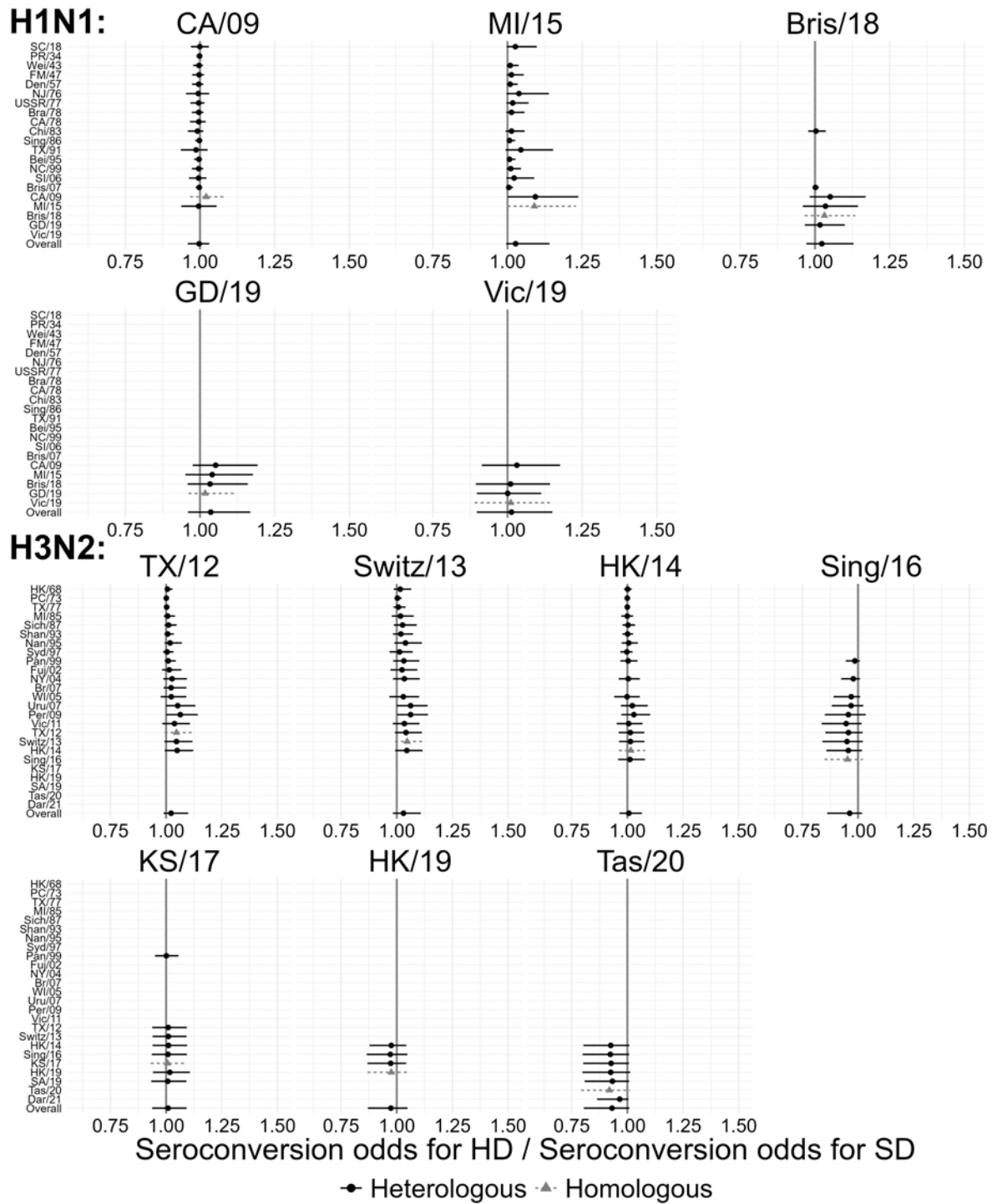


Figure 44: Exponentiated cACE estimates for each assay strain, within vaccine strains

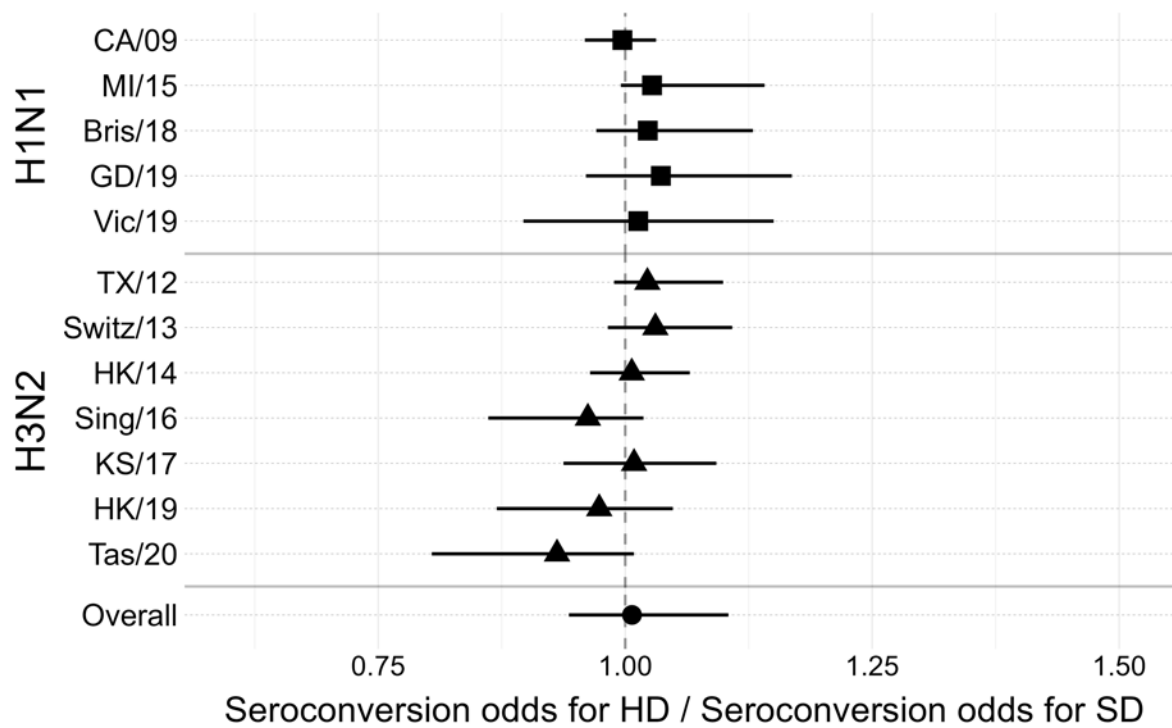


Figure 45: Exponentiated ACE estimates for each vaccine strain and overall.

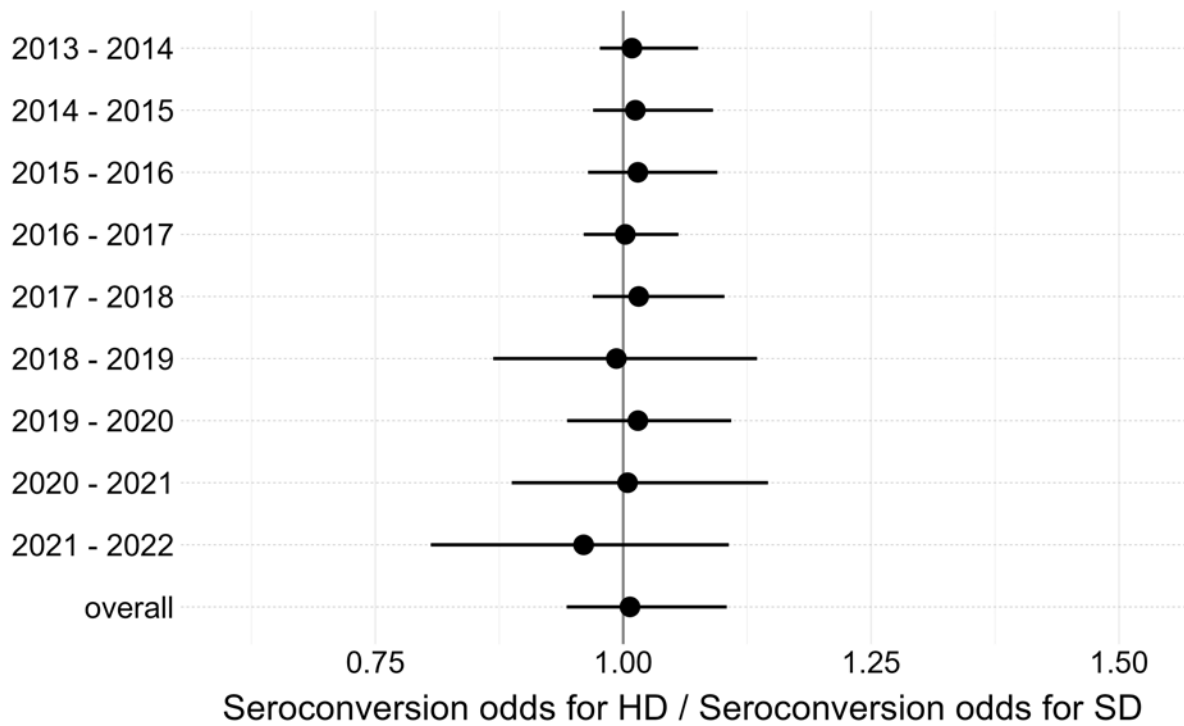


Figure 46: Exponentiated cACE for each season, over all vaccine strains and assay strains.

Session information

The complete R session information for all of our required packages is shown here.

Finding R package dependencies ... Done!

R version 4.4.1 (2024-06-14 ucrt)
Platform: x86_64-w64-mingw32/x64
Running under: Windows 10 x64 (build 19045)

Matrix products: default

locale:

[1] LC_COLLATE=English_United States.utf8
[2] LC_CTYPE=English_United States.utf8
[3] LC_MONETARY=English_United States.utf8
[4] LC_NUMERIC=C
[5] LC_TIME=English_United States.utf8

time zone: America/New_York

tzcode source: internal

attached base packages:

[1] stats graphics grDevices utils datasets methods base

other attached packages:

[1] renv_1.0.7 rmarkdown_2.27 dplyr_1.1.4 yaml_2.3.8
[5] softbib_0.0.2 readr_2.1.5 knitr_1.47 here_1.0.1
[9] flextable_0.9.6

loaded via a namespace (and not attached):

[1] generics_0.1.3	utf8_1.2.4	fontLiberation_0.1.0
[4] xml2_1.3.6	httpcode_0.3.0	hms_1.1.3
[7] digest_0.6.36	magrittr_2.0.3	evaluate_0.24.0
[10] grid_4.4.1	fastmap_1.2.0	rprojroot_2.0.4
[13] jsonlite_1.8.8	zip_2.3.1	crul_1.4.2
[16] promises_1.3.0	fansi_1.0.6	fontBitstreamVera_0.1.1
[19] textshaping_0.4.0	cli_3.6.3	shiny_1.8.1.1
[22] rlang_1.1.4	fontquiver_0.2.1	crayon_1.5.3
[25] withr_3.0.0	gfonts_0.2.0	gdtools_0.3.7
[28] tools_4.4.1	officer_0.6.6	tzdb_0.4.0

[31]	uuid_1.2-0	httpuv_1.6.15	curl_5.2.1
[34]	vctrs_0.6.5	R6_2.5.1	mime_0.12
[37]	lifecycle_1.0.4	ragg_1.3.2	pkgconfig_2.0.3
[40]	pillar_1.9.0	later_1.3.2	data.table_1.15.4
[43]	glue_1.7.0	Rcpp_1.0.12	systemfonts_1.1.0
[46]	tidyselect_1.2.1	xfun_0.45	tibble_3.2.1
[49]	rstudioapi_0.16.0	xtable_1.8-4	htmltools_0.5.8.1
[52]	compiler_4.4.1	askpass_1.2.0	openssl_2.2.0

References

- [1] Couch RB, Winokur P, Brady R, et al. [Safety and immunogenicity of a high dosage trivalent influenza vaccine among elderly subjects](#). *Vaccine*. 2007;25:7656–7663.
- [2] Falsey AR, Treanor JJ, Tornieporth N, et al. [Randomized, double-blind controlled phase 3 trial comparing the immunogenicity of high-dose and standard-dose influenza vaccine in adults 65 years of age and older](#). *The Journal of Infectious Diseases*. 2009;200:172–180.
- [3] DiazGranados CA, Dunning AJ, Jordanov E, et al. [High-dose trivalent influenza vaccine compared to standard dose vaccine in elderly adults: Safety, immunogenicity and relative efficacy during the 2009–2010 season](#). *Vaccine*. 2013;31:861–866.
- [4] DiazGranados CA, Dunning AJ, Kimmel M, et al. [Efficacy of High-Dose versus Standard-Dose Influenza Vaccine in Older Adults](#). *New England Journal of Medicine*. 2014;371:635–645.
- [5] DiazGranados CA, Dunning AJ, Robertson CA, et al. [Efficacy and immunogenicity of high-dose influenza vaccine in older adults by age, comorbidities, and frailty](#). *Vaccine*. 2015;33:4565–4571.
- [6] Lee JKH, Lam GKL, Shin T, et al. [Efficacy and effectiveness of high-dose influenza vaccine in older adults by circulating strain and antigenic match: An updated systematic review and meta-analysis](#). *Vaccine*. 2021;39:A24–A35.
- [7] Chang L-J, Meng Y, Janoszyk H, et al. [Safety and immunogenicity of high-dose quadrivalent influenza vaccine in adults \$\geq 65\$ years of age: A phase 3 randomized clinical trial](#). *Vaccine*. 2019;37:5825–5834.

- [8] [Chaves SS, Naeger S, Lounaci K, et al. High-Dose Influenza Vaccine Is Associated With Reduced Mortality Among Older Adults With Breakthrough Influenza Even When There Is Poor Vaccine-Strain Match.](#) *Clinical Infectious Diseases*. 2023;77:1032–1042.
- [9] [Wilkinson K, Wei Y, Szwajcer A, et al. Efficacy and safety of high-dose influenza vaccine in elderly adults: A systematic review and meta-analysis.](#) *Vaccine*. 2017;35:2775–2780.
- [10] [Samson SI, Leventhal PS, Salamand C, et al. Immunogenicity of high-dose trivalent inactivated influenza vaccine: A systematic review and meta-analysis.](#) *Expert Review of Vaccines*. 2019;18:295–308.
- [11] [Dunning AJ, DiazGranados CA, Voloshen T, et al. Correlates of Protection against Influenza in the Elderly: Results from an Influenza Vaccine Efficacy Trial.](#) *Clinical and Vaccine Immunology*. 2016;23:228–235.
- [12] [Li APY, Cohen CA, Leung NHL, et al. Immunogenicity of standard, high-dose, MF59-adjuvanted, and recombinant-HA seasonal influenza vaccination in older adults.](#) *npj Vaccines*. 2021;6:25.
- [13] [Lee JKH, Lam GKL, Shin T, et al. Efficacy and effectiveness of high-dose versus standard-dose influenza vaccination for older adults: A systematic review and meta-analysis.](#) *Expert Review of Vaccines*. 2018;17:435–443.
- [14] [Izurieta HS, Thadani N, Shay DK, et al. Comparative effectiveness of high-dose versus standard-dose influenza vaccines in US residents aged 65 years and older from 2012 to 2013 using Medicare data: A retrospective cohort analysis.](#) *The Lancet Infectious Diseases*. 2015;15:293–300.
- [15] [Izurieta HS, Lu M, Kelman J, et al. Comparative Effectiveness of Influenza Vaccines Among US Medicare Beneficiaries Ages 65 Years and Older During the 2019-2020 Season.](#) *Clinical Infectious Diseases: An Official Publication of the Infectious Diseases Society of America*. 2021;73:e4251–e4259.
- [16] [Robison SG, Thomas AR. Assessing the effectiveness of high-dose influenza vaccine in preventing hospitalization among seniors, and observations on the limitations of effectiveness study design.](#) *Vaccine*. 2018;36:6683–6687.
- [17] [Hsiao A, Yee A, Fireman B, et al. Recombinant or Standard-Dose Influenza Vaccine in Adults under 65 Years of Age.](#) *New England Journal of Medicine*. 2023;389:2245–2255.

- [18] Doyle JD, Beacham L, Martin ET, et al. [Relative and Absolute Effectiveness of High-Dose and Standard-Dose Influenza Vaccine Against Influenza-Related Hospitalization Among Older Adults—United States, 2015–2017](#). *Clinical Infectious Diseases*. 2021;72:995–1003.
- [19] Paudel M, Mahmud S, Buikema A, et al. [Relative vaccine efficacy of high-dose versus standard-dose influenza vaccines in preventing probable influenza in a Medicare Fee-for-Service population](#). *Vaccine*. 2020;38:4548–4556.
- [20] Naleway AL, Kim SS, Flannery B, et al. [Immunogenicity of High-Dose Egg-Based, Recombinant, and Cell Culture–Based Influenza Vaccines Compared With Standard-Dose Egg-Based Influenza Vaccine Among Health Care Personnel Aged 18–65 Years in 2019–2020](#). *Open Forum Infectious Diseases*. 2023;10:ofad223.
- [21] Schmader KE, Liu CK, Flannery B, et al. [Immunogenicity of adjuvanted versus high-dose inactivated influenza vaccines in older adults: A randomized clinical trial](#). *Immunity & Ageing*. 2023;20:30.
- [22] Coleman BL, Sanderson R, Haag MDM, et al. [Effectiveness of the MF59-adjuvanted trivalent or quadrivalent seasonal influenza vaccine among adults 65 years of age or older, a systematic review and meta-analysis](#). *Influenza and Other Respiratory Viruses*. 2021;15:813–823.
- [23] Dugan HL, Henry C, Wilson PC. [Aging and influenza vaccine-induced immunity](#). *Cellular Immunology*. 2020;348:103998.
- [24] Arevalo P, McLean HQ, Belongia EA, et al. [Earliest infections predict the age distribution of seasonal influenza A cases](#). Cooper BS, Ferguson NM, Cooper BS, et al., editors. *eLife*. 2020;9:e50060.
- [25] Vieira MC, Donato CM, Arevalo P, et al. [Lineage-specific protection and immune imprinting shape the age distributions of influenza B cases](#). *Nature Communications*. 2021;12:4313.
- [26] Gostic KM, Ambrose M, Worobey M, et al. [Potent protection against H5N1 and H7N9 influenza via childhood hemagglutinin imprinting](#). *Science*. 2016;354:722–726.
- [27] Gostic KM, Bridge R, Brady S, et al. [Childhood immune imprinting to influenza A shapes birth year-specific risk during seasonal H1N1 and H3N2 epidemics](#). *PLOS Pathogens*. 2019;15:e1008109.

- [28] Wood SN. Thin-plate regression splines. *Journal of the Royal Statistical Society (B)*. 2003;65:95–114.
- [29] Wood SN. Stable and efficient multiple smoothing parameter estimation for generalized additive models. *Journal of the American Statistical Association*. 2004;99:673–686.
- [30] Wood SN. Fast stable restricted maximum likelihood and marginal likelihood estimation of semiparametric generalized linear models. *Journal of the Royal Statistical Society (B)*. 2011;73:3–36.
- [31] Wood SN, N., Pya, et al. Smoothing parameter and model selection for general smooth models (with discussion). *Journal of the American Statistical Association*. 2016;111:1548–1575.
- [32] Wood SN. Generalized additive models: An introduction with R. 2nd ed. Chapman and Hall/CRC; 2017.
- [33] Pedersen EJ, Miller DL, Simpson GL, et al. [Hierarchical generalized additive models in ecology: An introduction with mgcv](#). *PeerJ*. 2019;7:e6876.
- [34] Lewandowski D, Kurowicka D, Joe H. [Generating random correlation matrices based on vines and extended onion method](#). *Journal of Multivariate Analysis*. 2009;100:1989–2001.
- [35] Stan Development Team. Stan Modeling Language Users Guide and Reference Manual. 2022.
- [36] Prior Choice Recommendations · stan-dev/stan Wiki. GitHub. <https://github.com/stan-dev/stan>;
- [37] Bürkner P-C. [Brms: An R Package for Bayesian Multilevel Models Using Stan](#). *Journal of Statistical Software*. 2017;80:1–28.
- [38] Bürkner P-C. [Advanced Bayesian Multilevel Modeling with the R Package brms](#). *The R Journal*. 2018;10:395.
- [39] Gabry J, Češnovar R, Johnson A. Cmdstanr: R interface to 'CmdStan'. 2023.
- [40] Betancourt M. A Conceptual Introduction to Hamiltonian Monte Carlo [Internet]. arXiv; 2018 [cited 2024 Jun 11]. Available from: <https://arxiv.org/abs/1701.02434>.

- [41] Kay M. [ggdist: Visualizations of distributions and uncertainty in the grammar of graphics](#). IEEE Transactions on Visualization and Computer Graphics. 2024;30:414–424.
- [42] Kay M. [ggdist: Visualizations of distributions and uncertainty](#). 2024.
- [43] COOKE P. [Statistical inference for bounds of random variables](#). Biometrika. 1979;66:367–374.
- [44] Loh W-Y. [Estimating an Endpoint of a Distribution with Resampling Methods](#). The Annals of Statistics. 1984;12:1543–1550.
- [45] Sheather SJ, Jones MC. A Reliable Data-Based Bandwidth Selection Method for Kernel Density Estimation. Journal of the Royal Statistical Society Series B (Methodological) [Internet]. 1991 [cited 2024 Jun 11];53:683–690. Available from: <https://www.jstor.org/stable/2345597>.
- [46] Gouma S, Zost SJ, Parkhouse K, et al. [Comparison of Human H3N2 Antibody Responses Elicited by Egg-Based, Cell-Based, and Recombinant Protein-Based Influenza Vaccines During the 2017-2018 Season](#). Clinical Infectious Diseases. 2020;71:1447–1453.
- [47] Liu F, Gross FL, Jefferson SN, et al. [Age-specific effects of vaccine egg adaptation and immune priming on A\(H3N2\) antibody responses following influenza vaccination](#). The Journal of Clinical Investigation. 2021;131.
- [48] Yang D, Dalton JE. A unified approach to measuring the effect size between two groups using SAS®. SAS Global Forum 2012. 2012;
- [49] Saul B. Smd: Compute standardized mean differences. 2024.
- [50] Cohen J. Statistical power analysis for the behavioral sciences. 2nd ed. London, England: Routledge; 2013.
- [51] Sawilowsky S. [New Effect Size Rules of Thumb](#). Journal of Modern Applied Statistical Methods. 2009;8.
- [52] Gelman A, Carlin JB, Stern HS, et al. Bayesian Data Analysis. 2021;
- [53] Vehtari A, Gelman A, Simpson D, et al. Rank-normalization, folding, and localization: An improved \widehat{R} for assessing convergence of MCMC [Internet]. arXiv; 2021 [cited 2024 Nov 3]. Available from: <https://arxiv.org/abs/1903.08008>.